

# GFZ

Helmholtz Centre  
**POTS DAM**

HELMHOLTZ CENTRE POTSDAM  
**GFZ GERMAN RESEARCH CENTRE  
FOR GEOSCIENCES**

Gottfried Grünthal, Dietrich Stromeyer, Christian Bosse

## **The data sets of the earthquake model for the probabilistic seismic hazard assessment of Germany, version 2016**

**Report on supplementary material  
for the respective publication**

Scientific Technical Report STR17/05 - Data

Recommended citation:

Grünthal, G., Stromeyer, D., Bosse, C. (2017): The data sets of the earthquake model for the probabilistic seismic hazard assessment of Germany, version 2016 - Report on supplementary material for the respective publication, (Scientific Technical Report STR - Data; 17/05), Potsdam: GFZ German Research Centre for Geosciences.  
DOI: <http://doi.org/10.2312/GFZ.b103-17056>

Supplementary datasets described in this report:

Grünthal, G., Stromeyer, D., Bosse, C. (2018): The Source Model of the Probabilistic Seismic Hazard Assessment (PSHA) of Germany - Version 2016. V. 1.0. GFZ Data Services.  
DOI: <http://doi.org/10.5880/GFZ.2.6.2018.001>

Respective publication:

Grünthal G, Stromeyer D, Bosse C, Cotton F, Bindi D (2018) The probabilistic seismic hazard assessment of Germany: version 2016, considering the range of epistemic uncertainties and aleatory variability. Bull Earthquake Engineering: 1-57.  
DOI: <http://doi.org/10.1007/s10518-018-0315-y>

## Imprint

HELMHOLTZ CENTRE POTSDAM  
**GFZ GERMAN RESEARCH CENTRE  
FOR GEOSCIENCES**

Telegrafenberg  
D-14473 Potsdam

Published in Potsdam, Germany  
2017

ISSN 2190-7110

DOI: <http://doi.org/10.2312/GFZ.b103-17056>  
URN: urn:nbn:de:kobv:b103-17056

This work is published in the GFZ series  
Scientific Technical Report (STR)  
and electronically available at GFZ website  
[www.gfz-potsdam.de](http://www.gfz-potsdam.de)



G. Grünthal, D. Stromeyer, C. Bosse

**The data sets of the earthquake model for  
the probabilistic seismic hazard assessment  
of Germany, version 2016**

**Report on supplementary material  
for the respective publication**

## **Table of Contents**

|  |    |
|--|----|
| Abbreviations .....  | 3  |
| Abstract .....   | 4  |
| 1. Introduction .....  | 5  |
| 2. Seismicity .....  | 6  |
| 2.1. Induced seismicity .....  | 6  |
| 2.2. Seismicity related to photolineations .....                           | 9  |
| 2.3. Completeness of catalogued magnitudes .....                           | 11 |
| 3. Models of seismic sources .....   | 12 |
| 4. Probability density functions of maximum magnitudes .....               | 19 |
| 5. Seismicity rates .....  | 21 |
| 6. Depth distributions .....   | 58 |
| 7. Tectonic regimes .....  | 61 |
| 8. Additional results of the probabilistic seismic hazard assessment ..... | 62 |
| 8.1. Probabilistic seismic hazard maps .....                               | 62 |
| 8.2. Deaggregations .....  | 81 |
| 8.3. The parameters of the EC 8 elastic design spectral shapes .....       | 82 |
| 9. Comparison with results of the new Swiss earthquake hazard model .....  | 83 |
| 10. Available Datasets .....   | 85 |
| 11. References .....   | 87 |

## Abbreviations

|                 |  |
|-----------------|--|
| CSS             | composite seismic source   |
| DIBt            | Deutsches Institut für Bautechnik  |
| EC 8            | Eurocode 8   |
| GMPE            | ground motion prediction equation  |
| LASZ            | large scale areal source zone  |
| meanSRA         | mean of the amplitudes of periods $T(0.1s, 0.15s, 0.2s)$ in the UHS representing the plateau at a grid point [ $m/s^2$ ] |
| $M_w$           | moment magnitude   |
| $M_{max}$       | maximum expected magnitude   |
| $M_{max}^{obs}$ | maximum observed magnitude   |
| PDF             | probability density function   |
| PGA             | peak ground acceleration [ $m/s^2$ ]   |
| PSHA            | probabilistic seismic hazard assessment  |
| RP              | mean return period [a]   |
| SRA             | spectral response acceleration [ $m/s^2$ ]   |
| SSAZ            | small scale seismic source zone  |
| SSZ             | seismic source zone  |
| UHS             | uniform hazard response spectrum   |

## **Abstract**

The Scientific Technical Report describes supplementary material to the publication by *Grünthal et al. (2018)* on the earthquake model for the probabilistic seismic hazard assessment (PSHA) of Germany, version 2016. In particular, it contains detailed information, additional figures, tables and electronic data concerning seismicity, seismic source zone models, maximum magnitudes, seismicity rates of the seismic source zones, model data related to distributions of focal depth and tectonic regime parameters. It also supplies seismic hazard maps for Germany with a broad range of parametrizations.

## 1. Introduction

The re-evaluation of the probabilistic seismic hazard of Germany, in the version of 2016, has been elaborated on behalf of the German Institute for Civil Engineering (DIBt). The descriptions of the related earthquake model as input for the analysis, as well as the presentation of the respective basic results, are subject of the article by *Grünthal et al.* (2018). However, the earthquake model with all its elements and parameters, including their epistemic uncertainties and aleatory variabilities, is rather complex and beyond the scope of the abovementioned publication. Therefore, the entire set of model parameters and input data are compiled within this report as supporting and supplementary material to *Grünthal et al.* (2018). Moreover, the model parameters and input data are made available also in electronic form (*Grünthal et al.* 2018a). Though, to avoid repetitions, the usage of these data requires detailed information of *Grünthal et al.* (2018).

## **2. Seismicity**

### **2.1. Induced seismicity**

The probabilistic seismic hazard assessment (PSHA) of Germany is based on the needs of the National Annex (NA) [DIN EN 1998-1/NA:2011-01(2011)] to the Eurocode 8 [DIN EN 1998-1:2010-12 (2010)] and in agreement with our research contract with the DIBt on natural tectonic earthquakes (cf. chapter 2 in *Grünthal et al. 2018*). However, the issue of induced seismicity, with several widely felt events in the last decades, has become well-covered by the media and received much public attention. Because of this common interest, some light is shed on this aspect of induced seismicity, where we can rely on the review article by *Grünthal (2014)* on different types of induced seismicity observed in Germany and its immediate surroundings. The differentiation is made therein in induced seismic events due to mining of coal, potash and salt mining, ore mining, hydrocarbon exploitation, geothermal projects, water reservoirs and precipitation. The latter type is in a way a natural phenomenon and rather a triggering mechanism; hence this type of events is used for the presented PSHA. For a clearer distinction between tectonic and induced seismicity, *Grünthal (2014)* suggested to make a clear differentiation in the terminology of both types; i.e. to use strictly the term “induced seismic events” versus “natural tectonic earthquakes” (or simply “earthquakes”).

Fig 2-1 shows the observed seismicity in Germany and its immediate surroundings (tectonic earthquakes and induced seismic events), discriminated into the types mentioned above. The concentration of the induced events on respective coal mining areas or project sites is obvious. The precipitation triggered events are connected with karst areas (see *Grünthal, 2014*, for more details). Particularly revealing is the temporal occurrence of magnitudes of the different types of induced seismic events subdivided into mining districts (Fig. 2-2). We can recognize that the respective activities started with certain human manipulations in the underground. On the other hand, there is obviously a decrease in the magnitudes of several types of induced seismicity connected with a better of exploitation processes, fracking activities or stabilization measures in the underground to avoid “Seismic event of economic concern” (SEECo - introduced as technical term *Grünthal (2014)*). Another issue, which can clearly be noticed in Fig. 2-2, is the termination of seismicity of induced events after the stop of respective projects or mining activity in certain districts. Such obvious temporal changes in the seismic activities of



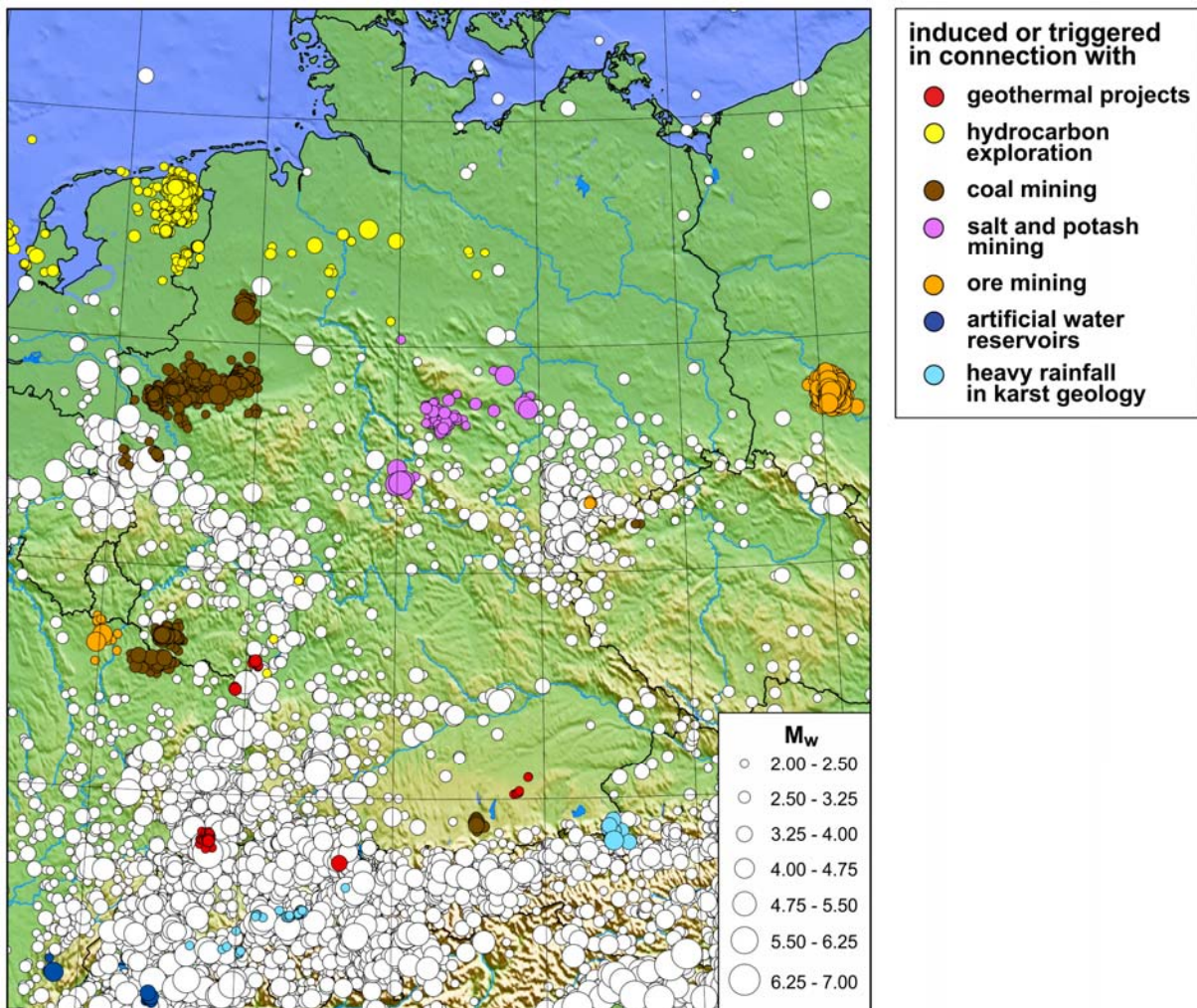


**Figure 2-1.** Natural tectonic seismicity (white circles) and induced seismic events in Germany and surroundings; according to Grünthal (2014) – though based on a data file extended up to 2016.

induced events in dependence of human manipulations in the underground make any probabilistic forecast, such as a PSHA, extremely difficult. Any PSHA concerning induced seismic events which does not consider such striking temporal effects will be of reduced validity.

One of the parameters that provides a preliminary insight into the hazard potential of an area is the maximum observed magnitude  $M_{max}^{obs}$ . Fig. 2-3 shows the ranking of  $M_{max}^{obs}$  for the different types of induced seismic events in Germany and immediate surroundings. All magnitudes used here are moment magnitudes  $M_w$ . The  $M_{max}^{obs} = 6.6$  of natural tectonic earthquakes (i.e.; the 1365 Basel earthquake, c.f. Grünthal et al. 2018) is by far the largest event observed in the region. It is followed by the  $M_w$  5.4 Völkershäuser seismic event in a potash mining area, of rank 2, which was caused by an obvious undersizing of pillars in the potash mining horizon. Since such a mining engineering approach is unlikely to be

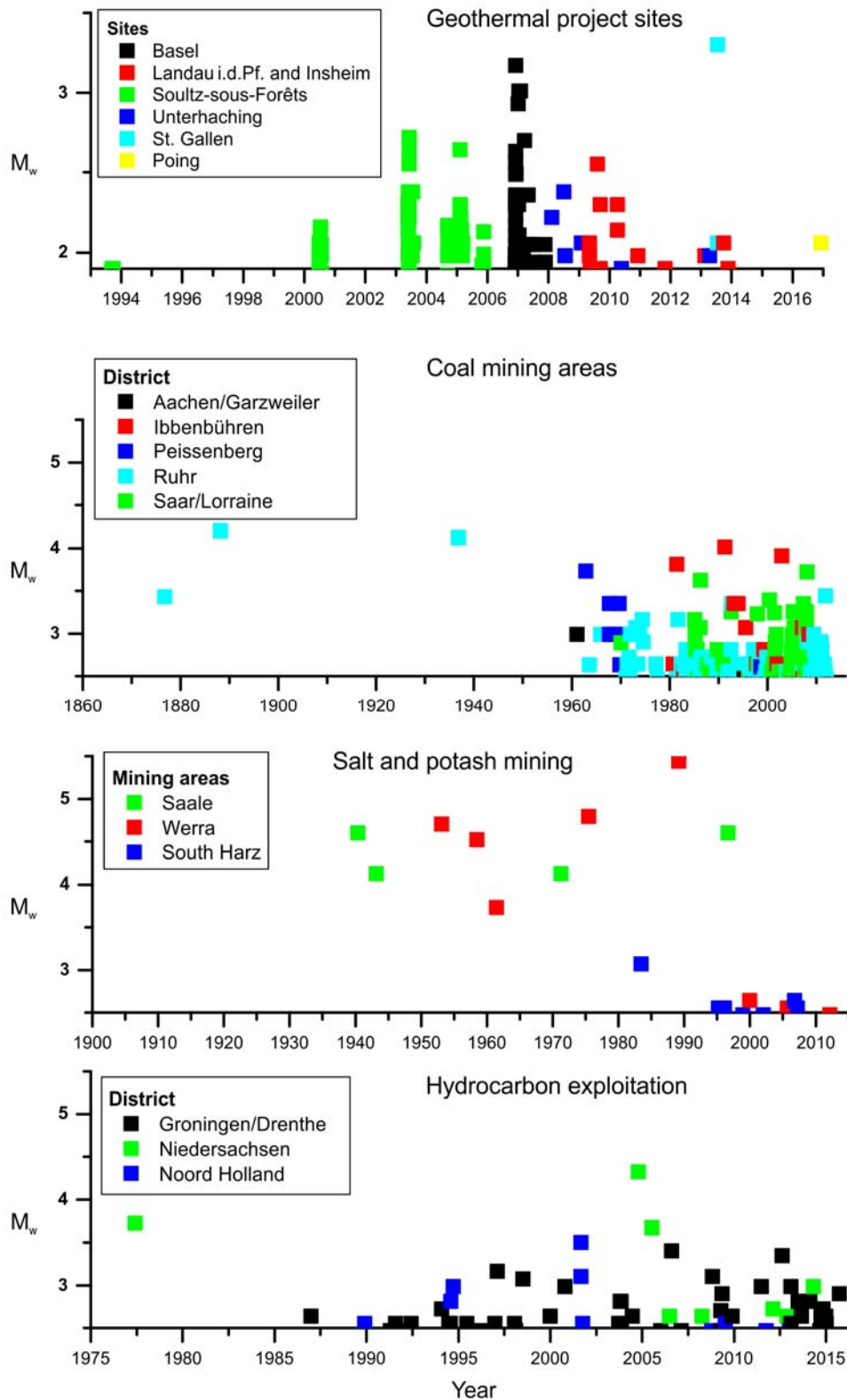


**Figure 2-2.** Temporal occurrence of induced seismic events specified according to event types and mining districts; according to Grünthal (2014) – though based on a data file extended up to 2016.

repeated, a similar event becomes considerably less probable in future. The  $M_{max}^{obs}$  values of the other types of induced seismicity are much lower.

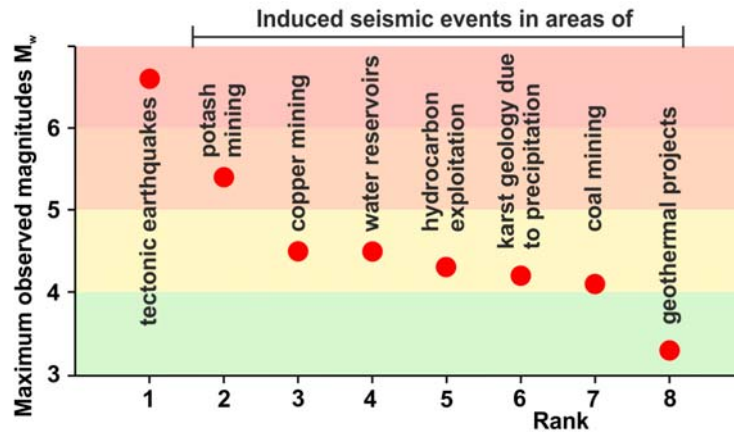


**Figure 2-3.** Ranking of the maximum observed magnitude  $M_{max}^{obs}$  of the different sources of seismicity in Germany and immediate surroundings, differentiated into natural tectonic earthquakes and observed types of induced seismic events up to 2016; modified after Grünthal (2014).

A quantitatively more refined comparison is possible with yearly frequency-magnitude relations of the different event types. With respect to such graphs we refer to Fig. 7 of Grünthal (2014).

## 2.2. Seismicity related to photolineations

The relationship of seismicity with regional tectonic settings has already been described to some extent in chapter 3 of Grünthal *et al.* (2018). There, it has been mentioned that prominent seismicity features cannot be associated readily with classical tectonic faults but rather with fracture lineaments detected from high resolution data from ERS-1/2 radar mosaics, Landsat-TM, Aster-DEM, and X-SAR-SRTM. This characteristic shall be supported here with two respective maps. The first example refers to the seismicity of the Hohenzollernalb (HZA), the spot of seismic activity that commenced in 1911 with a  $M_w$  5.7 event, followed by several damaging earthquakes, the most recent in 1978. Ongoing activity can be observed in that focal zone of the HZA, which is located around  $9^\circ\text{N}$  and  $48.2\text{-}48.5^\circ\text{E}$  (Fig. 2-4). The figure shows both the precisely located seismicity from 1995-2016, alongside the tectonic faults and photolineations of Figs. 3-1, and 3-2 of Grünthal *et al.* (2018) for the southwest part of the target area and surroundings. The coincidence of the seismicity in a narrow band around  $9^\circ\text{N}$  and  $48.2\text{-}48.5^\circ\text{E}$  with almost N-S striking photolineations is obvious.

The other example, which highlights the importance of photolineations in relation to understanding the seismicity of certain regions, concerns the Vogtland-Leipzig zone (cf.

chapter 3 of Grünthal et al. 2018). Fig. 2-5 shows the well located seismicity of this N-S elongated zone from 1995-2016.

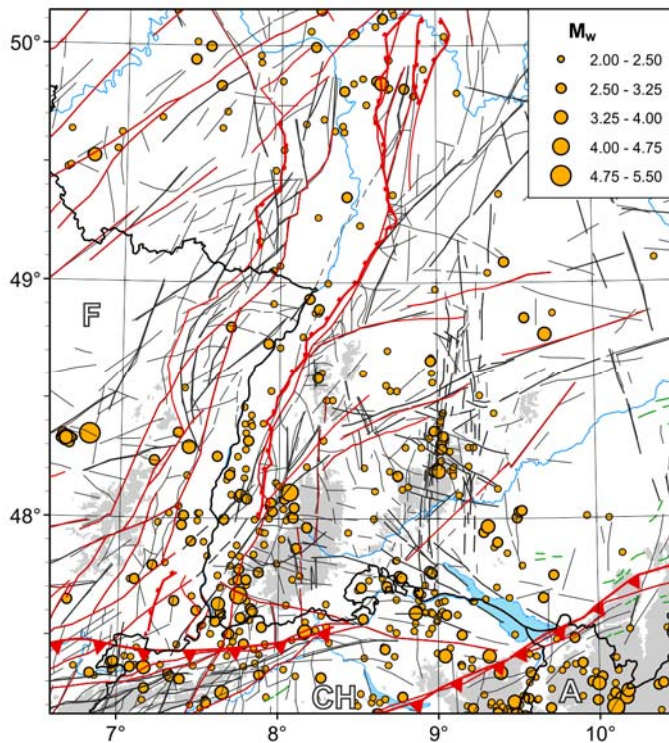


**Figure 2-4.** Seismicity in the southwest part of the target area and surroundings from 1995-2016 in connection with tectonic faults and photolineations of Figs. 3-1 and 3-2 of Grünthal et al. (2018).

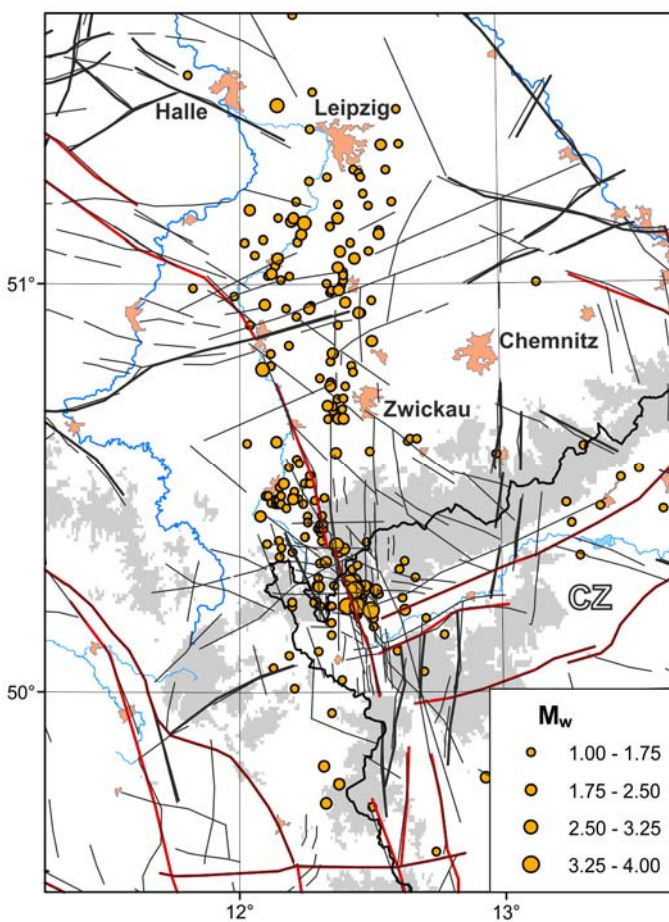


**Figure 2-5.** Seismicity in the Vogtland-Leipzig zone from 1995-2016 in connection with tectonic faults and photolineations of Fig. 3-1 and 3-2 of Grünthal et al. (2018).

### 2.3. Completeness of catalogued magnitudes

A basic element for the calculation of yearly rates of catalogued earthquake magnitude classes is the sufficient temporal completeness of events per class. This has been described in many of our earlier seismic hazard studies, such as Grünthal *et al.* (1998). Therein and in further studies, we have employed an approach for the completeness assessment from a historical perspective in combination with graphs of the cumulative number of events with time; i.e. the slope method. Since the development of our statistical method (Hakimhashemi & Grünthal 2012) we usually apply both methods in parallel. The results based on both approaches are generally very similar. In case of differences, standard deviations of maximum likelihood estimates of Gutenberg-Richter  $b$ -values decide which datum to use. As described in Grünthal *et al.* (2018), we determined the following completeness times for the west and southwest of our target area, i.e. in the regions of elevated seismicity of Germany: for  $M_w = 3.5-4.5$  a sufficient completeness time since about 1870, for  $M_w = 4.5-5$  since about 1800,  $M_w = 5-5.5$  since 1650,  $M_w = 5.5-6$  since 1450 and for  $M_w = 6-6.5$  since 1250.

For the illustration of the determination of the completeness times, we use here the descriptive slope method, which is intuitively accessible (Fig. 2-6a and b). Both graphs show the cumulative plots of earthquake occurrences with time for half magnitude classes with their centres at  $M_w$  1.75 to 5.75. The abscissae of the graphs were chosen such that they provide sufficient time resolution to determine the point (or time range) where the slopes of the cumulative graphs change. To improve the readability in the graphs, the vertical steps indicating an event with time are normalized in such a way that the end points of the cumulative graphs on the right vertical axis have a small difference with the largest magnitude on top. For the interpretation, the graphs are checked to verify the more or less constant slope of the cumulative plots for each magnitude class viewed from the catalogue end towards historical times and starting with lower magnitude classes. After having determined such a point where the smoothed slope of the cumulative graph of a magnitude class significantly decreases towards history, the procedure is repeated for the next larger class. Its completeness range is assumed to be not shorter than that for the next lower class. Concerning the largest magnitude class (or classes) with usually sparse data, additionally, cultural-historical information is used to determine the likely availability of written testimonies within the respective region.

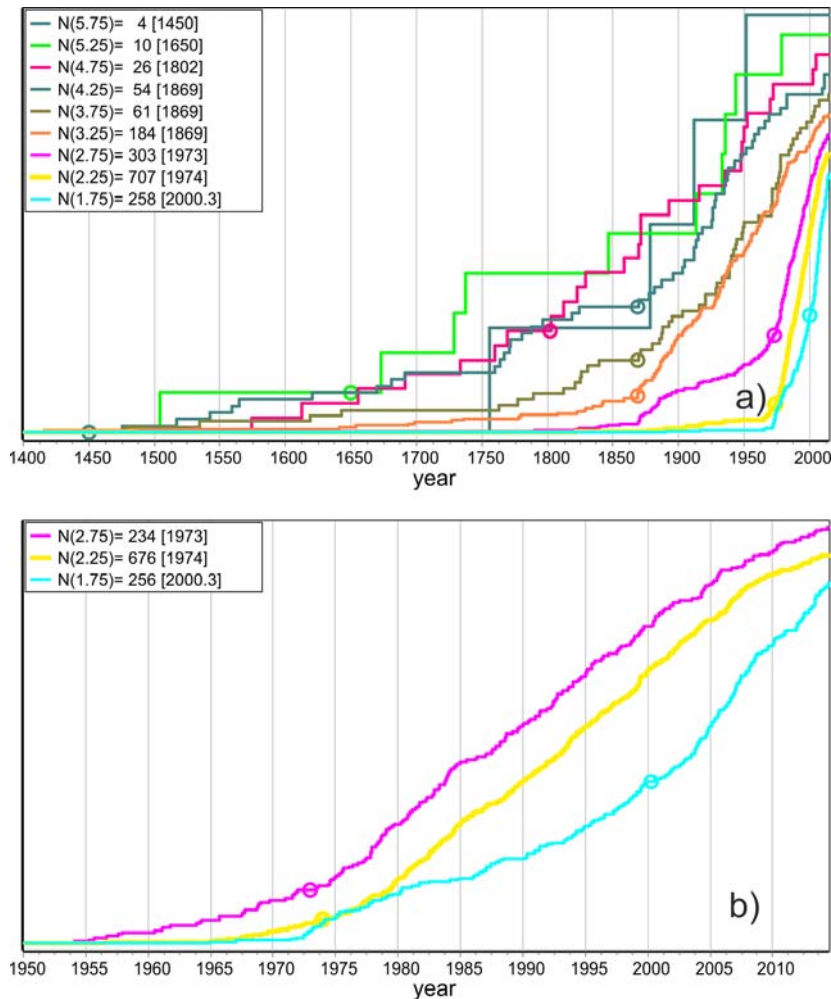


**Figure 2-6.** Illustrations of the determination of the completeness times of catalogued earthquakes for the west and south-west regions of Germany with elevated seismicity as cumulative plots of earthquake occurrences with time for half magnitude classes with their centres at 1.75 to 5.75 (a) and with spread horizontal time axis (b) for the three smallest magnitude classes. The determined completeness times are marked as small circles for each magnitude class. The legend contains the numbers of catalogued earthquakes for corresponding magnitude classes within their completeness windows.

### 3. Models of seismic sources

The input model of the reassessment of the seismic hazard of Germany is composed of five areal seismic source zone (SSZ) models A, B, C, D and E (cf. chapter 4 of *Grünthal et al.* 2018). While this paper shows the configuration of SSZ model A in full, only parts of the others are presented therein. Here, we provide all SSZ models; i.e. the large scale areal seismic source zone (LASZ) models and the small scale areal seismic source zone (SASZ) models, in their entirety together with the enlarged part of the target area for a better readability of the finer SSZ model there (Figs. 3-1 to 3-5). The polygon traces for each SSZ are supplied in the electronic Annex.

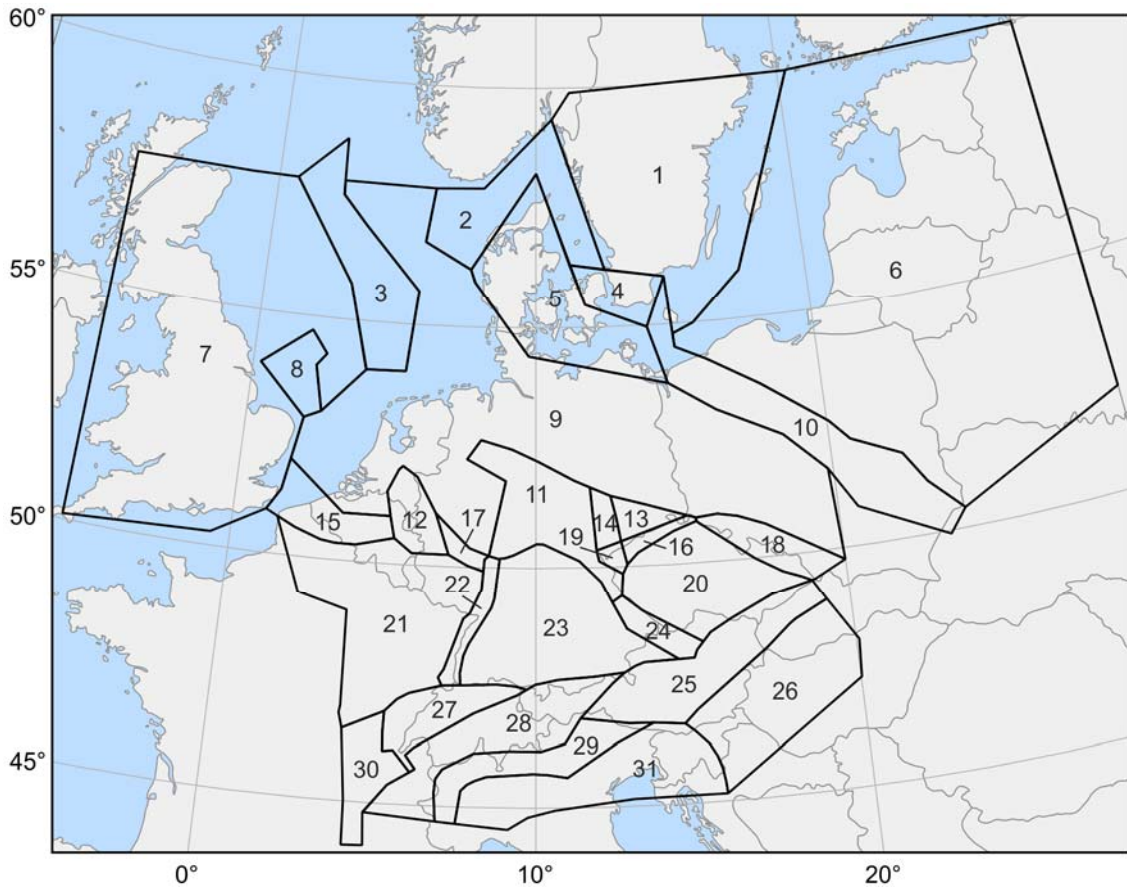


Figure 3-1. The large scale areal seismic source zone (LASZ) model A.

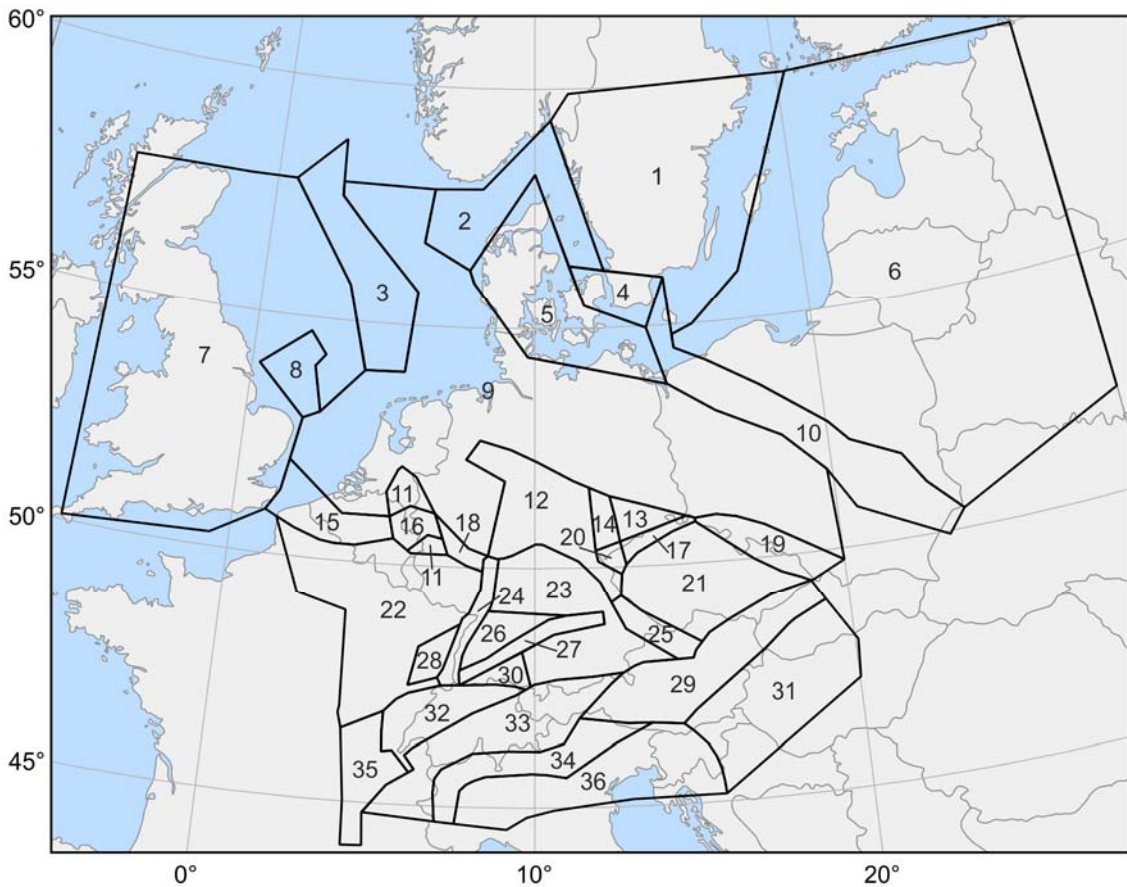


Figure 3-2. The LASZ model B.

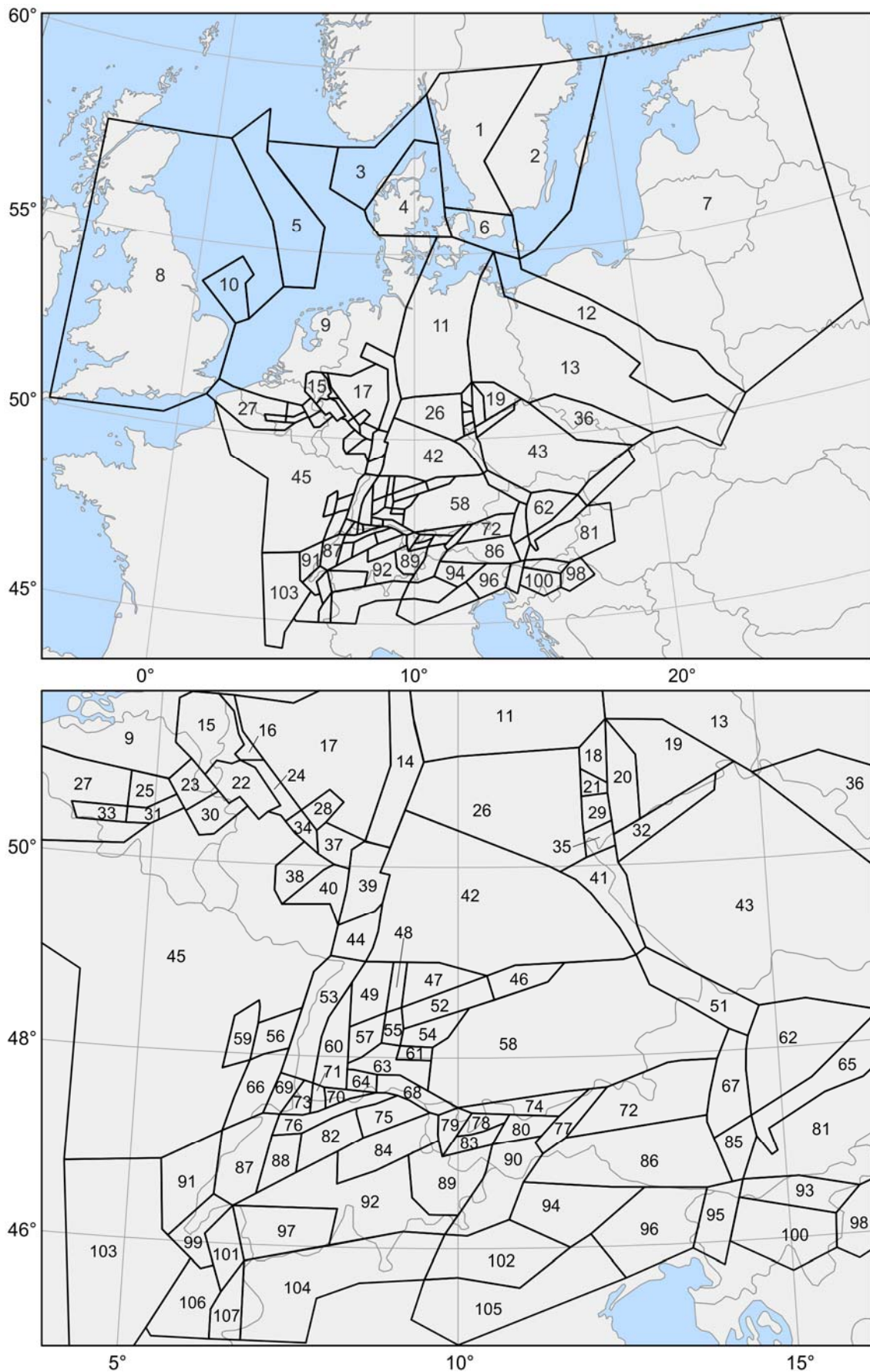


Figure 3-3. The SASZ model C; the entire model above; an enlarged section with the SW part below.



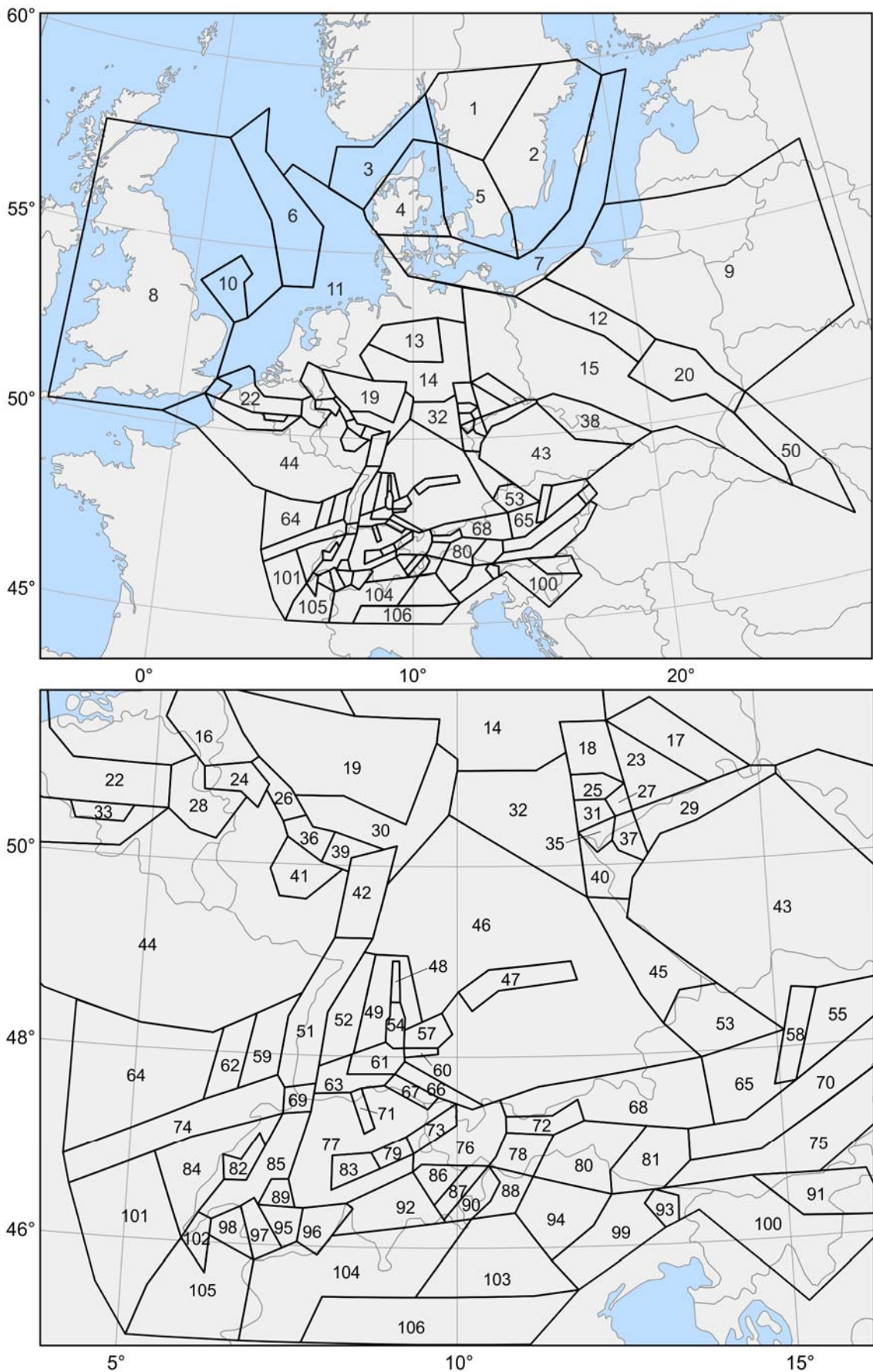


Figure 3-4. The SASZ model D; the entire model above; an enlarged section with the SW part below.

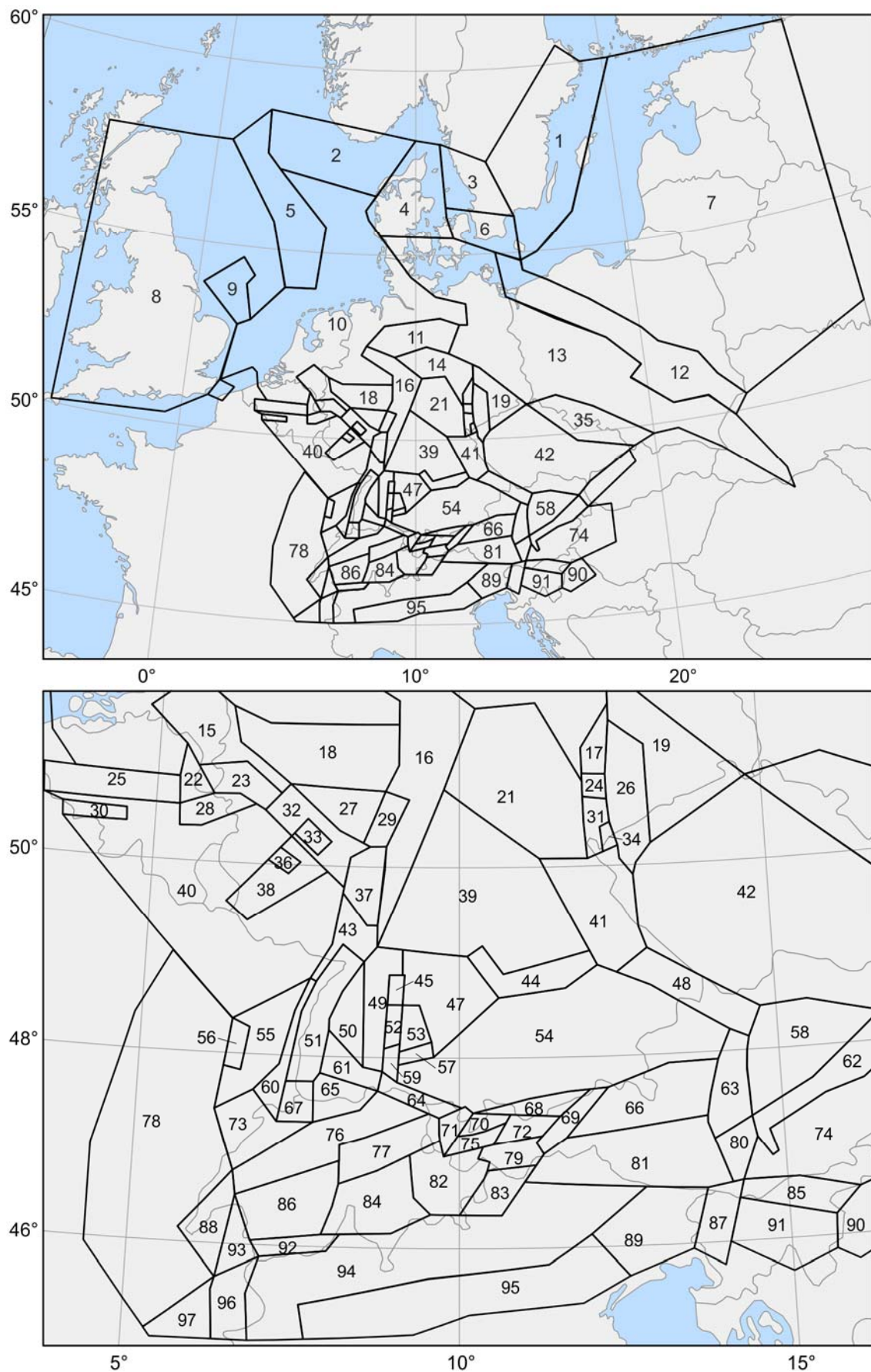
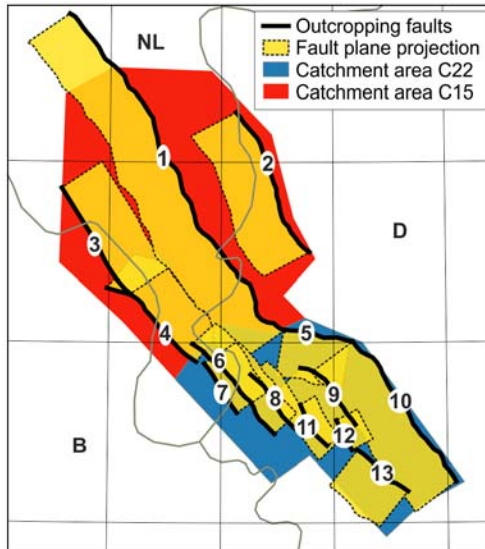
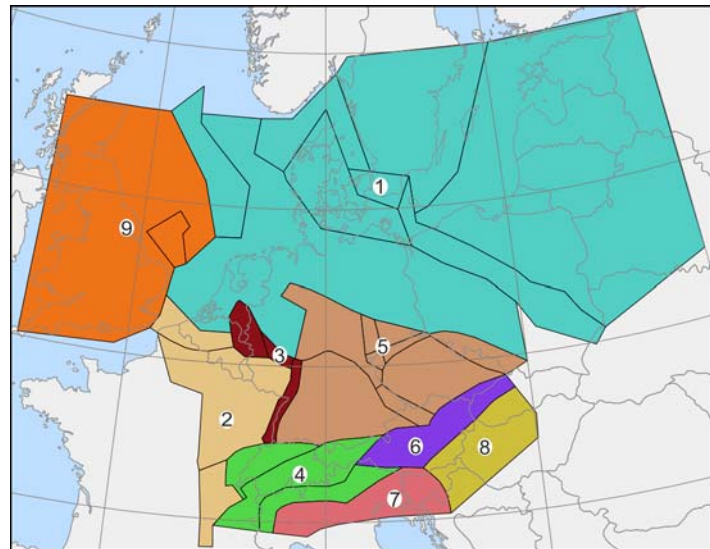


Figure 3-5. The SASZ model E; the entire model above; an enlarged section with the SW part below.



**Figure 3-6.** Geometry of composite seismic sources (CSS) for the Lower Rhine Graben (Vanneste *et al.* 2013) and corresponding catchment areas of the SASZ model C.



**Figure 3-7.** The model of superzones, within which separate kernels were derived.

**Table 3-1.** Parameters of the CSS for the Lower Rhine graben according to Vanneste *et al.* (2013) in the ascending numbering of Fig. 3-6. A dip marked with (\*) refers to faults striking from NW to SO otherwise from SO to NW.

| No. | Name    | Dip [°] | Width [km] | Length [km] | Area [km <sup>2</sup> ] | Max. depth [km] | Fault type | $M_{max}$ | $\sigma(M_{max})$ |
|-----|---------|---------|------------|-------------|-------------------------|-----------------|------------|-----------|-------------------|
| 1   | NLCS001 | 57.5    | 29.6       | 123.8       | 3664                    | 25.0            | normal     | 7.1       | 0.3               |
| 2   | DECS004 | 57.5    | 29.6       | 51.1        | 1483                    | 25.0            | normal     | 7.1       | 0.3               |
| 3   | BECS002 | 57.5*   | 27.7       | 39.2        | 1086                    | 23.5            | normal     | 6.9       | 0.3               |
| 4   | BECS001 | 57.5*   | 25.1       | 37.1        | 931                     | 21.2            | normal     | 6.9       | 0.3               |
| 5   | DECS002 | 57.5    | 27.5       | 21.3        | 586                     | 23.2            | normal     | 6.6       | 0.3               |
| 6   | NLCS002 | 57.5*   | 17.7       | 38.3        | 678                     | 14.9            | normal     | 6.9       | 0.3               |
| 7   | NLCS003 | 57.5*   | 22.3       | 18.4        | 410                     | 18.8            | normal     | 6.6       | 0.3               |
| 8   | DECS005 | 57.5*   | 12.1       | 21.8        | 264                     | 10.2            | normal     | 6.6       | 0.3               |
| 9   | DECS001 | 57.5    | 29.6       | 25.5        | 755                     | 25.0            | normal     | 6.9       | 0.3               |
| 10  | DECS003 | 57.5    | 29.6       | 55.0        | 1628                    | 25.0            | normal     | 7.1       | 0.3               |
| 11  | DECS006 | 57.5*   | 10.2       | 15.3        | 156                     | 8.7             | normal     | 6.5       | 0.3               |
| 12  | DECS007 | 57.5*   | 13.8       | 10.4        | 144                     | 11.6            | normal     | 6.3       | 0.3               |
| 13  | DECS008 | 57.5    | 26.2       | 20.6        | 540                     | 22.1            | normal     | 6.6       | 0.3               |

Model C contains additionally composite seismic fault sources (CSS) for the Lower Rhine graben (Fig. 3-6, Tab. 3-1) derived from the NW-SE striking CSS model by Vanneste *et al.* (2013). The determination of rates is based on the seismicity of two catchment sub-areas C15 and C22 and is described in chapter 4.3 of Grünthal *et al.* (2018).

The PSHA makes use of two zoneless models, which apply procedures of smoothing the observed seismicity. The corresponding bandwidth functions were determined from the

**Table 3-2.** Combination of LASZs of model A to build nine kernel superzones KSZ. Parameters  $c_1$  and  $c_2$  of the magnitude dependent bandwidth function  $H(M) = c_1 \exp(c_2 M)$ .

| DSZ | LASZ (model A)                              | $c_1$  | $c_2$  |
|-----|---|--------|--------|
| 1   | A09, A05, A04, A01, A10, A06, A03, A02      | 8.9563 | 0.5546 |
| 2   | A21, A30, A15                               | 1.6416 | 0.7063 |
| 3   | A12, A17, A22                               | 0.1332 | 1.0916 |
| 4   | A27, A28, A29                               | 0.2482 | 0.8766 |
| 5   | A11, A23, A14, A13, A19, A16, A24, A20, A18 | 2.2363 | 0.4969 |
| 6   | A25   | 0.5867 | 0.7360 |
| 7   | A31   | 0.0450 | 1.0849 |
| 8   | A26   | 1.0834 | 0.5775 |
| 9   | A07, A08                                    | 4.1962 | 0.5470 |

areal distribution of the observed seismicity within nine respective superzones. This superzone model is shown in Fig. 3-7; here related to the SSZ model A. The polygon traces of each superzone for deriving the bandwidth functions are also part of the electronic annex. The parameters of the bandwidth functions of each superzone are provided in Tab. 3-2. Fig. 3-8 presents the shapes of the bandwidth functions together with the data of the mean nearest event distances for all these superzones. This figure also illustrates the truncated version of the bandwidth functions we use for the PSHA.

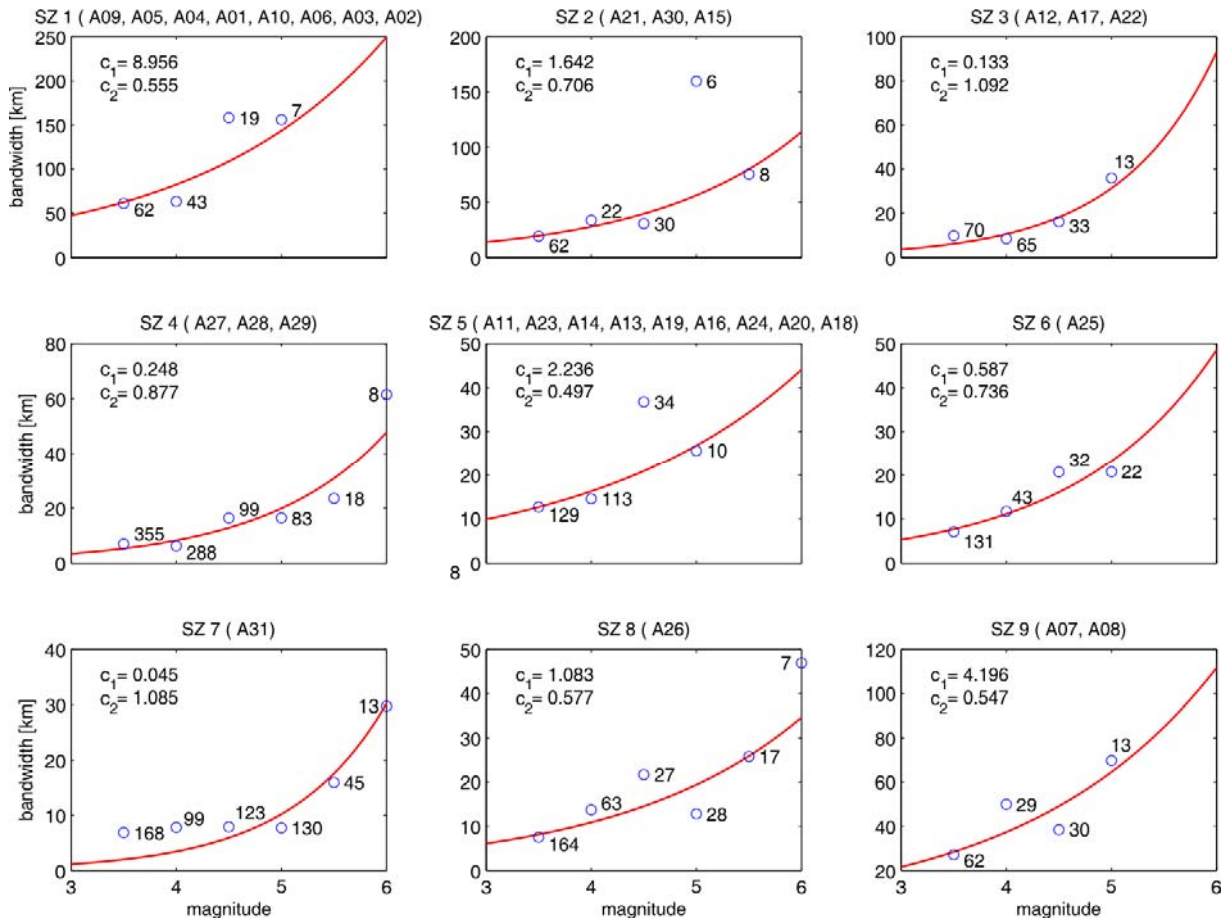


**Figure 3-8.** Shapes of the bandwidth functions together with the data of the mean nearest event distances for the kernel superzones.

#### 4. Probability density functions of maximum magnitudes

The probability density functions (PDF) of maximum magnitudes ( $M_{max}$ ) were also derived for the respective  $M_{max}$  superzone model (cf. chapter 5.1 of Grünthal *et al.* 2018). The calculation of the PDF requires different prior functions of  $M_{max}$  and different truncation parameters according to different tectonic terranes. The model of tectonic terranes used for the approach is shown in Fig. 4-1. The resulting  $M_{max}$ -superzone model, derived from the  $b$ -value superzone-model (cf. next chapter) is provided in Fig. 4-2. The polygon traces of each zone are part of the electronic annex. The shapes of the PDFs of each  $M_{max}$ -superzone with their discretized five  $M_{max,i}$  are presented in Fig. 4-3. Table 4-1 provides the discretized values of the  $M_{max,i}$  for each superzone

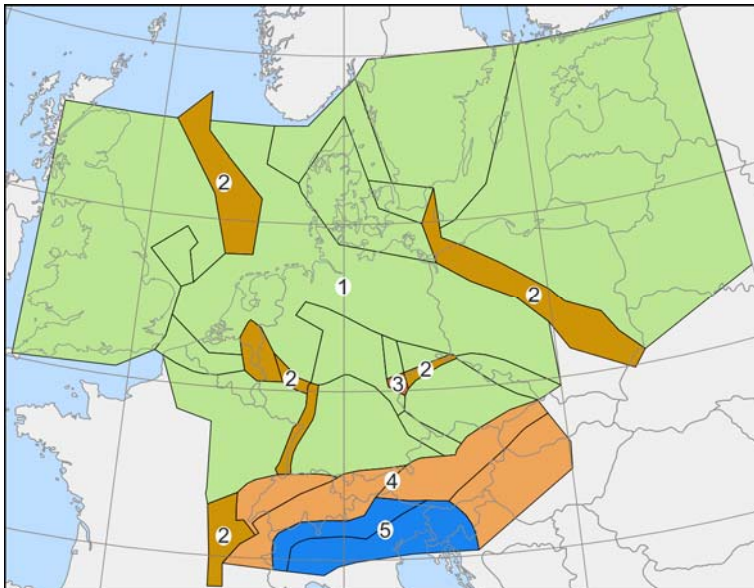


**Figure 4-1.** The model of tectonic terranes that define the use of different prior functions of  $M_{max}$  and truncation parameters.

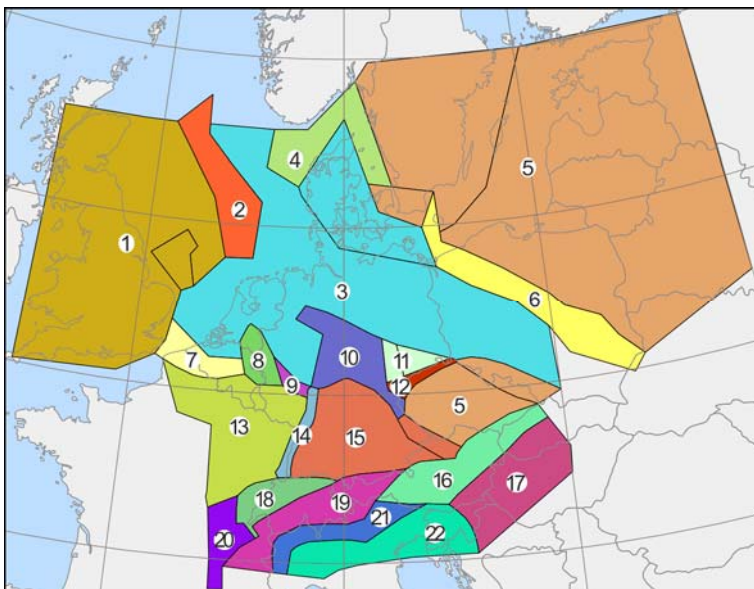


**Figure 4-2.** The  $M_{max}$ -superzone model.

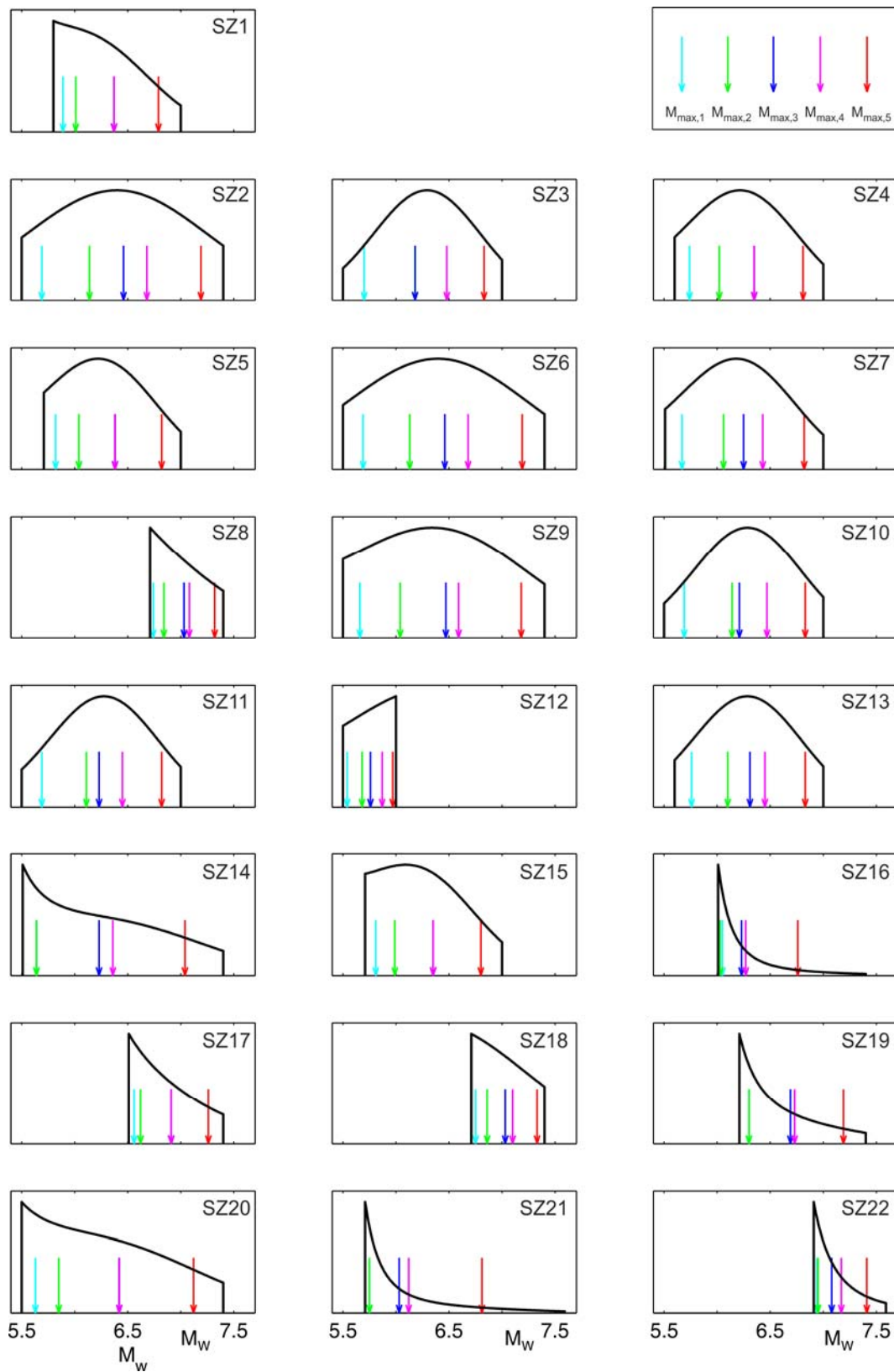


**Figure 4-3.** Shapes of the PDFs for each  $M_{max}$  superzone with their truncations. The discretized  $M_{max,i}$  of equal weights are shown as well.

**Table 4-1.** Discrete  $M_{max}$  distribution of model A (Min for Fit High) for all 22 superzones (see Fig. 4-3) with equal weights of 0.2.

| SZ Number | $M_{max,1}$ | $M_{max,2}$ | $M_{max,3}$ | $M_{max,4}$ | $M_{max,5}$ |
|-----------|-------------|-------------|-------------|-------------|-------------|
| 1         | 5.89        | 6.01        | 6.37        | 6.37        | 6.79        |
| 2         | 5.69        | 6.14        | 6.46        | 6.68        | 7.19        |
| 3         | 5.70        | 6.18        | 6.18        | 6.48        | 6.83        |
| 4         | 5.74        | 6.02        | 6.35        | 6.35        | 6.81        |
| 5         | 5.82        | 6.04        | 6.38        | 6.38        | 6.82        |
| 6         | 5.69        | 6.13        | 6.46        | 6.68        | 7.19        |
| 7         | 5.67        | 6.06        | 6.25        | 6.43        | 6.82        |
| 8         | 6.74        | 6.84        | 7.03        | 7.08        | 7.32        |
| 9         | 5.66        | 6.04        | 6.47        | 6.59        | 7.18        |
| 10        | 5.69        | 6.14        | 6.21        | 6.47        | 6.83        |
| 11        | 5.69        | 6.11        | 6.23        | 6.45        | 6.82        |
| 12        | 5.54        | 5.68        | 5.76        | 5.87        | 5.97        |
| 13        | 5.76        | 6.10        | 6.31        | 6.45        | 6.83        |
| 14        | 5.64        | 5.64        | 6.23        | 6.36        | 7.04        |
| 15        | 5.81        | 5.99        | 6.35        | 6.35        | 6.80        |
| 16        | 6.05        | 6.03        | 6.23        | 6.27        | 6.76        |
| 17        | 6.56        | 6.62        | 6.91        | 6.91        | 7.26        |
| 18        | 6.75        | 6.86        | 7.03        | 7.10        | 7.33        |
| 19        | 6.30        | 6.30        | 6.69        | 6.73        | 7.19        |
| 20        | 5.63        | 5.85        | 6.42        | 6.42        | 7.12        |
| 21        | 5.75        | 5.75        | 6.03        | 6.12        | 6.81        |
| 22        | 6.94        | 6.95        | 7.08        | 7.17        | 7.41        |

## 5. Seismicity rates

The seismicity rates per superzone (cf. chapter 5.2 of Grünthal *et al.* 2018) were calculated using a minimum of 70 events in each respective zone. The model of these superzones for  $b$  values is shown in Fig. 5-1. This superzone model is the basic one of the six superzone models we use for our approach. This prime  $b$ -value superzone-model is derived from the large scale seismic source zone model A. Its zones, which are tectonically related to each other, were combined such that at least 70 events would be available for the derivation of the seismicity parameters. This combination of zones is only necessary in areas of very low seismicity. So, it is obvious that the  $b$ -value superzone-model (with 18 superzones) is very similar to our SSZ model A.

The  $M_{max}$ -superzone model requires a specification of those  $b$ -value superzones, which are a combination of different tectonic terranes, which necessitates the use of different prior functions of  $M_{max}$  and different truncation parameters. This means that four of the  $b$ -value superzone-models needed to be split up which results in 22  $M_{max}$  superzones.

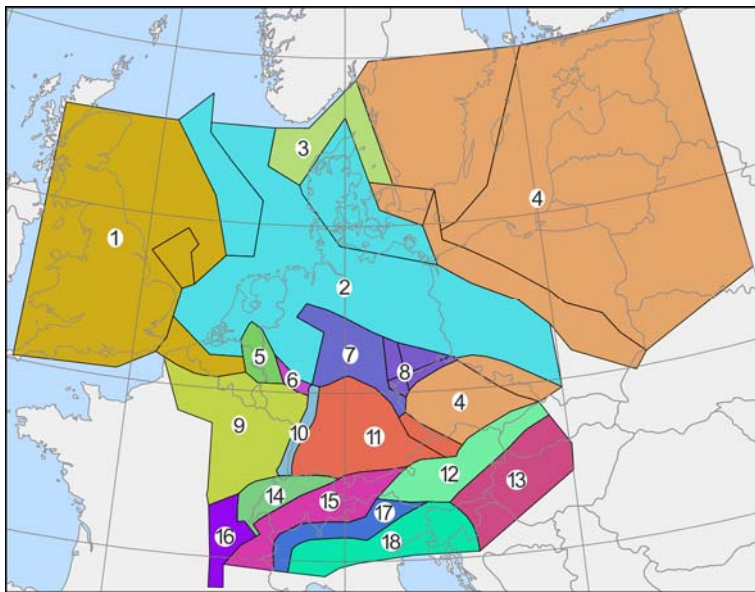


**Figure 5-1.** The  $b$ -value superzone-model with the SSZ of Model A for comparison.

The superzone model of the kernels (see above) is a generalization of the  $b$ -value superzone-model to nine superzones. The same model is applied also as superzone model of focal depth (see below). And finally, the superzone model of tectonic regimes required a split up of two superzones of the latter, which results in eleven superzones of the model for the tectonic regime (see below).

The determination of the seismicity rate parameters necessitates the differentiation of two versions for the minimum for fit (cf. chapter 5.2.3 of *Grünthal et al. 2018*). This could be applied in about 35% of the SSZs. The magnitude frequency graphs of the zones of the  $b$ -value superzone-model are shown in Fig. 5-2 with the minimum magnitude for the fit at low values and  $M_{max,3}$ .

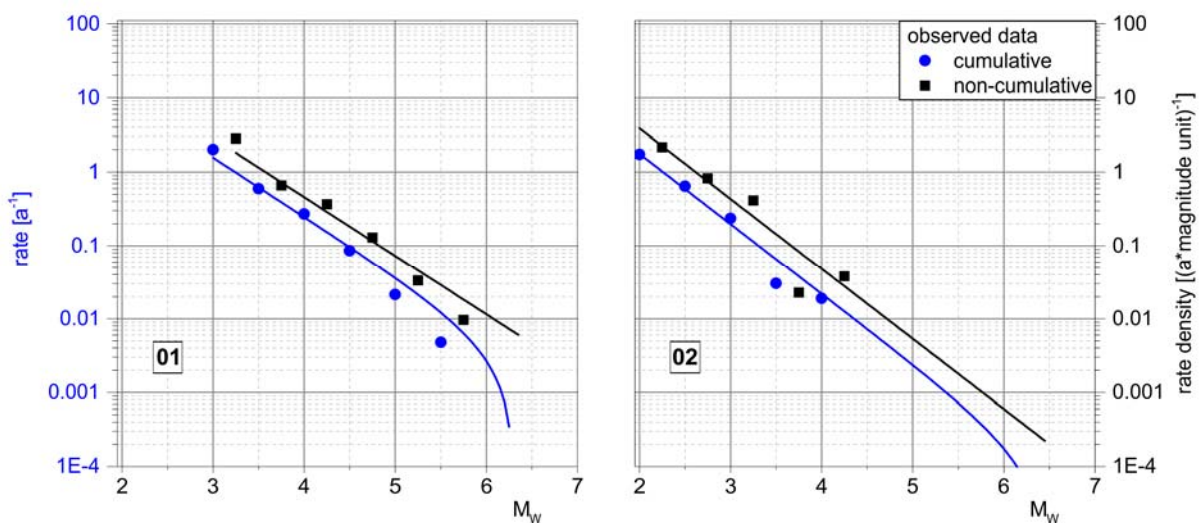


**Figure 5-2.** Frequency-magnitude graphs of the zones of the  $b$ -value superzone model with the minimum magnitude for the fit at low values and  $M_{max,3}$ . The cumulative and the non-cumulative form are given.



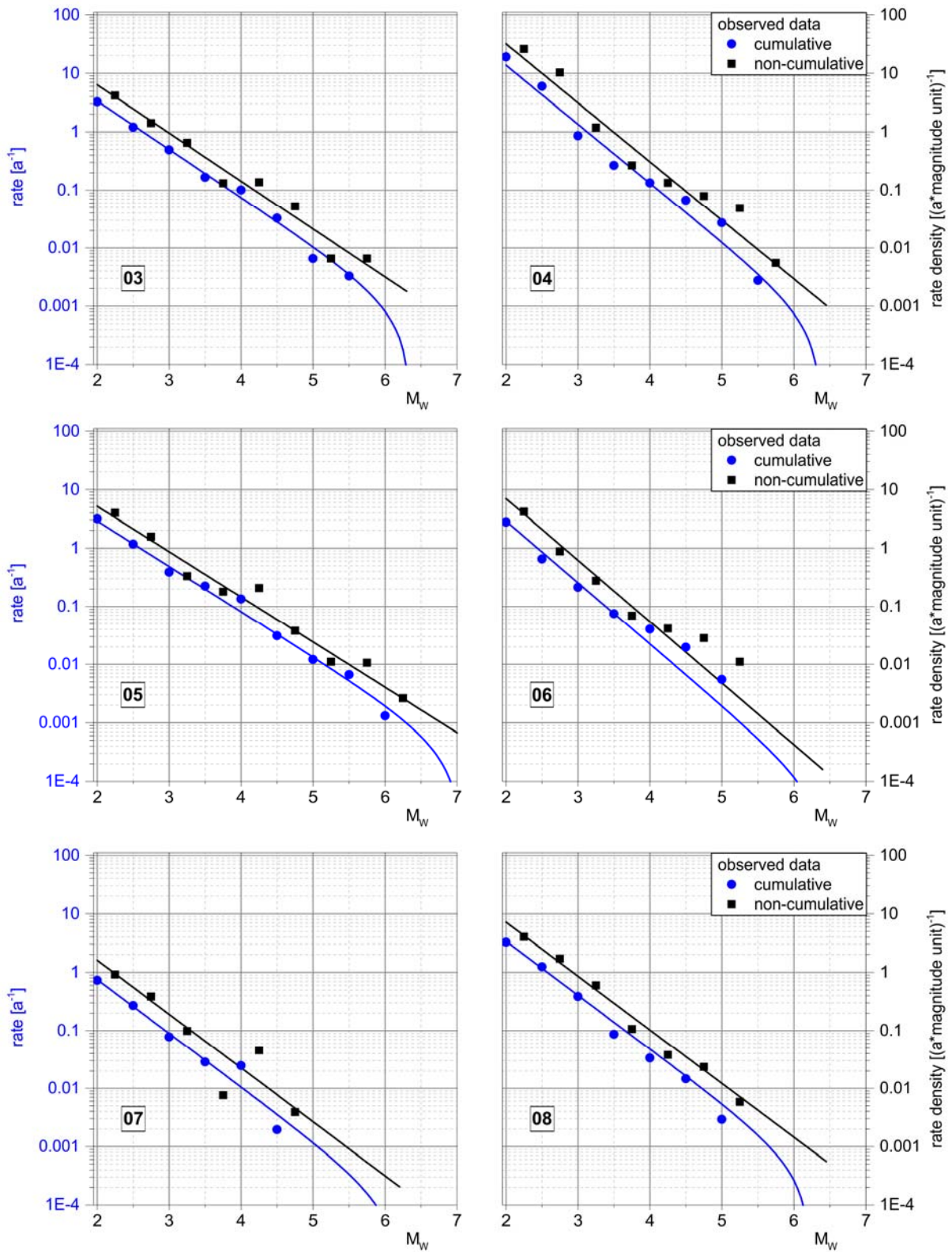


Figure 5-2. Continued.

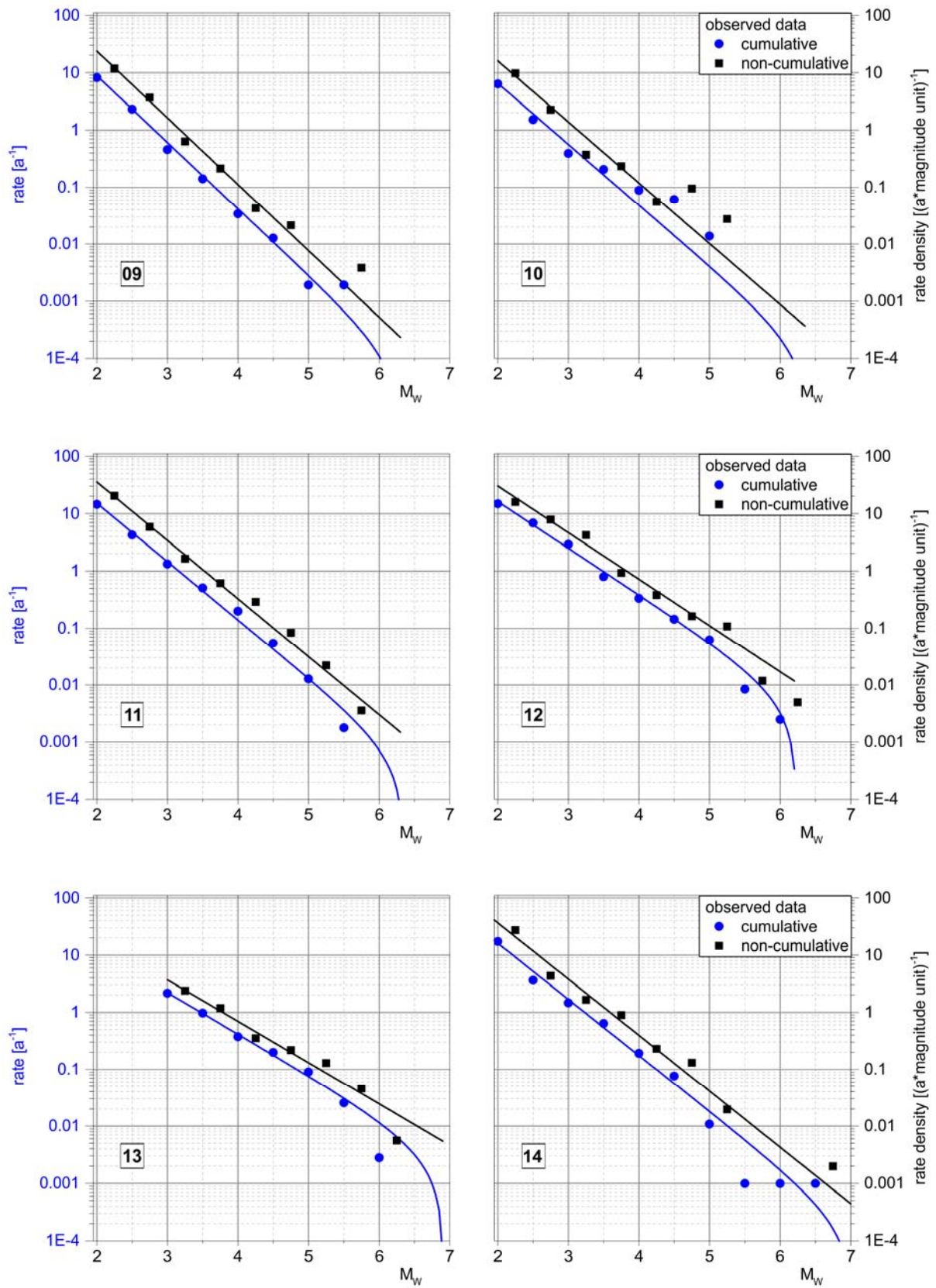


Figure 5-2. Continued.

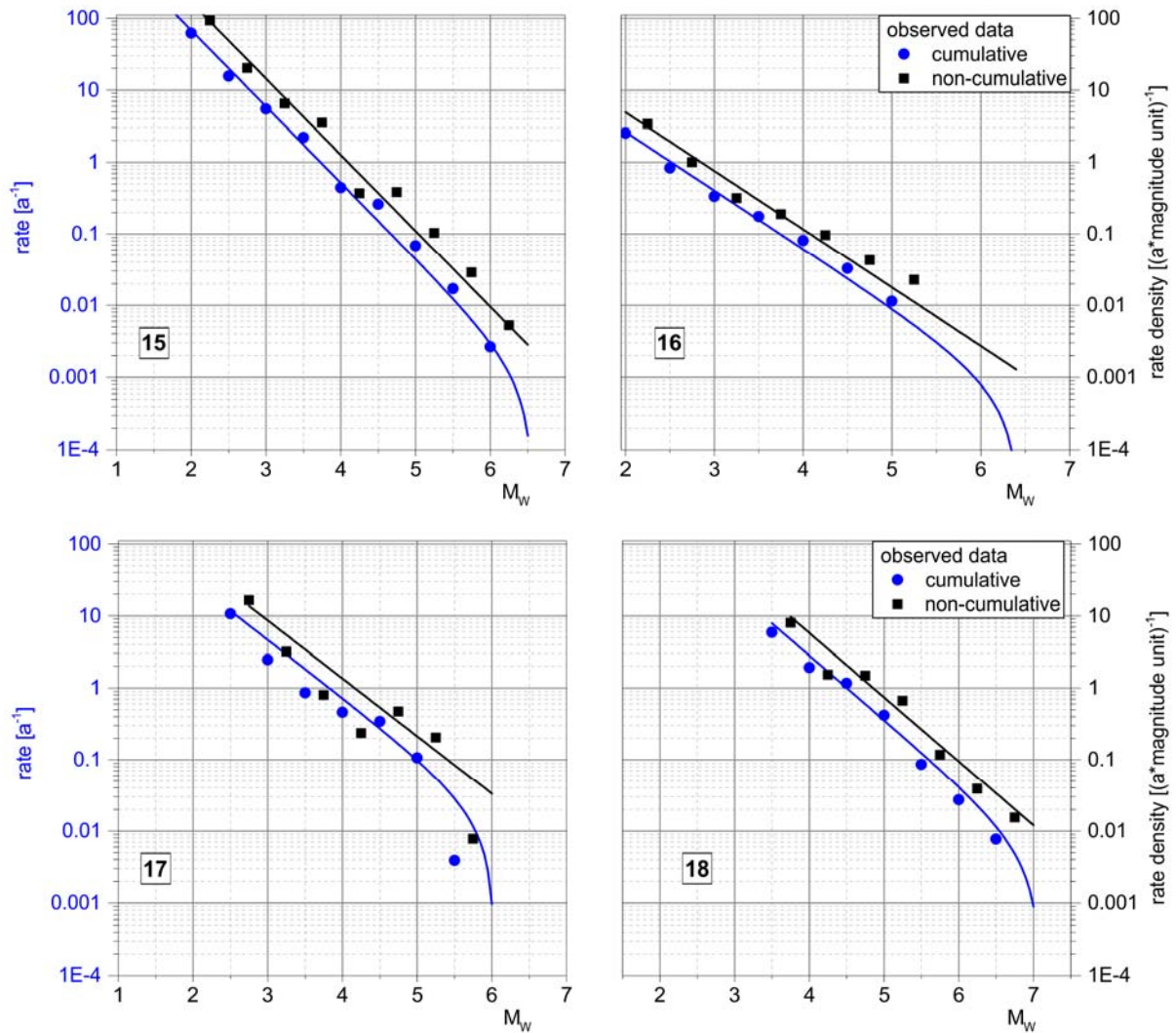
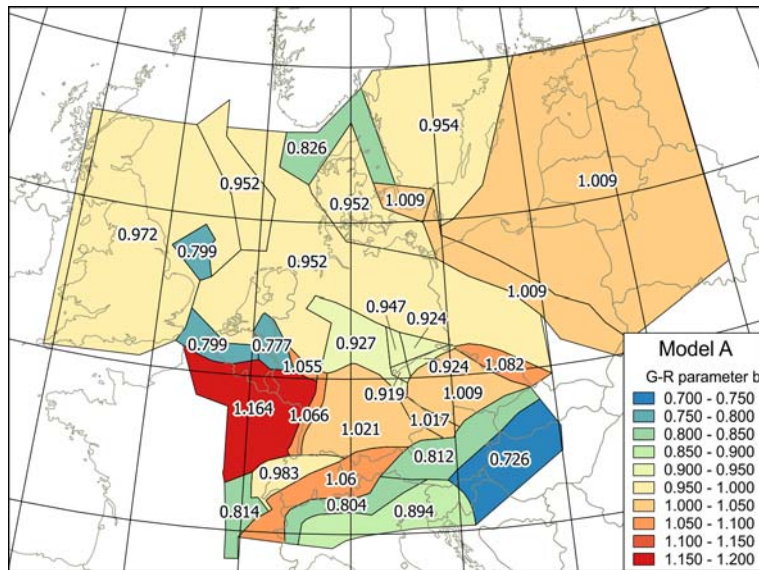
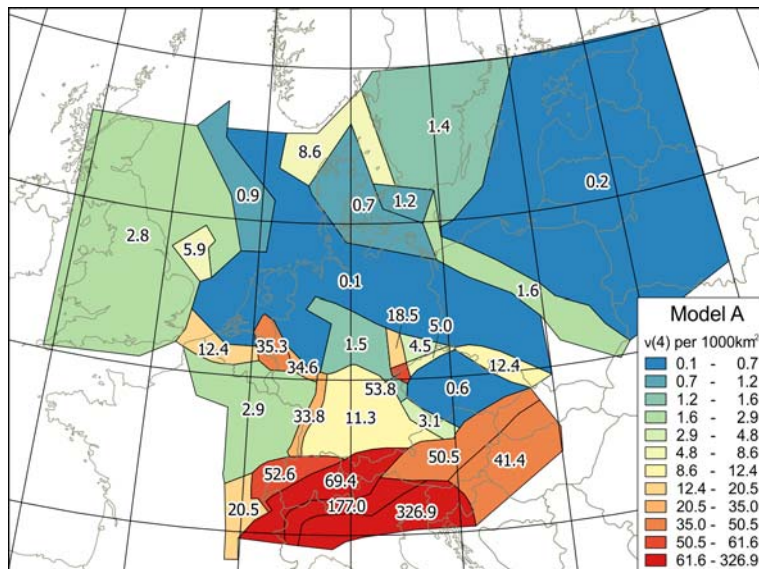


Figure 5-2. Continued.

Fig. 5-3 provides the areal variation of  $b$  values in the SSZ of model A. The variation of the  $a$  value, given as the rate  $\nu$  for  $M_w = 4.0$  and normalized to  $1000 \text{ km}^2$ , is presented in Fig. 5-4. The parameters of the frequency-magnitude relation  $a$  and  $b$  with the parameters of the covariance matrix as measure of the uncertainty for the different  $M_{max,i}$  per zone are provided in Tab. 5-1a-e for the SSZ models A, B, C, D and E. This table contains the two versions for the minimum fit.



**Figure 5-3.** The areal variation of  $b$  values in the SSZ of model A.



**Figure 5-4.** The variation of  $a$  values, given as the rate  $\nu$  for  $M_w = 4.0$  and normalized to 1000 km<sup>2</sup>.

Additionally, those SSZs, where the distinction of the minimum for fit to lower and higher magnitudes could be made, are shown in Fig. 5-5. It enables the easily ascertainable respective information.

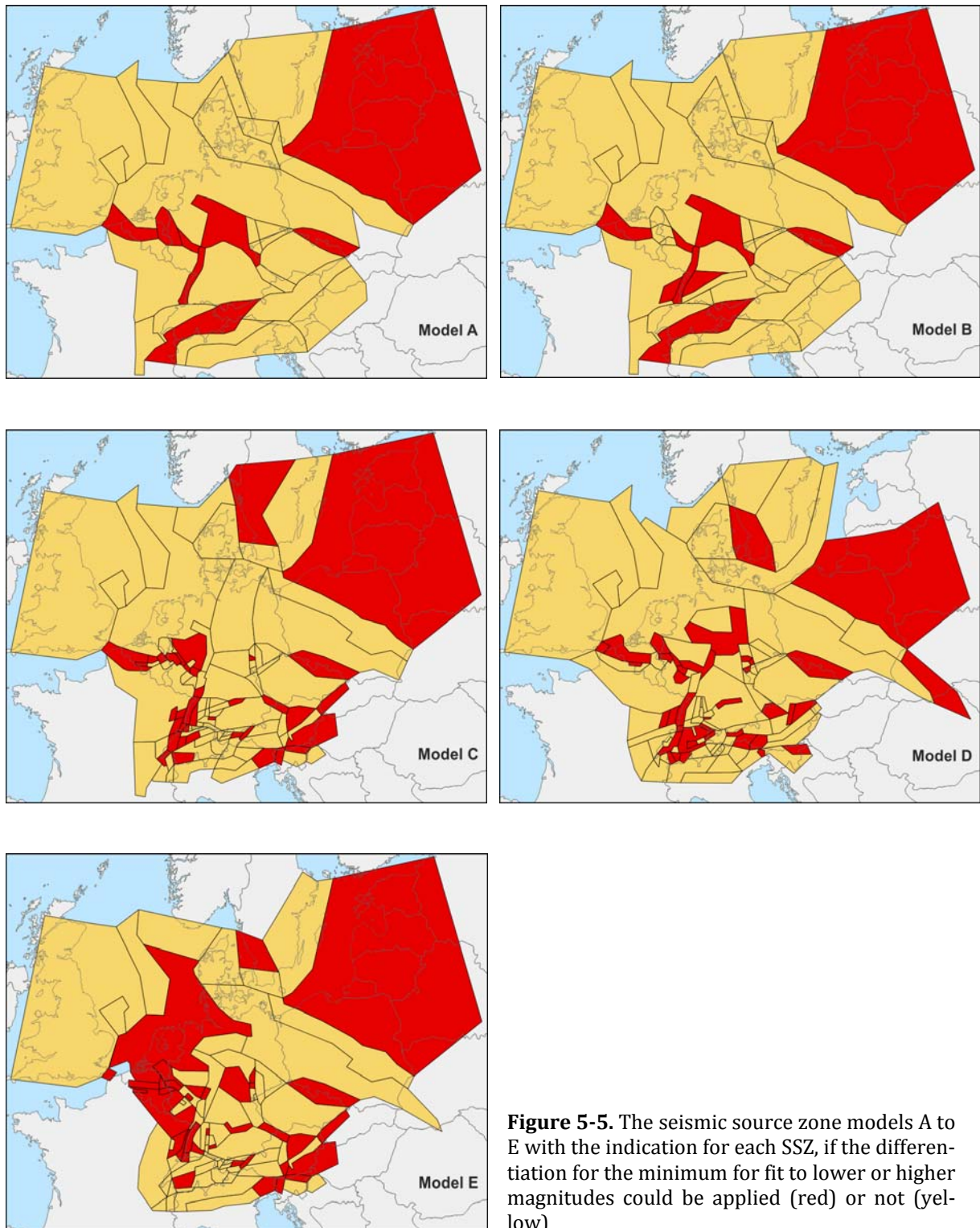


**Figure 5-5.** The seismic source zone models A to E with the indication for each SSZ, if the differentiation for the minimum for fit to lower or higher magnitudes could be applied (red) or not (yellow)





The data sets of the earthquake model for the PSHA of Germany

|            | minimum for fit high |       |       |          |          |          | minimum for fit low |       |       |          |          |          |
|------------|----------------------|-------|-------|----------|----------|----------|---------------------|-------|-------|----------|----------|----------|
|            | $M_{max.i}$          | $a$   | $b$   | $C_{aa}$ | $C_{ab}$ | $C_{bb}$ | $M_{max.i}$         | $a$   | $b$   | $C_{aa}$ | $C_{ab}$ | $C_{bb}$ |
| <b>A28</b> | 6,30                 | 5,142 | 1,169 | 0,420    | 0,0823   | 0,0163   | 6,27                | 4,336 | 1,059 | 0,000692 | 0,000263 | 0,000107 |
|            | 6,30                 | 5,142 | 1,169 | 0,420    | 0,0823   | 0,0163   | 6,27                | 4,336 | 1,059 | 0,000692 | 0,000263 | 0,000107 |
|            | 6,69                 | 5,381 | 1,218 | 0,375    | 0,0736   | 0,0145   | 6,56                | 4,338 | 1,060 | 0,000688 | 0,000261 | 0,000107 |
|            | 6,73                 | 5,381 | 1,218 | 0,375    | 0,0736   | 0,0145   | 6,69                | 4,338 | 1,060 | 0,000688 | 0,000261 | 0,000107 |
|            | 7,19                 | 5,443 | 1,230 | 0,361    | 0,0707   | 0,0140   | 7,11                | 4,338 | 1,060 | 0,000686 | 0,000260 | 0,000107 |
| <b>A29</b> | 5,75                 | 3,348 | 0,804 | 0,0316   | 0,00744  | 0,00187  | 5,75                | 3,348 | 0,804 | 0,0316   | 0,00744  | 0,00187  |
|            | 5,75                 | 3,348 | 0,804 | 0,0316   | 0,00744  | 0,00187  | 5,75                | 3,348 | 0,804 | 0,0316   | 0,00744  | 0,00187  |
|            | 6,03                 | 3,348 | 0,804 | 0,0316   | 0,00744  | 0,00187  | 6,03                | 3,348 | 0,804 | 0,0316   | 0,00744  | 0,00187  |
|            | 6,12                 | 3,430 | 0,828 | 0,0292   | 0,00684  | 0,00172  | 6,12                | 3,430 | 0,828 | 0,0292   | 0,00684  | 0,00172  |
|            | 6,81                 | 3,532 | 0,857 | 0,0260   | 0,00604  | 0,00152  | 6,81                | 3,532 | 0,857 | 0,0260   | 0,00604  | 0,00152  |
|            | 5,63                 | 2,306 | 0,808 | 0,0106   | 0,00375  | 0,00147  | 5,63                | 2,306 | 0,808 | 0,0106   | 0,00375  | 0,00147  |
| <b>A30</b> | 5,85                 | 2,306 | 0,808 | 0,0106   | 0,00375  | 0,00147  | 5,85                | 2,306 | 0,808 | 0,0106   | 0,00375  | 0,00147  |
|            | 6,42                 | 2,321 | 0,814 | 0,0102   | 0,00363  | 0,00143  | 6,42                | 2,321 | 0,814 | 0,0102   | 0,00363  | 0,00143  |
|            | 6,42                 | 2,321 | 0,814 | 0,0102   | 0,00363  | 0,00143  | 6,42                | 2,321 | 0,814 | 0,0102   | 0,00363  | 0,00143  |
|            | 7,12                 | 2,329 | 0,818 | 0,0100   | 0,00354  | 0,00139  | 7,12                | 2,329 | 0,818 | 0,0100   | 0,00354  | 0,00139  |
|            | 6,94                 | 4,201 | 0,864 | 0,0407   | 0,00808  | 0,00164  | 6,94                | 4,201 | 0,864 | 0,0407   | 0,00808  | 0,00164  |
| <b>A31</b> | 6,95                 | 4,201 | 0,864 | 0,0407   | 0,00808  | 0,00164  | 6,95                | 4,201 | 0,864 | 0,0407   | 0,00808  | 0,00164  |
|            | 7,08                 | 4,339 | 0,894 | 0,0367   | 0,00727  | 0,00148  | 7,08                | 4,339 | 0,894 | 0,0367   | 0,00727  | 0,00148  |
|            | 7,17                 | 4,339 | 0,894 | 0,0367   | 0,00727  | 0,00148  | 7,17                | 4,339 | 0,894 | 0,0367   | 0,00727  | 0,00148  |
|            | 7,41                 | 4,339 | 0,894 | 0,0367   | 0,00727  | 0,00148  | 7,41                | 4,339 | 0,894 | 0,0367   | 0,00727  | 0,00148  |
|            | 6,94                 | 4,201 | 0,864 | 0,0407   | 0,00808  | 0,00164  | 6,94                | 4,201 | 0,864 | 0,0407   | 0,00808  | 0,00164  |
|            | 6,95                 | 4,201 | 0,864 | 0,0407   | 0,00808  | 0,00164  | 6,95                | 4,201 | 0,864 | 0,0407   | 0,00808  | 0,00164  |







|            | minimum for fit high |       |       |          |          |          | minimum for fit low |       |       |          |          |          |
|------------|----------------------|-------|-------|----------|----------|----------|---------------------|-------|-------|----------|----------|----------|
|            | $M_{max.i}$          | $a$   | $b$   | $C_{aa}$ | $C_{ab}$ | $C_{bb}$ | $M_{max.i}$         | $a$   | $b$   | $C_{aa}$ | $C_{ab}$ | $C_{bb}$ |
| <b>B29</b> | 6,05                 | 3,081 | 0,804 | 0,00464  | 0,00143  | 0,000472 | 6,05                | 3,081 | 0,804 | 0,00464  | 0,00143  | 0,000472 |
|            | 6,03                 | 3,081 | 0,804 | 0,00464  | 0,00143  | 0,000472 | 6,03                | 3,081 | 0,804 | 0,00464  | 0,00143  | 0,000472 |
|            | 6,23                 | 3,105 | 0,812 | 0,00431  | 0,00132  | 0,000433 | 6,23                | 3,105 | 0,812 | 0,00431  | 0,00132  | 0,000433 |
|            | 6,27                 | 3,105 | 0,812 | 0,00431  | 0,00132  | 0,000433 | 6,27                | 3,105 | 0,812 | 0,00431  | 0,00132  | 0,000433 |
|            | 6,76                 | 3,122 | 0,818 | 0,00418  | 0,00128  | 0,000419 | 6,76                | 3,122 | 0,818 | 0,00418  | 0,00128  | 0,000419 |
| <b>B30</b> | 5,80                 | 3,182 | 1,070 | 0,0207   | 0,00745  | 0,00281  | 5,81                | 3,182 | 1,070 | 0,0207   | 0,00745  | 0,00281  |
|            | 5,97                 | 3,182 | 1,070 | 0,0207   | 0,00745  | 0,00281  | 5,99                | 3,182 | 1,070 | 0,0207   | 0,00745  | 0,00281  |
|            | 6,34                 | 3,189 | 1,072 | 0,0203   | 0,00733  | 0,00277  | 6,35                | 3,189 | 1,072 | 0,0203   | 0,00733  | 0,00277  |
|            | 6,34                 | 3,189 | 1,072 | 0,0203   | 0,00733  | 0,00277  | 6,35                | 3,189 | 1,072 | 0,0203   | 0,00733  | 0,00277  |
|            | 6,79                 | 3,192 | 1,074 | 0,0202   | 0,00727  | 0,00274  | 6,80                | 3,192 | 1,074 | 0,0202   | 0,00727  | 0,00274  |
| <b>B31</b> | 6,56                 | 2,745 | 0,726 | 0,0171   | 0,00442  | 0,00118  | 6,56                | 2,745 | 0,726 | 0,0171   | 0,00442  | 0,00118  |
|            | 6,62                 | 2,745 | 0,726 | 0,0171   | 0,00442  | 0,00118  | 6,62                | 2,745 | 0,726 | 0,0171   | 0,00442  | 0,00118  |
|            | 6,91                 | 2,745 | 0,726 | 0,0171   | 0,00442  | 0,00118  | 6,91                | 2,745 | 0,726 | 0,0171   | 0,00442  | 0,00118  |
|            | 6,91                 | 2,745 | 0,726 | 0,0171   | 0,00442  | 0,00118  | 6,91                | 2,745 | 0,726 | 0,0171   | 0,00442  | 0,00118  |
|            | 7,26                 | 2,763 | 0,731 | 0,0167   | 0,00431  | 0,00115  | 7,26                | 2,763 | 0,731 | 0,0167   | 0,00431  | 0,00115  |
| <b>B32</b> | 6,75                 | 3,528 | 0,983 | 0,00264  | 0,000959 | 0,000379 | 6,75                | 3,528 | 0,983 | 0,00264  | 0,000959 | 0,000379 |
|            | 6,86                 | 3,528 | 0,983 | 0,00264  | 0,000959 | 0,000379 | 6,86                | 3,528 | 0,983 | 0,00264  | 0,000959 | 0,000379 |
|            | 7,03                 | 3,528 | 0,983 | 0,00264  | 0,000959 | 0,000379 | 7,03                | 3,528 | 0,983 | 0,00264  | 0,000959 | 0,000379 |
|            | 7,10                 | 3,530 | 0,984 | 0,00263  | 0,000955 | 0,000377 | 7,10                | 3,530 | 0,984 | 0,00263  | 0,000955 | 0,000377 |
|            | 7,33                 | 3,530 | 0,984 | 0,00263  | 0,000955 | 0,000377 | 7,33                | 3,530 | 0,984 | 0,00263  | 0,000955 | 0,000377 |
| <b>B33</b> | 6,30                 | 5,142 | 1,169 | 0,420    | 0,0823   | 0,0163   | 6,27                | 4,336 | 1,059 | 0,000692 | 0,000263 | 0,000107 |
|            | 6,30                 | 5,142 | 1,169 | 0,420    | 0,0823   | 0,0163   | 6,27                | 4,336 | 1,059 | 0,000692 | 0,000263 | 0,000107 |
|            | 6,69                 | 5,381 | 1,218 | 0,375    | 0,0736   | 0,0145   | 6,56                | 4,338 | 1,060 | 0,000688 | 0,000261 | 0,000107 |
|            | 6,73                 | 5,381 | 1,218 | 0,375    | 0,0736   | 0,0145   | 6,69                | 4,338 | 1,060 | 0,000688 | 0,000261 | 0,000107 |
|            | 7,19                 | 5,443 | 1,230 | 0,361    | 0,0707   | 0,0140   | 7,11                | 4,338 | 1,060 | 0,000686 | 0,000260 | 0,000107 |
| <b>B34</b> | 5,75                 | 3,348 | 0,804 | 0,0316   | 0,00744  | 0,00187  | 5,75                | 3,348 | 0,804 | 0,0316   | 0,00744  | 0,00187  |
|            | 5,75                 | 3,348 | 0,804 | 0,0316   | 0,00744  | 0,00187  | 5,75                | 3,348 | 0,804 | 0,0316   | 0,00744  | 0,00187  |
|            | 6,03                 | 3,348 | 0,804 | 0,0316   | 0,00744  | 0,00187  | 6,03                | 3,348 | 0,804 | 0,0316   | 0,00744  | 0,00187  |
|            | 6,12                 | 3,430 | 0,828 | 0,0292   | 0,00684  | 0,00172  | 6,12                | 3,430 | 0,828 | 0,0292   | 0,00684  | 0,00172  |
|            | 6,81                 | 3,532 | 0,857 | 0,0260   | 0,00604  | 0,00152  | 6,81                | 3,532 | 0,857 | 0,0260   | 0,00604  | 0,00152  |
| <b>B35</b> | 5,63                 | 2,306 | 0,808 | 0,0106   | 0,00375  | 0,00147  | 5,63                | 2,306 | 0,808 | 0,0106   | 0,00375  | 0,00147  |
|            | 5,85                 | 2,306 | 0,808 | 0,0106   | 0,00375  | 0,00147  | 5,85                | 2,306 | 0,808 | 0,0106   | 0,00375  | 0,00147  |
|            | 6,42                 | 2,321 | 0,814 | 0,0102   | 0,00363  | 0,00143  | 6,42                | 2,321 | 0,814 | 0,0102   | 0,00363  | 0,00143  |
|            | 6,42                 | 2,321 | 0,814 | 0,0102   | 0,00363  | 0,00143  | 6,42                | 2,321 | 0,814 | 0,0102   | 0,00363  | 0,00143  |
|            | 7,12                 | 2,329 | 0,818 | 0,0100   | 0,00354  | 0,00139  | 7,12                | 2,329 | 0,818 | 0,0100   | 0,00354  | 0,00139  |
| <b>B36</b> | 6,94                 | 4,201 | 0,864 | 0,0407   | 0,00808  | 0,00164  | 6,94                | 4,201 | 0,864 | 0,0407   | 0,00808  | 0,00164  |
|            | 6,95                 | 4,201 | 0,864 | 0,0407   | 0,00808  | 0,00164  | 6,95                | 4,201 | 0,864 | 0,0407   | 0,00808  | 0,00164  |
|            | 7,08                 | 4,339 | 0,894 | 0,0367   | 0,00727  | 0,00148  | 7,08                | 4,339 | 0,894 | 0,0367   | 0,00727  | 0,00148  |
|            | 7,17                 | 4,339 | 0,894 | 0,0367   | 0,00727  | 0,00148  | 7,17                | 4,339 | 0,894 | 0,0367   | 0,00727  | 0,00148  |
|            | 7,41                 | 4,339 | 0,894 | 0,0367   | 0,00727  | 0,00148  | 7,41                | 4,339 | 0,894 | 0,0367   | 0,00727  | 0,00148  |

















|             | minimum for fit high |       |       |          |          |          | minimum for fit low |       |       |          |          |          |
|-------------|----------------------|-------|-------|----------|----------|----------|---------------------|-------|-------|----------|----------|----------|
|             | $M_{max,i}$          | $a$   | $b$   | $C_{aa}$ | $C_{ab}$ | $C_{bb}$ | $M_{max,i}$         | $a$   | $b$   | $C_{aa}$ | $C_{ab}$ | $C_{bb}$ |
| <b>C099</b> | 5,63                 | 3,080 | 1,052 | 0,0549   | 0,00515  | 0,00113  | 5,63                | 2,440 | 1,040 | 0,00691  | 0,00136  | 0,000552 |
|             | 5,89                 | 3,080 | 1,052 | 0,0549   | 0,00515  | 0,00113  | 5,87                | 2,440 | 1,040 | 0,00691  | 0,00136  | 0,000552 |
|             | 6,45                 | 3,091 | 1,056 | 0,0548   | 0,00509  | 0,00111  | 6,45                | 2,446 | 1,043 | 0,00685  | 0,00134  | 0,000543 |
|             | 6,46                 | 3,091 | 1,056 | 0,0548   | 0,00509  | 0,00111  | 6,45                | 2,446 | 1,043 | 0,00685  | 0,00134  | 0,000543 |
|             | 7,14                 | 3,100 | 1,059 | 0,0546   | 0,00504  | 0,00110  | 7,14                | 2,450 | 1,044 | 0,00681  | 0,00132  | 0,000537 |
| <b>C100</b> | 6,92                 | 2,211 | 0,593 | 0,0319   | 0,00702  | 0,00162  | 6,93                | 2,211 | 0,593 | 0,0319   | 0,00702  | 0,00162  |
|             | 7,06                 | 2,320 | 0,621 | 0,0288   | 0,00630  | 0,00145  | 6,93                | 2,211 | 0,593 | 0,0319   | 0,00702  | 0,00162  |
|             | 6,94                 | 2,211 | 0,593 | 0,0319   | 0,00702  | 0,00162  | 7,03                | 2,211 | 0,593 | 0,0319   | 0,00702  | 0,00162  |
|             | 7,11                 | 2,320 | 0,621 | 0,0288   | 0,00630  | 0,00145  | 7,11                | 2,320 | 0,621 | 0,0288   | 0,00630  | 0,00145  |
|             | 7,34                 | 2,320 | 0,621 | 0,0288   | 0,00630  | 0,00145  | 7,33                | 2,320 | 0,621 | 0,0288   | 0,00630  | 0,00145  |
| <b>C101</b> | 6,30                 | 1,928 | 0,834 | 0,0290   | 0,0104   | 0,00415  | 6,29                | 2,440 | 1,049 | 0,00329  | 0,000228 | 0,000101 |
|             | 6,30                 | 1,928 | 0,834 | 0,0290   | 0,0104   | 0,00415  | 6,32                | 2,440 | 1,049 | 0,00329  | 0,000228 | 0,000101 |
|             | 6,70                 | 1,933 | 0,836 | 0,0287   | 0,0103   | 0,00409  | 6,72                | 2,442 | 1,050 | 0,00329  | 0,000226 | 0,000100 |
|             | 6,72                 | 1,933 | 0,836 | 0,0287   | 0,0103   | 0,00409  | 6,72                | 2,442 | 1,050 | 0,00329  | 0,000226 | 0,000100 |
|             | 7,18                 | 1,936 | 0,837 | 0,0285   | 0,0102   | 0,00406  | 7,19                | 2,442 | 1,050 | 0,00328  | 0,000226 | 0,000098 |
| <b>C102</b> | 5,61                 | 3,007 | 0,798 | 0,0359   | 0,00794  | 0,00199  | 5,61                | 3,007 | 0,798 | 0,0359   | 0,00794  | 0,00199  |
|             | 5,61                 | 3,007 | 0,798 | 0,0359   | 0,00794  | 0,00199  | 5,61                | 3,007 | 0,798 | 0,0359   | 0,00794  | 0,00199  |
|             | 6,16                 | 3,081 | 0,820 | 0,0336   | 0,00735  | 0,00184  | 6,16                | 3,081 | 0,820 | 0,0336   | 0,00735  | 0,00184  |
|             | 6,31                 | 3,081 | 0,820 | 0,0336   | 0,00735  | 0,00184  | 6,31                | 3,081 | 0,820 | 0,0336   | 0,00735  | 0,00184  |
|             | 7,05                 | 3,210 | 0,856 | 0,0292   | 0,00623  | 0,00155  | 7,05                | 3,210 | 0,856 | 0,0292   | 0,00623  | 0,00155  |
| <b>C103</b> | 5,64                 | 2,041 | 0,718 | 0,00388  | 0,00146  | 0,000668 | 5,64                | 2,041 | 0,718 | 0,00388  | 0,00146  | 0,000668 |
|             | 5,64                 | 2,041 | 0,718 | 0,00388  | 0,00146  | 0,000668 | 5,64                | 2,041 | 0,718 | 0,00388  | 0,00146  | 0,000668 |
|             | 6,18                 | 2,053 | 0,724 | 0,00377  | 0,00141  | 0,000645 | 6,18                | 2,053 | 0,724 | 0,00377  | 0,00141  | 0,000645 |
|             | 6,33                 | 2,053 | 0,724 | 0,00377  | 0,00141  | 0,000645 | 6,33                | 2,053 | 0,724 | 0,00377  | 0,00141  | 0,000645 |
|             | 7,00                 | 2,058 | 0,727 | 0,00371  | 0,00138  | 0,000633 | 7,00                | 2,058 | 0,727 | 0,00371  | 0,00138  | 0,000633 |
| <b>C104</b> | 5,61                 | 2,744 | 0,798 | 0,0341   | 0,00741  | 0,00199  | 5,61                | 2,744 | 0,798 | 0,0341   | 0,00741  | 0,00199  |
|             | 5,61                 | 2,744 | 0,798 | 0,0341   | 0,00741  | 0,00199  | 5,61                | 2,744 | 0,798 | 0,0341   | 0,00741  | 0,00199  |
|             | 6,16                 | 2,814 | 0,820 | 0,0319   | 0,00684  | 0,00184  | 6,16                | 2,814 | 0,820 | 0,0319   | 0,00684  | 0,00184  |
|             | 6,31                 | 2,814 | 0,820 | 0,0319   | 0,00684  | 0,00184  | 6,31                | 2,814 | 0,820 | 0,0319   | 0,00684  | 0,00184  |
|             | 7,05                 | 2,935 | 0,856 | 0,0278   | 0,00575  | 0,00155  | 7,05                | 2,935 | 0,856 | 0,0278   | 0,00575  | 0,00155  |
| <b>C105</b> | 6,92                 | 2,639 | 0,712 | 0,0387   | 0,00831  | 0,00196  | 6,93                | 2,481 | 0,675 | 0,0128   | 0,00211  | 0,000482 |
|             | 7,06                 | 2,699 | 0,728 | 0,0358   | 0,00764  | 0,00181  | 6,93                | 2,481 | 0,675 | 0,0128   | 0,00211  | 0,000482 |
|             | 6,94                 | 2,639 | 0,712 | 0,0387   | 0,00831  | 0,00196  | 7,03                | 2,481 | 0,675 | 0,0128   | 0,00211  | 0,000482 |
|             | 7,11                 | 2,699 | 0,728 | 0,0358   | 0,00764  | 0,00181  | 7,11                | 2,556 | 0,695 | 0,0119   | 0,00192  | 0,000438 |
|             | 7,34                 | 2,699 | 0,728 | 0,0358   | 0,00764  | 0,00181  | 7,33                | 2,556 | 0,695 | 0,0119   | 0,00192  | 0,000438 |
| <b>C106</b> | 6,30                 | 2,398 | 0,915 | 0,00489  | 0,00226  | 0,00124  | 6,29                | 2,398 | 0,915 | 0,00489  | 0,00226  | 0,00124  |
|             | 6,30                 | 2,398 | 0,915 | 0,00489  | 0,00226  | 0,00124  | 6,32                | 2,398 | 0,915 | 0,00489  | 0,00226  | 0,00124  |
|             | 6,70                 | 2,399 | 0,915 | 0,00486  | 0,00225  | 0,00123  | 6,72                | 2,399 | 0,915 | 0,00486  | 0,00225  | 0,00123  |
|             | 6,72                 | 2,399 | 0,915 | 0,00486  | 0,00225  | 0,00123  | 6,72                | 2,399 | 0,915 | 0,00486  | 0,00225  | 0,00123  |
|             | 7,18                 | 2,400 | 0,916 | 0,00486  | 0,00225  | 0,00123  | 7,19                | 2,400 | 0,916 | 0,00486  | 0,00225  | 0,00123  |
| <b>C107</b> | 6,30                 | 2,847 | 1,075 | 0,00410  | 0,00218  | 0,00132  | 6,29                | 2,847 | 1,075 | 0,00410  | 0,00218  | 0,00132  |
|             | 6,30                 | 2,847 | 1,075 | 0,00410  | 0,00218  | 0,00132  | 6,32                | 2,847 | 1,075 | 0,00410  | 0,00218  | 0,00132  |
|             | 6,70                 | 2,847 | 1,075 | 0,00409  | 0,00217  | 0,00132  | 6,72                | 2,847 | 1,075 | 0,00409  | 0,00217  | 0,00132  |
|             | 6,72                 | 2,847 | 1,075 | 0,00409  | 0,00217  | 0,00132  | 6,72                | 2,847 | 1,075 | 0,00409  | 0,00217  | 0,00132  |
|             | 7,18                 | 2,847 | 1,075 | 0,00409  | 0,00217  | 0,00131  | 7,19                | 2,847 | 1,075 | 0,00409  | 0,00217  | 0,00131  |

















|             | minimum for fit high |       |       |          |          |          | minimum for fit low |       |       |          |          |          |
|-------------|----------------------|-------|-------|----------|----------|----------|---------------------|-------|-------|----------|----------|----------|
|             | $M_{max,i}$          | $a$   | $b$   | $C_{aa}$ | $C_{ab}$ | $C_{bb}$ | $M_{max,i}$         | $a$   | $b$   | $C_{aa}$ | $C_{ab}$ | $C_{bb}$ |
| <b>D099</b> | 6,83                 | 2,908 | 0,749 | 0,0283   | 0,00629  | 0,00154  | 6,82                | 2,648 | 0,688 | 0,0125   | 0,00227  | 0,000523 |
|             | 6,83                 | 2,908 | 0,749 | 0,0283   | 0,00629  | 0,00154  | 6,84                | 2,648 | 0,688 | 0,0125   | 0,00227  | 0,000523 |
|             | 6,96                 | 2,908 | 0,749 | 0,0283   | 0,00629  | 0,00154  | 6,93                | 2,648 | 0,688 | 0,0125   | 0,00227  | 0,000523 |
|             | 7,00                 | 2,908 | 0,749 | 0,0283   | 0,00629  | 0,00154  | 7,00                | 2,648 | 0,688 | 0,0125   | 0,00227  | 0,000523 |
|             | 7,26                 | 2,956 | 0,763 | 0,0266   | 0,00586  | 0,00144  | 7,25                | 2,717 | 0,706 | 0,0117   | 0,00207  | 0,000478 |
| <b>D100</b> | 6,83                 | 2,538 | 0,632 | 0,0226   | 0,00507  | 0,00119  | 6,82                | 2,538 | 0,632 | 0,0226   | 0,00507  | 0,00119  |
|             | 6,83                 | 2,538 | 0,632 | 0,0226   | 0,00507  | 0,00119  | 6,84                | 2,538 | 0,632 | 0,0226   | 0,00507  | 0,00119  |
|             | 6,96                 | 2,538 | 0,632 | 0,0226   | 0,00507  | 0,00119  | 6,93                | 2,538 | 0,632 | 0,0226   | 0,00507  | 0,00119  |
|             | 7,00                 | 2,538 | 0,632 | 0,0226   | 0,00507  | 0,00119  | 7,00                | 2,538 | 0,632 | 0,0226   | 0,00507  | 0,00119  |
|             | 7,26                 | 2,631 | 0,655 | 0,0206   | 0,00460  | 0,00108  | 7,25                | 2,631 | 0,655 | 0,0206   | 0,00460  | 0,00108  |
| <b>D101</b> | 5,68                 | 1,878 | 0,794 | 0,00856  | 0,00352  | 0,00174  | 5,68                | 1,878 | 0,794 | 0,00856  | 0,00352  | 0,00174  |
|             | 6,12                 | 1,885 | 0,798 | 0,00840  | 0,00343  | 0,00170  | 6,12                | 1,885 | 0,798 | 0,00840  | 0,00343  | 0,00170  |
|             | 6,46                 | 1,885 | 0,798 | 0,00840  | 0,00343  | 0,00170  | 6,46                | 1,885 | 0,798 | 0,00840  | 0,00343  | 0,00170  |
|             | 6,67                 | 1,888 | 0,799 | 0,00831  | 0,00339  | 0,00168  | 6,67                | 1,888 | 0,799 | 0,00831  | 0,00339  | 0,00168  |
|             | 7,19                 | 1,889 | 0,800 | 0,00827  | 0,00337  | 0,00167  | 7,19                | 1,889 | 0,800 | 0,00827  | 0,00337  | 0,00167  |
| <b>D102</b> | 5,65                 | 1,565 | 0,900 | 0,0167   | 0,00188  | 0,000713 | 5,62                | 1,821 | 1,000 | 0,0139   | 0,000840 | 0,000335 |
|             | 5,65                 | 1,565 | 0,900 | 0,0167   | 0,00188  | 0,000713 | 5,80                | 1,821 | 1,000 | 0,0139   | 0,000840 | 0,000335 |
|             | 6,29                 | 1,585 | 0,909 | 0,0165   | 0,00181  | 0,000686 | 6,40                | 1,828 | 1,003 | 0,0139   | 0,000826 | 0,000329 |
|             | 6,34                 | 1,585 | 0,909 | 0,0165   | 0,00181  | 0,000686 | 6,40                | 1,828 | 1,003 | 0,0139   | 0,000826 | 0,000329 |
|             | 7,06                 | 1,599 | 0,914 | 0,0164   | 0,00175  | 0,000664 | 7,12                | 1,831 | 1,005 | 0,0138   | 0,000816 | 0,000325 |
| <b>D103</b> | 5,74                 | 2,825 | 0,724 | 0,0356   | 0,00830  | 0,00210  | 5,74                | 3,021 | 0,775 | 0,0208   | 0,00475  | 0,00125  |
|             | 5,95                 | 2,825 | 0,724 | 0,0356   | 0,00830  | 0,00210  | 5,95                | 3,021 | 0,775 | 0,0208   | 0,00475  | 0,00125  |
|             | 5,74                 | 2,825 | 0,724 | 0,0356   | 0,00830  | 0,00210  | 5,74                | 3,021 | 0,775 | 0,0208   | 0,00475  | 0,00125  |
|             | 6,04                 | 2,825 | 0,724 | 0,0356   | 0,00830  | 0,00210  | 6,04                | 3,021 | 0,775 | 0,0208   | 0,00475  | 0,00125  |
|             | 6,66                 | 3,017 | 0,781 | 0,0286   | 0,00654  | 0,00165  | 6,66                | 3,168 | 0,820 | 0,0178   | 0,00394  | 0,00104  |
| <b>D104</b> | 5,74                 | 2,786 | 0,775 | 0,0228   | 0,00475  | 0,00125  | 5,74                | 2,786 | 0,775 | 0,0228   | 0,00475  | 0,00125  |
|             | 5,95                 | 2,786 | 0,775 | 0,0228   | 0,00475  | 0,00125  | 5,95                | 2,786 | 0,775 | 0,0228   | 0,00475  | 0,00125  |
|             | 5,74                 | 2,786 | 0,775 | 0,0228   | 0,00475  | 0,00125  | 5,74                | 2,786 | 0,775 | 0,0228   | 0,00475  | 0,00125  |
|             | 6,04                 | 2,786 | 0,775 | 0,0228   | 0,00475  | 0,00125  | 6,04                | 2,786 | 0,775 | 0,0228   | 0,00475  | 0,00125  |
|             | 6,66                 | 2,933 | 0,820 | 0,0198   | 0,00394  | 0,00104  | 6,66                | 2,933 | 0,820 | 0,0198   | 0,00394  | 0,00104  |
| <b>D105</b> | 6,28                 | 3,222 | 0,984 | 0,0123   | 0,000873 | 0,000269 | 6,29                | 3,411 | 1,043 | 0,0108   | 0,000435 | 0,000140 |
|             | 6,28                 | 3,222 | 0,984 | 0,0123   | 0,000873 | 0,000269 | 6,29                | 3,411 | 1,043 | 0,0108   | 0,000435 | 0,000140 |
|             | 6,59                 | 3,227 | 0,986 | 0,0123   | 0,000867 | 0,000265 | 6,62                | 3,412 | 1,044 | 0,0108   | 0,000434 | 0,000139 |
|             | 6,71                 | 3,227 | 0,986 | 0,0123   | 0,000867 | 0,000265 | 6,73                | 3,412 | 1,044 | 0,0108   | 0,000434 | 0,000139 |
|             | 7,13                 | 3,229 | 0,987 | 0,0123   | 0,000864 | 0,000264 | 7,15                | 3,412 | 1,044 | 0,0108   | 0,000433 | 0,000138 |
| <b>D106</b> | 6,83                 | 2,088 | 0,713 | 0,0238   | 0,00265  | 0,000628 | 6,82                | 1,979 | 0,688 | 0,0224   | 0,00227  | 0,000523 |
|             | 6,83                 | 2,088 | 0,713 | 0,0238   | 0,00265  | 0,000628 | 6,84                | 1,979 | 0,688 | 0,0224   | 0,00227  | 0,000523 |
|             | 6,96                 | 2,088 | 0,713 | 0,0238   | 0,00265  | 0,000628 | 6,93                | 1,979 | 0,688 | 0,0224   | 0,00227  | 0,000523 |
|             | 7,00                 | 2,088 | 0,713 | 0,0238   | 0,00265  | 0,000628 | 7,00                | 1,979 | 0,688 | 0,0224   | 0,00227  | 0,000523 |
|             | 7,26                 | 2,159 | 0,732 | 0,0228   | 0,00243  | 0,000577 | 7,25                | 2,048 | 0,706 | 0,0215   | 0,00207  | 0,000478 |



















## 6. Depth distributions

The depth distributions were calculated for a model of nine respective superzones (cf. chapter 8.3 of *Grünthal et al. 2018*). This superzone model is shown in Fig. 6-1. Also, this superzone model consists of a subsumption of the LASZ model A. It is identical to the superzone model of kernels as shown in Fig. 3-7. The polygon traces of the superzones of depth distributions are also part of the electronic annex. Fig. 6-2 presents the frequency of depth data in classes of 5 km for each superzone, the cumulative depth distributions and the mathematically optimized discretization of the depth occurrences according to *Miller and Rice (1983)* in form of three data pairs of respective depth values and corresponding weights. Additionally, these data are given for each depth distribution superzone in Tab. 6-1.

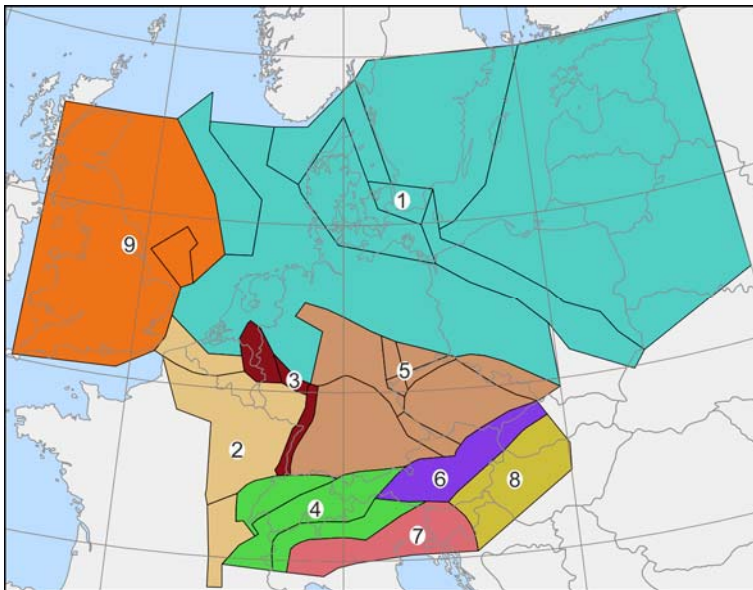


**Figure 6-1.** The depth superzone model.

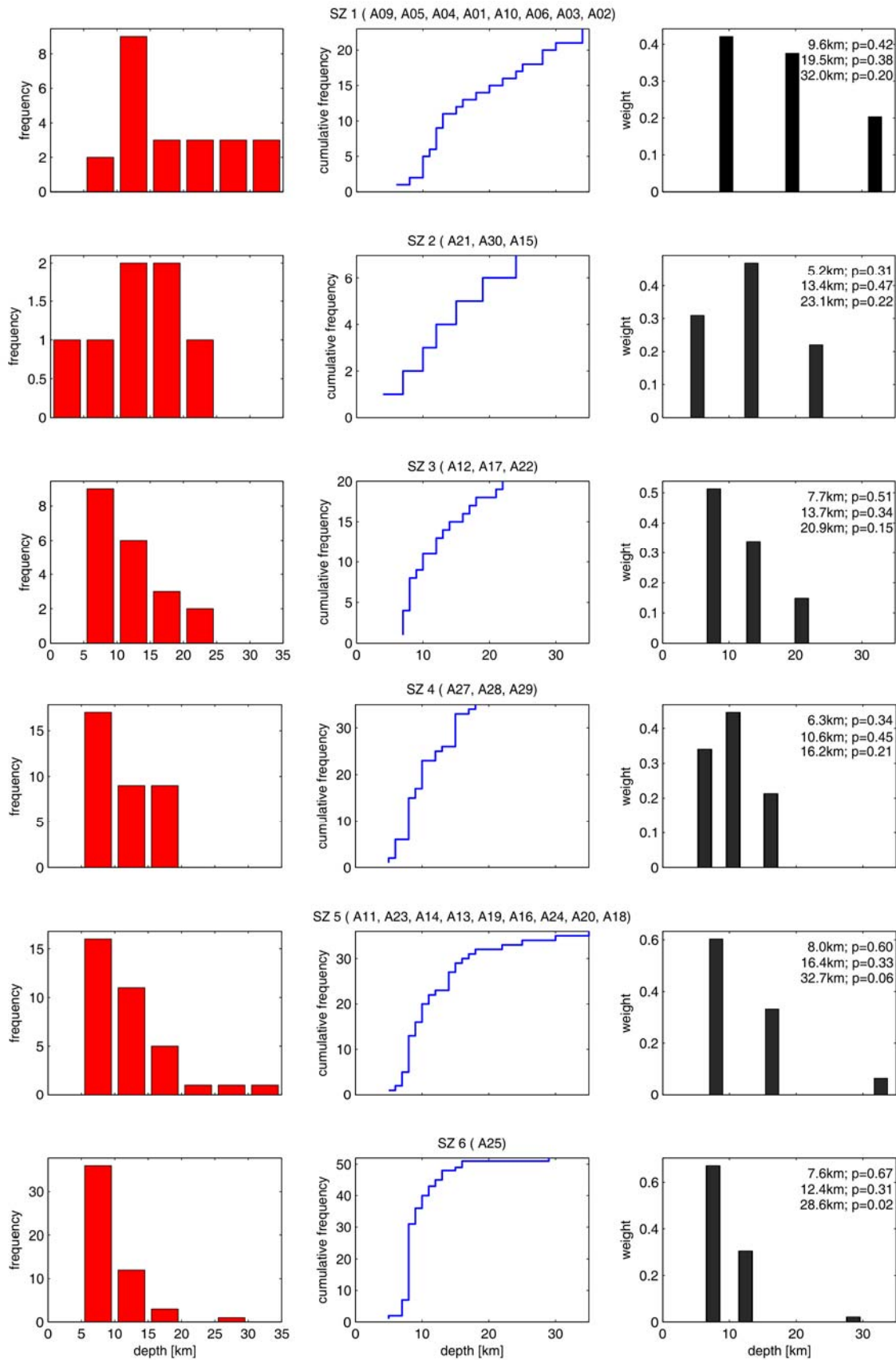


**Figure 6-2.** The depth distributions of the superzones. The frequency of depth data in classes of 5 km for each superzone (left), the cumulative depth distributions (middle) and the mathematically optimized discretization of the depth occurrences according to *Miller & Rice* (1983) in form of three data pairs of respective depth values and corresponding weights.

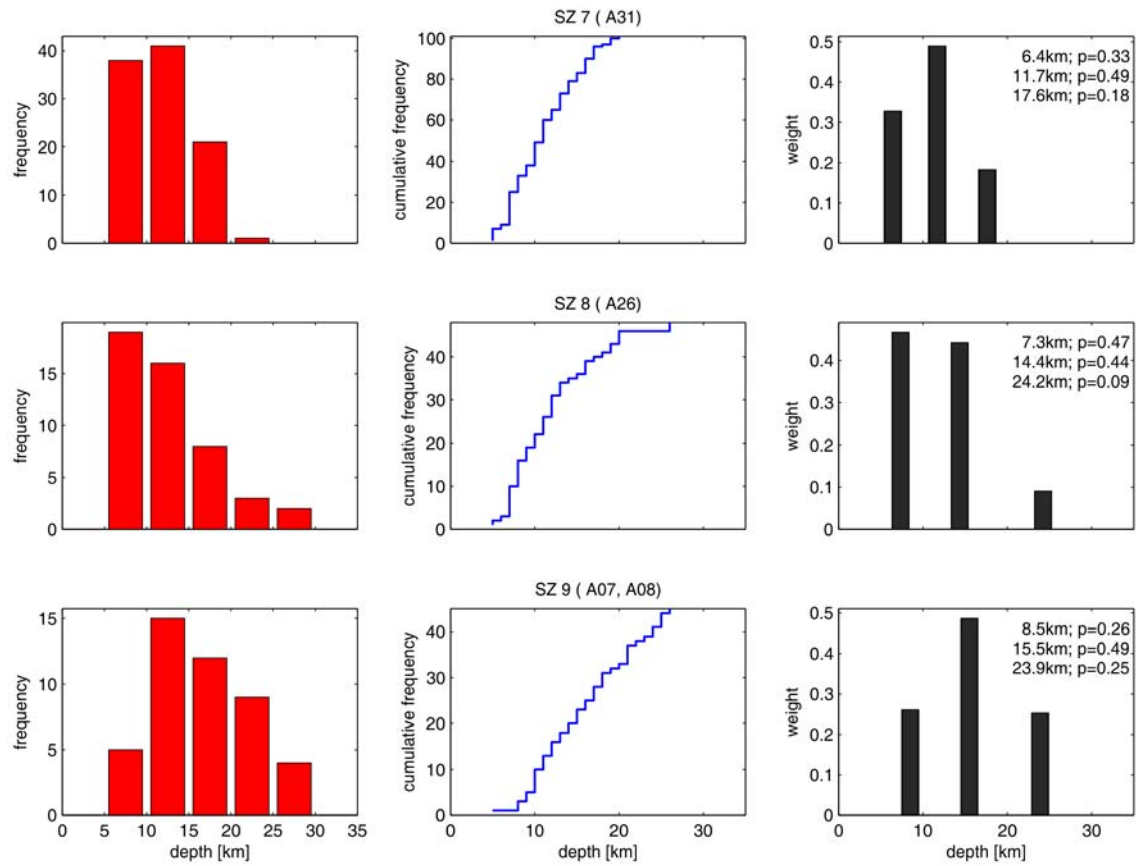


Figure 6-2. Continued.

**Table 6-1.** Combination of LASZs of model A to build nine depth superzones DSZ. Sampled depths distribution for each DSZ at three optimally selected depths with their corresponding weights.

| DSZ | LASZ (model A)                              | depths [km] |      |      | weights |       |       |
|-----|---|-------------|------|------|---------|-------|-------|
|     |   |             |      |      |         |       |       |
| 1   | A09, A05, A04, A01, A10, A06, A03, A02      | 9.6         | 19.5 | 32.0 | 0.421   | 0.376 | 0.203 |
| 2   | A21, A30, A15                               | 5.2         | 13.4 | 23.1 | 0.309   | 0.470 | 0.221 |
| 3   | A12, A17, A22                               | 7.7         | 13.7 | 20.9 | 0.513   | 0.338 | 0.149 |
| 4   | A27, A28, A29                               | 6.3         | 10.6 | 16.2 | 0.341   | 0.446 | 0.213 |
| 5   | A11, A23, A14, A13, A19, A16, A24, A20, A18 | 8.0         | 16.4 | 32.7 | 0.603   | 0.333 | 0.064 |
| 6   | A25   | 7.6         | 12.4 | 28.6 | 0.672   | 0.306 | 0.022 |
| 7   | A31   | 6.4         | 11.7 | 17.6 | 0.327   | 0.490 | 0.183 |
| 8   | A26   | 7.3         | 14.4 | 24.2 | 0.467   | 0.442 | 0.091 |
| 9   | A07, A08                                    | 8.5         | 15.5 | 23.9 | 0.261   | 0.486 | 0.253 |

## 7. Tectonic regimes

The parameters of the tectonic regime were derived for a model of eleven respective superzones (cf. chapter 8.5 of Grünthal *et al.* 2018), which are presented in Fig. 7-1 with the polygon traces as part of the electronic annex. The data source for deriving these parameters is the World Stress Map Database Release 2016 (Heidbach *et al.* 2016). The percentages of the occurrence of style-of-faulting within each of these eleven superzones are provided in Tab. 7-1.

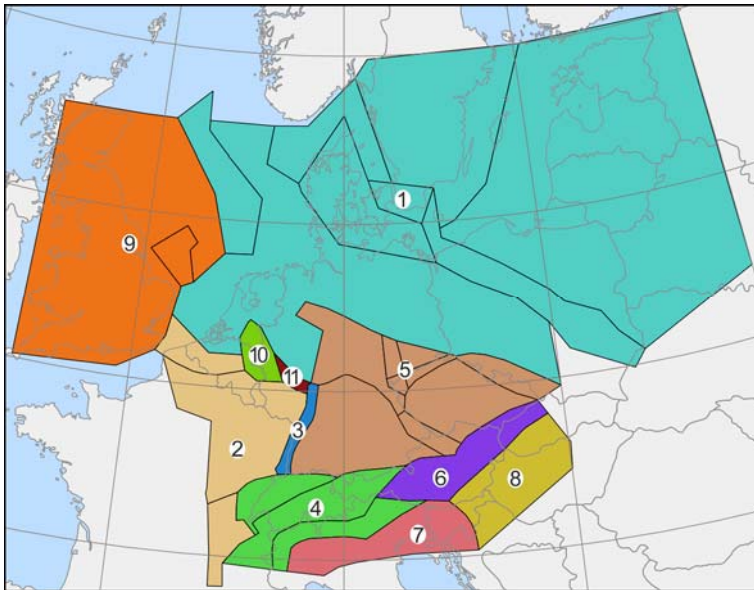


**Figure 7-1.** The superzone model used to derive the tectonic regime parameters.

**Table 7-1.** Combination of LASZs of model A to build eleven tectonic superzones TSZ. Weights of style-of-faulting for each TSZ according to the WSM database

| TSZ | LASZ (model A)                              | strike-slip | normal | thrust |
|-----|---|-------------|--------|--------|
| 1   | A09, A05, A04, A01, A10, A06, A03, A02      | 0.632       | 0.263  | 0.105  |
| 2   | A21, A30, A15                               | 0.571       | 0.214  | 0.214  |
| 3   | A22   | 0.500       | 0.500  | -      |
| 4   | A27, A28, A29                               | 0.538       | 0.299  | 0.167  |
| 5   | A11, A23, A14, A13, A19, A16, A24, A20, A18 | 0.727       | 0.258  | 0.015  |
| 6   | A25   | 0.816       | 0.053  | 0.132  |
| 7   | A31   | 0.315       | 0.076  | 0.609  |
| 8   | A26   | 0.520       | 0.080  | 0.400  |
| 9   | A07, A08                                    | 0.594       | 0.250  | 0.156  |
| 10  | A12   | 0.267       | 0.733  | -      |
| 11  | A17   | -           | 0.750  | 0.250  |

## 8. Additional results of the probabilistic seismic hazard assessment

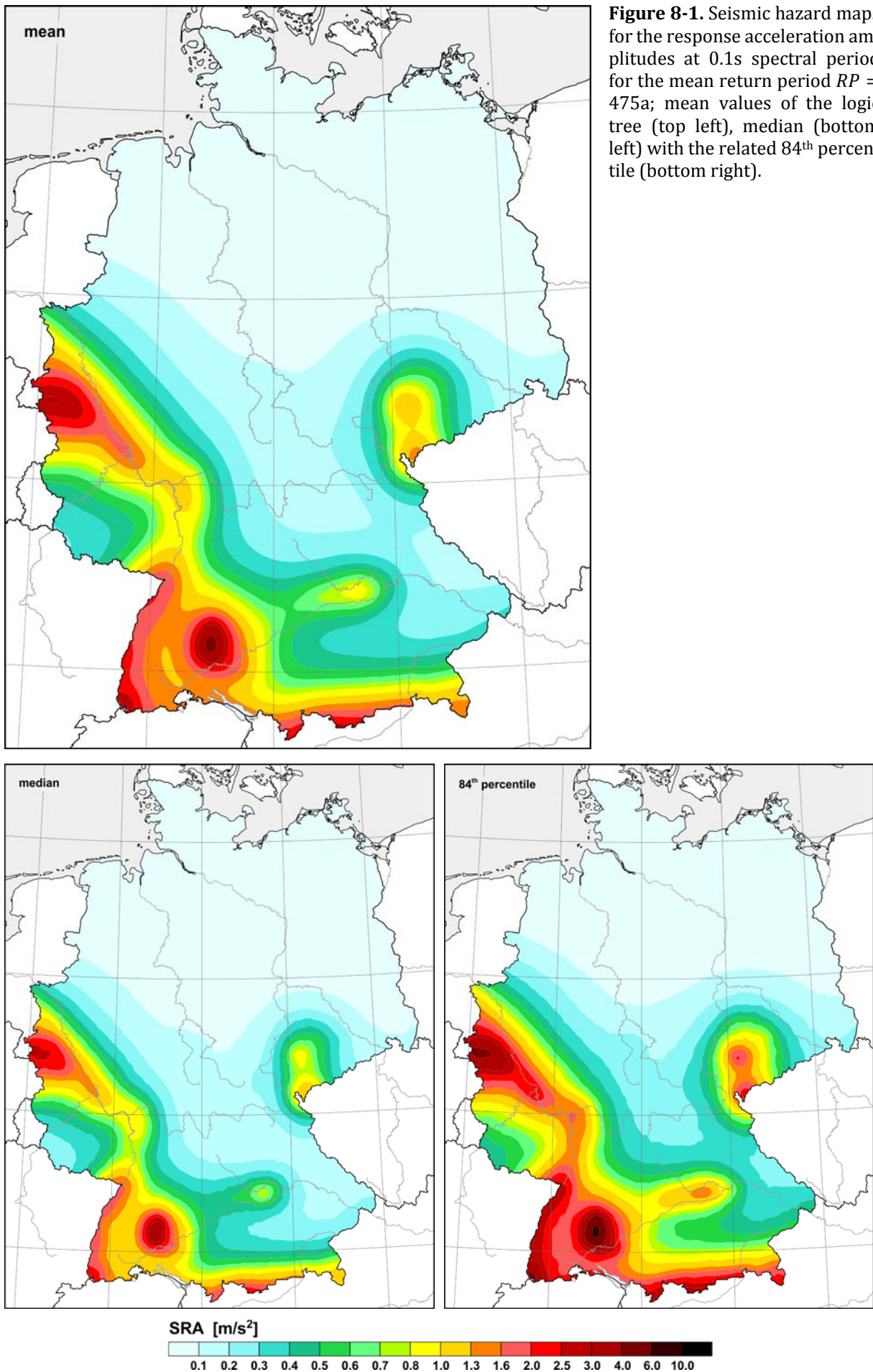
The results of the reassessment of the probabilistic seismic hazard of Germany are described in chapter 9 of *Grünthal et al. (2018)*. Here we provide additional probabilistic seismic hazard maps and deaggregation results for several selected sites.

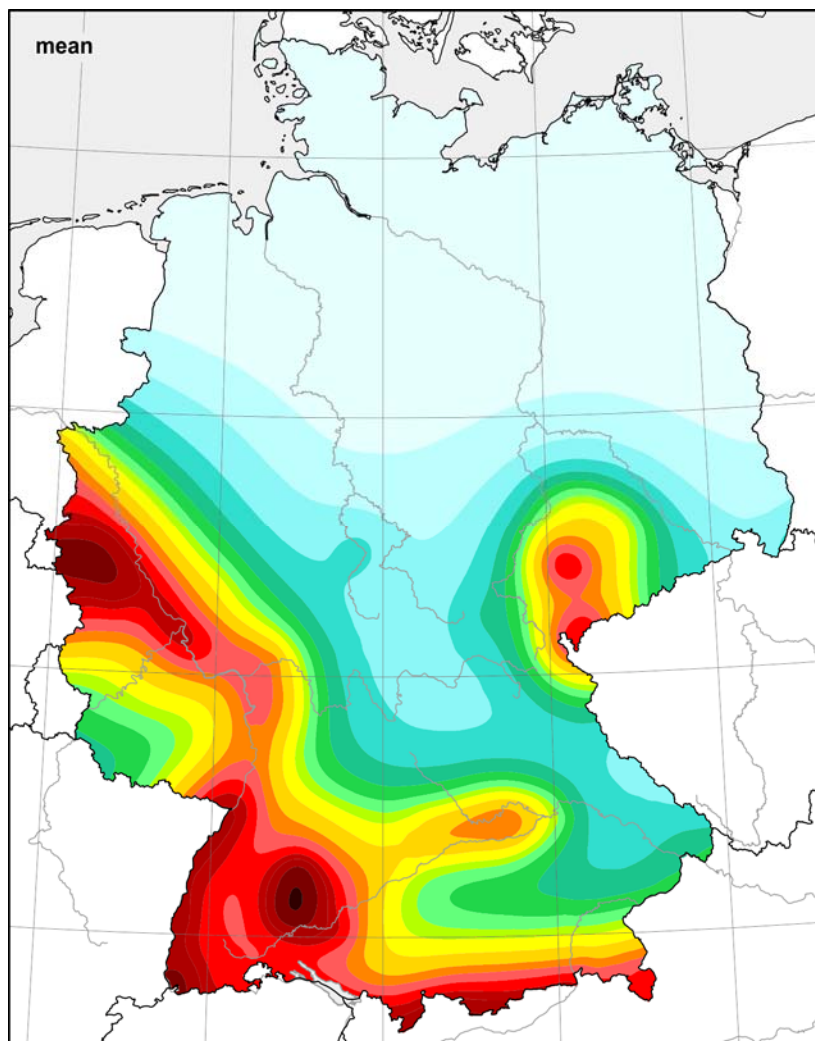
### 8.1. Probabilistic seismic hazard maps

While a selection of a few seismic hazard maps could be presented by *Grünthal et al. (2018)* only, we here show a more comprehensive set of maps. The hazard calculations were accomplished for rock underground conditions and characterized by an average shear wave velocity of the upper 30m  $v_{S30} = 800\text{m/s}$ , for the hazard levels of occurrence or exceedance probabilities of 10%, 5% and 2% within 50 years. These hazard levels correspond to the mean return periods  $RP = 475, 975$  and  $2475$  years (a). The horizontal 5% damped Uniform Hazard response Spectra (UHS) were computed for the spectral range of periods  $T$  of 0.02s-3.0s, for the weighted arithmetic mean of the results per each logic tree branch, the median, the 84<sup>th</sup> and the 16<sup>th</sup> percentile. The seismic hazard maps were generated for (1) the mean and the aforementioned percentiles for selected spectral response accelerations (SRA) of the UHS, (2) for the mean of the amplitudes of periods  $T$  in the UHS representing the plateau (0.1s, 0.15s, 0.2s), and (3) for peak ground accelerations (PGA).

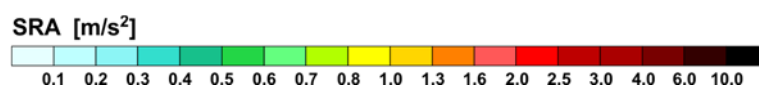
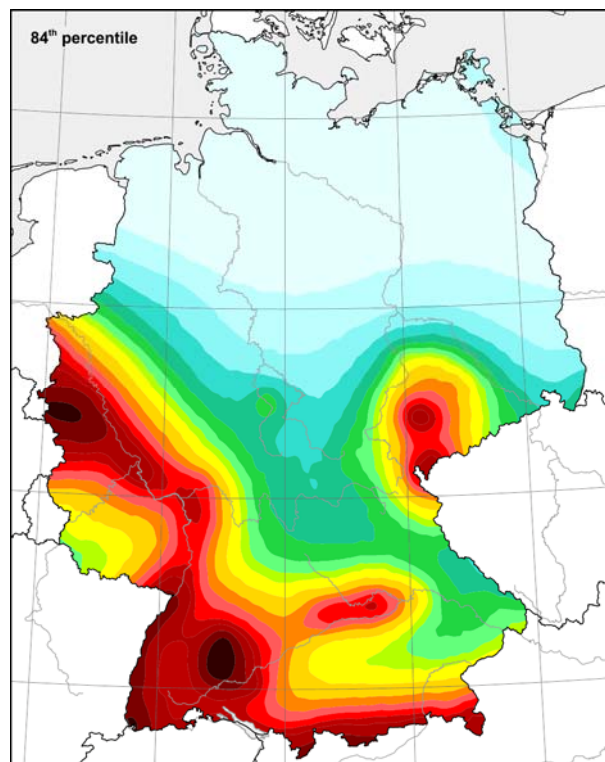
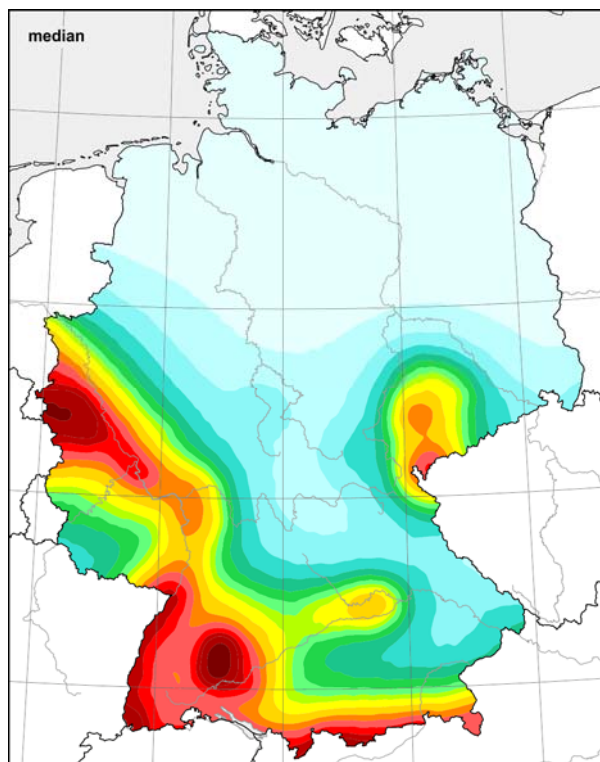
Here we present the seismic hazard maps for selected amplitudes of the UHS; i.e. for 0.1s for  $RP = 475\text{a}$  in form of the mean, the median with the 84<sup>th</sup> percentile (Fig. 8-1) and accordingly for  $RP = 975\text{a}$  (Fig. 8-2) and  $RP = 2475\text{a}$  (Fig. 8-3). The corresponding set of maps for 0.15s is shown in Figs. 8-4 to 8.6 as well as for 0.2s (Figs. 8-7 to 8-9). The PGA maps in the mentioned configuration are shown in Figs. 8-10 to 8-12. The mean of the amplitudes of periods  $T$  in the UHS representing the plateau (0.1s, 0.15s, 0.2s) at a grid point, abbreviated as meanSRA, are presented for the given results from the logic tree branches in Figs. 8-13 to 8-15. The corresponding maxSRA maps; i.e. the maxima of the amplitudes at the given three values of  $T$  at a grid point, are subject of the Figs. 8-16 to 8-18.

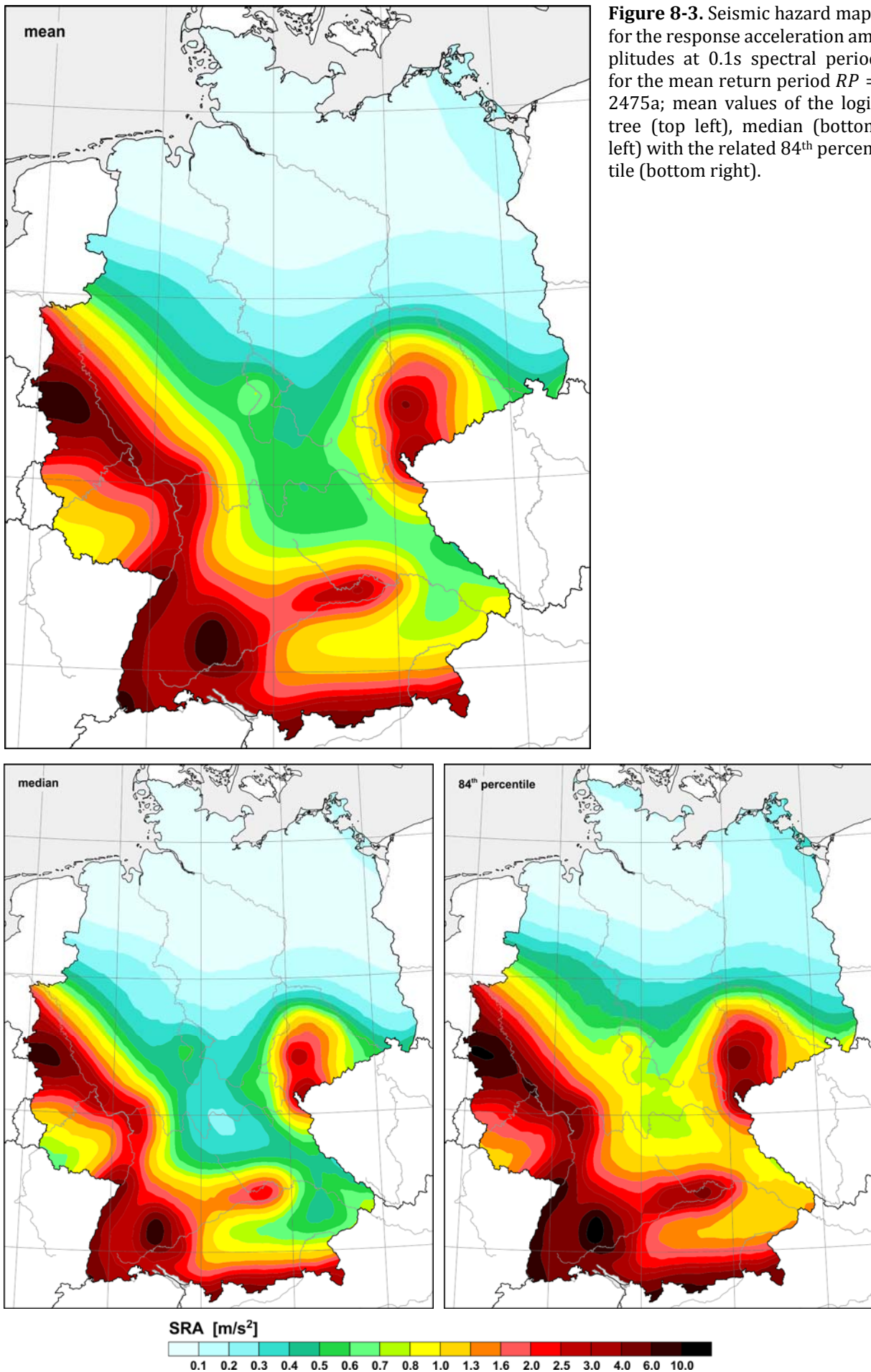




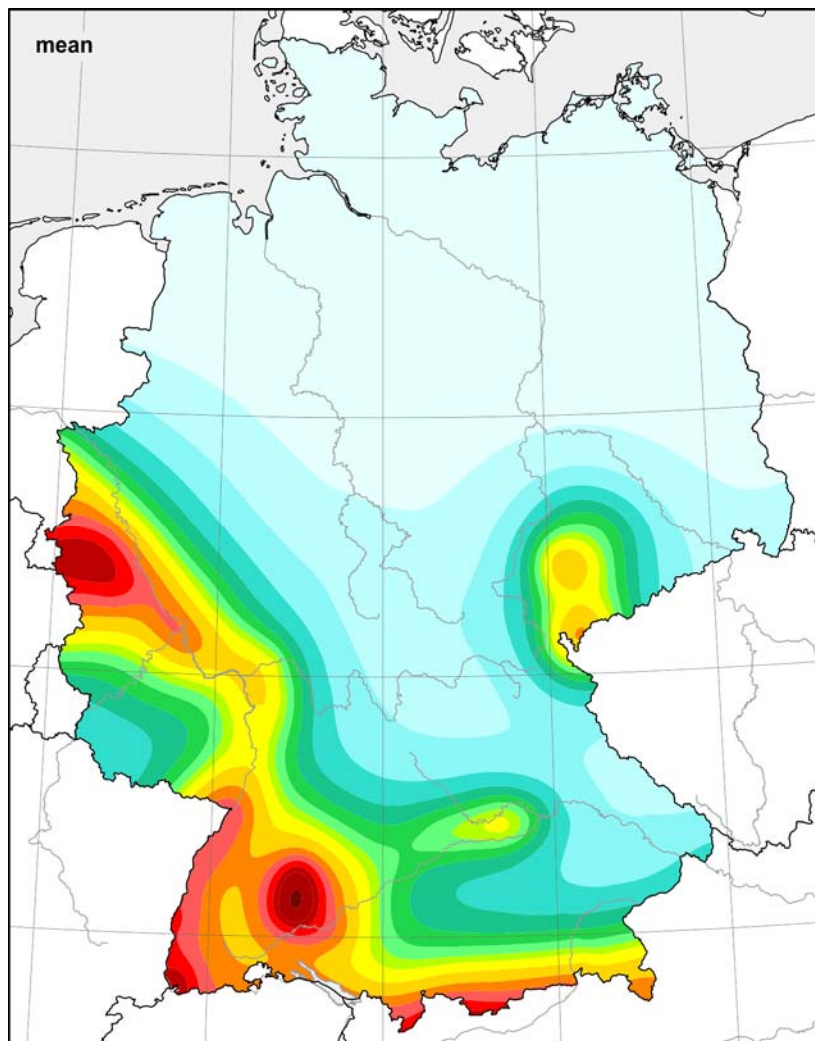


**Figure 8-2.** Seismic hazard maps for the response acceleration amplitudes at 0.1 s spectral period for the mean return period  $RP = 975$ a; mean values (top left), median (bottom left) with the related 84<sup>th</sup> percentile (bottom right).

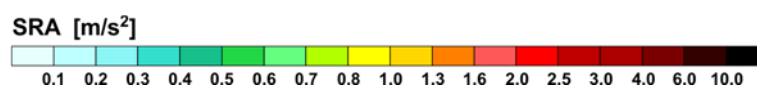
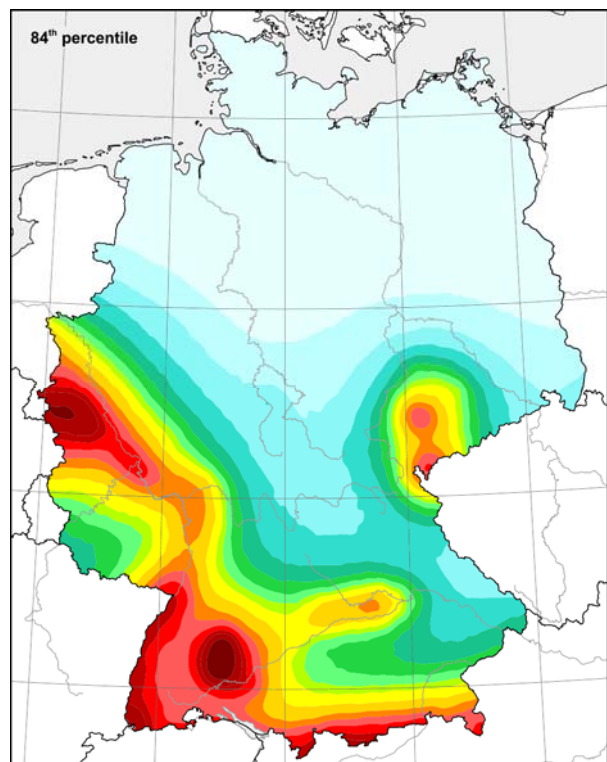
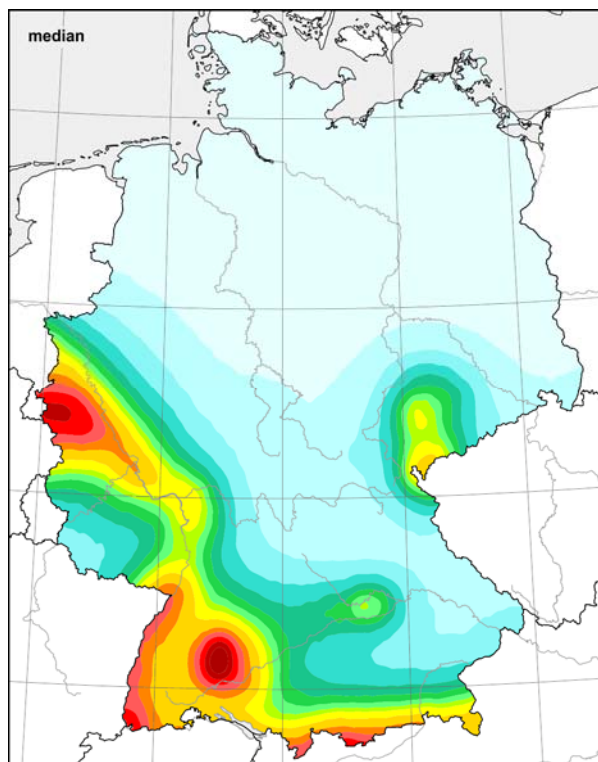


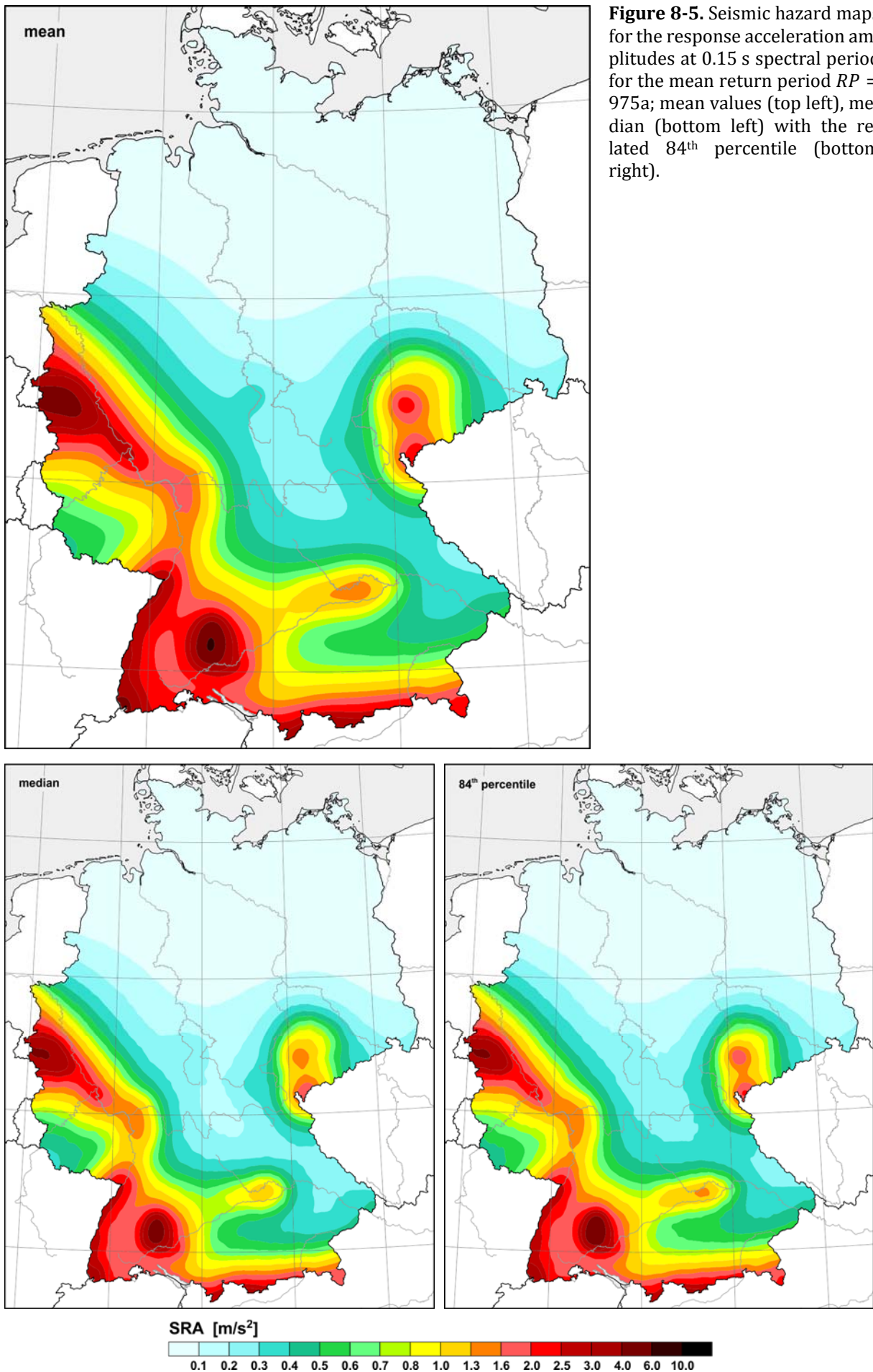


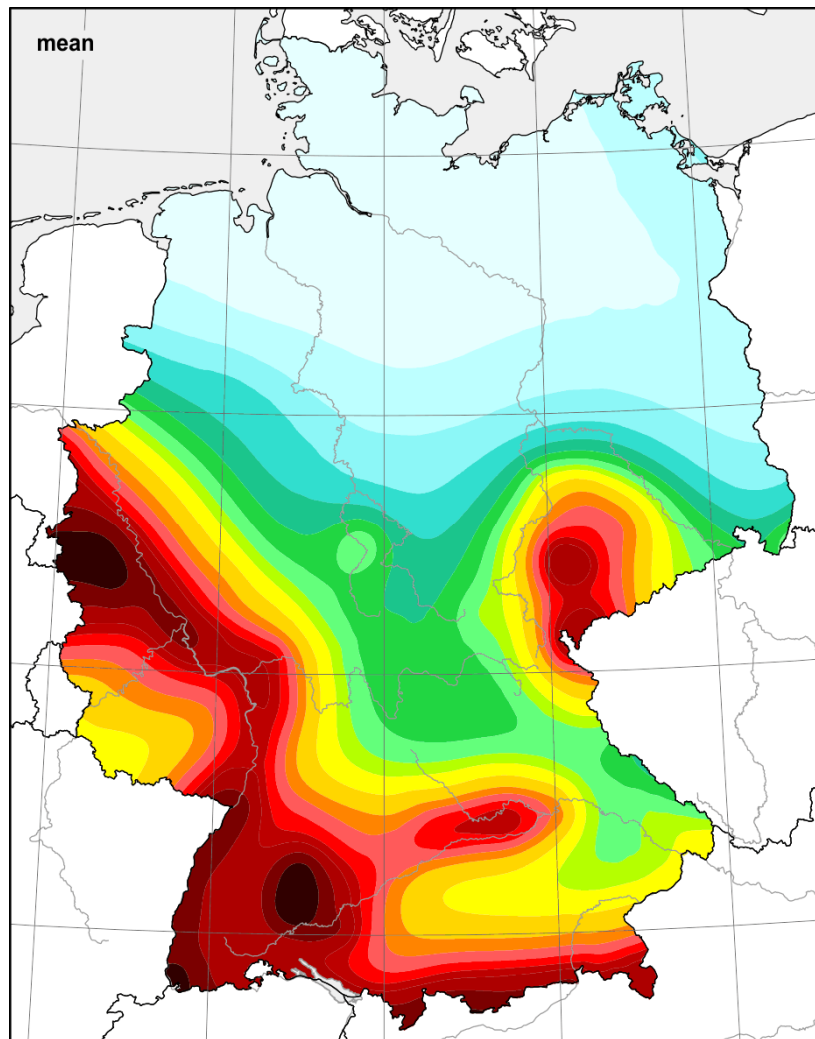
**Figure 8-3.** Seismic hazard maps for the response acceleration amplitudes at 0.1s spectral period for the mean return period  $RP = 2475a$ ; mean values of the logic tree (top left), median (bottom left) with the related 84<sup>th</sup> percentile (bottom right).



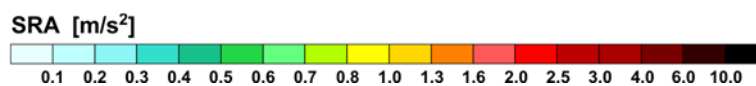
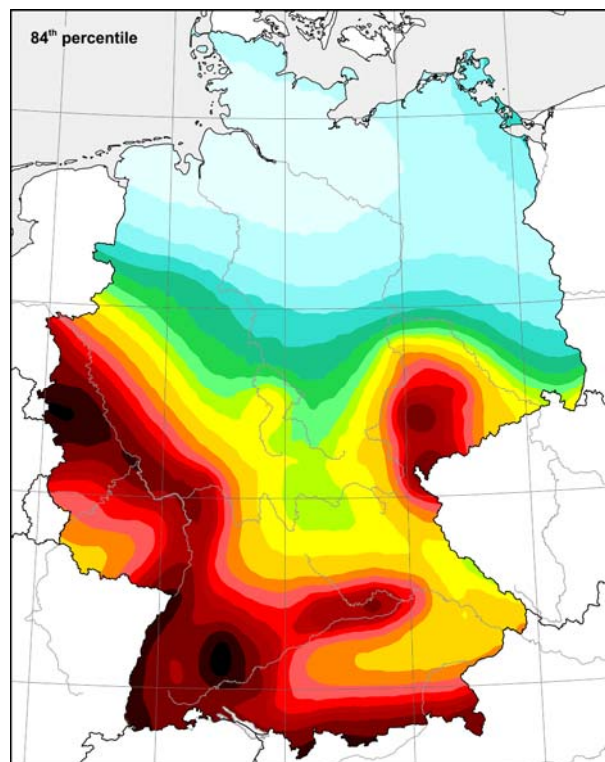
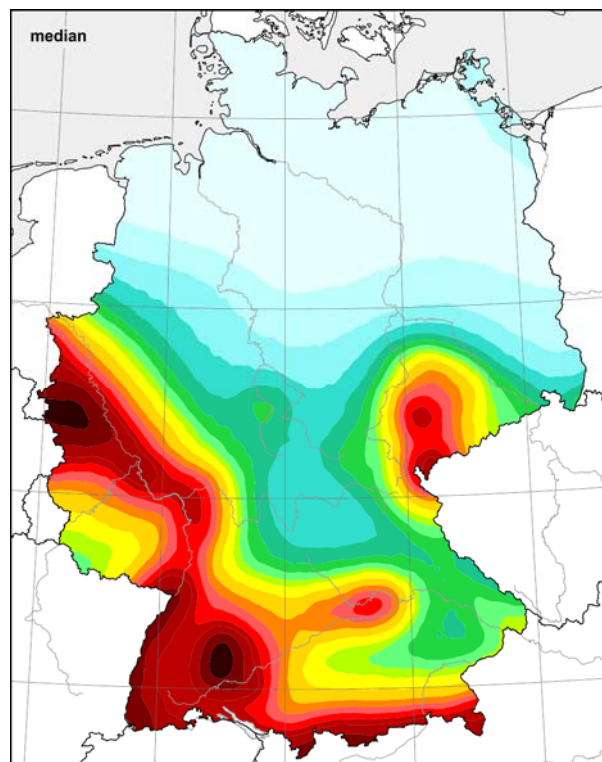
**Figure 8-4.** Seismic hazard maps for the response acceleration amplitudes at 0.15 s spectral period for the mean return period  $RP = 475$ a; mean values (top left), median (bottom left) with the related 84<sup>th</sup> percentile (bottom right).

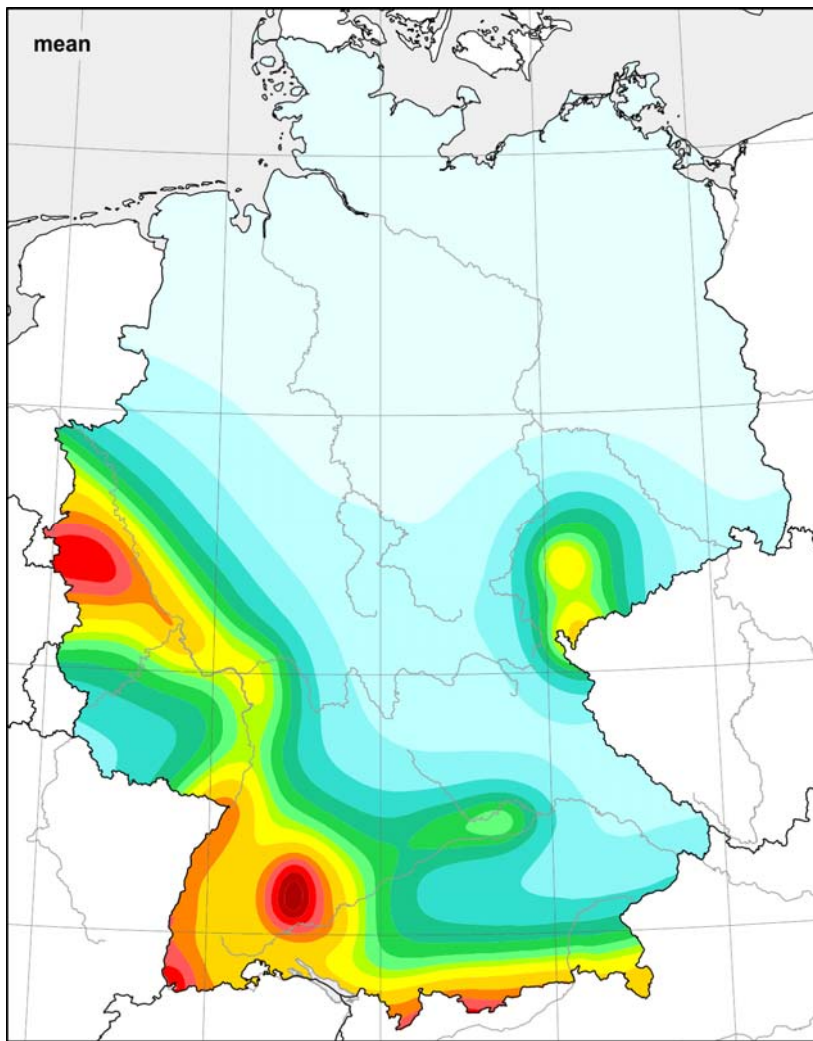




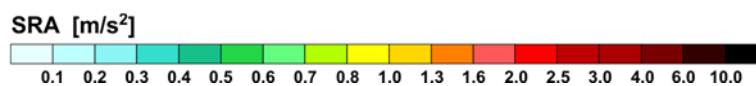
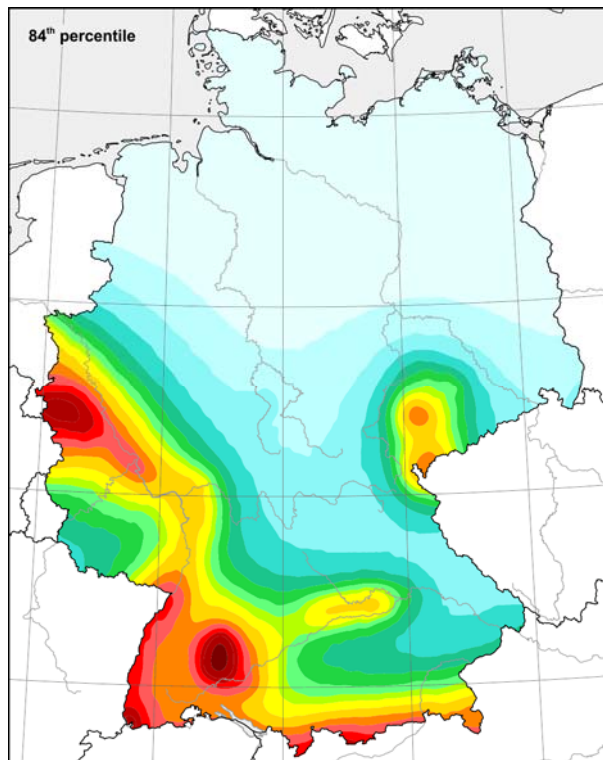
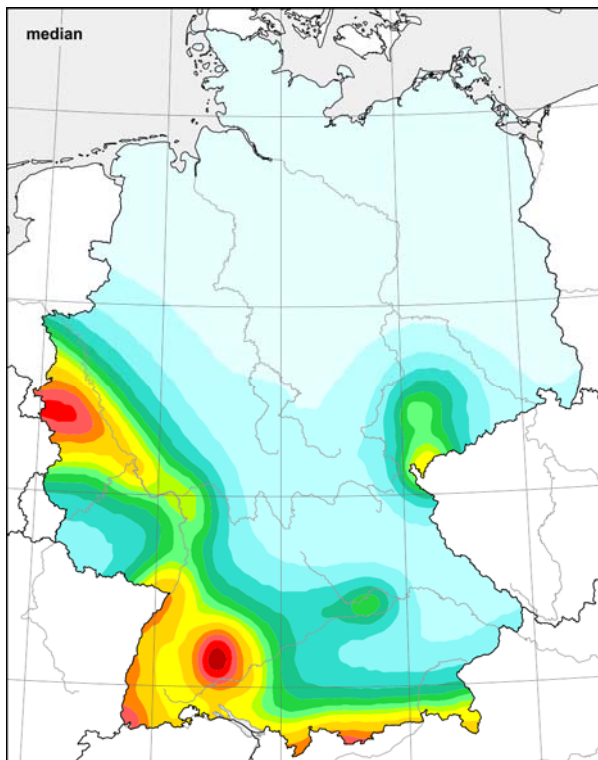


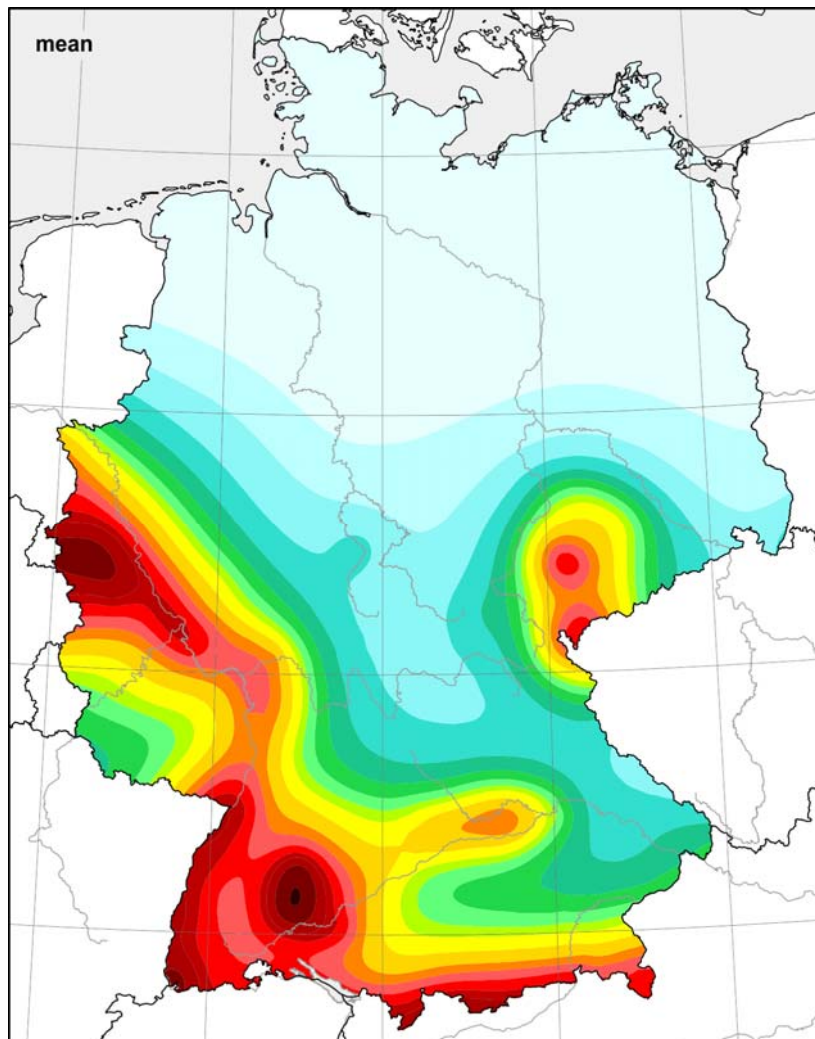
**Figure 8-6.** Seismic hazard maps for the response acceleration amplitudes at 0.15 s spectral period for the mean return period  $RP = 2475a$ ; mean values (top left), median (bottom left) with the related 84<sup>th</sup> percentile (bottom right).



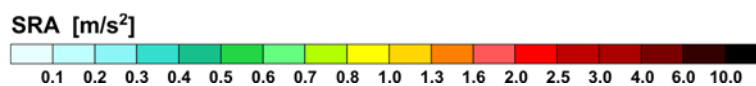
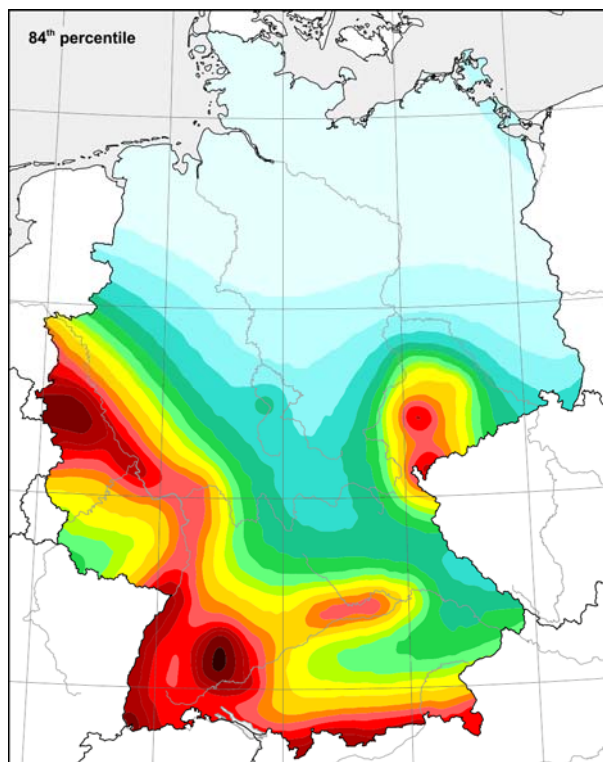
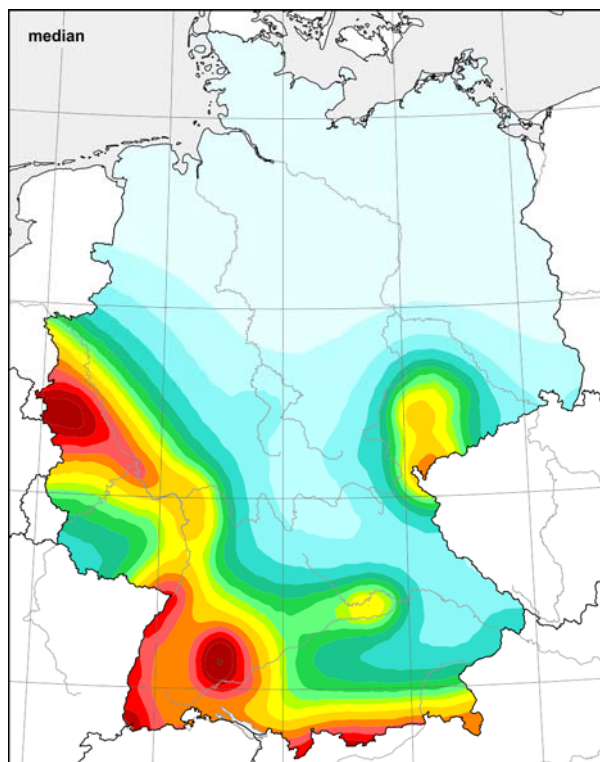


**Figure 8-7.** Seismic hazard maps for the response acceleration amplitudes at 0.20 s spectral period for the mean return period  $RP = 475a$ ; mean values (top left), median (bottom left) with the related 84<sup>th</sup> percentile (bottom right).

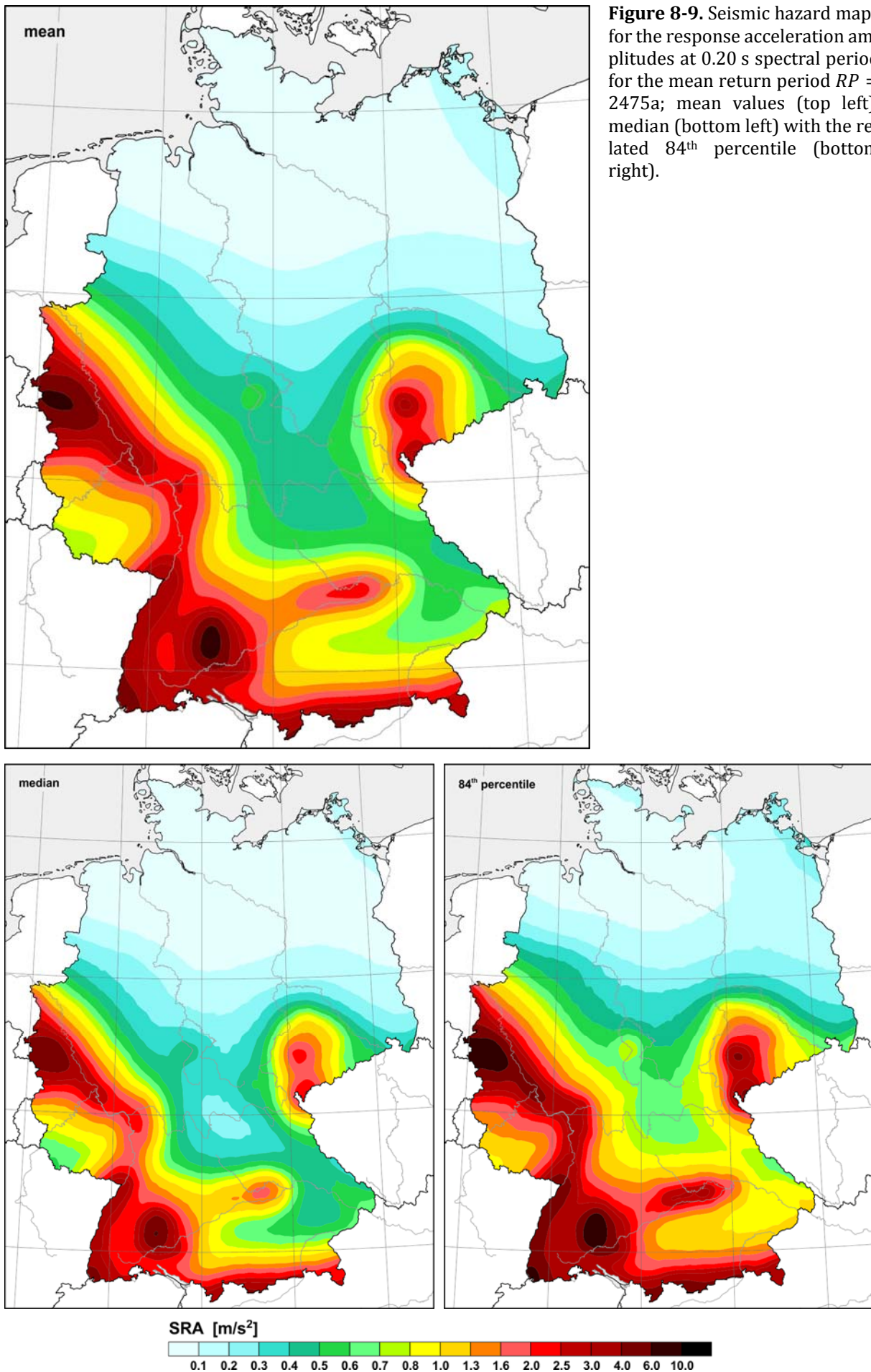




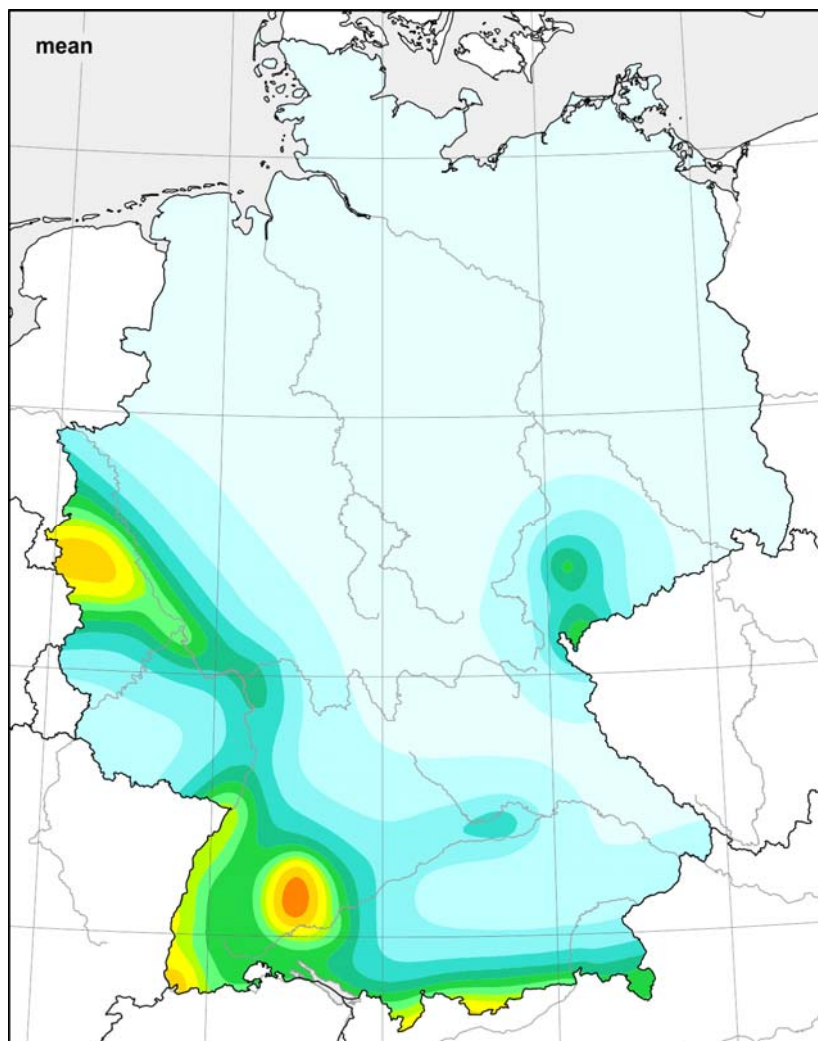
**Figure 8-8.** Seismic hazard maps for the response acceleration amplitudes at 0.20 s spectral period for the mean return period  $RP = 975a$ ; mean values (top left), median (bottom left) with the related 84<sup>th</sup> percentile (bottom right).



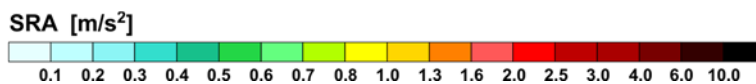
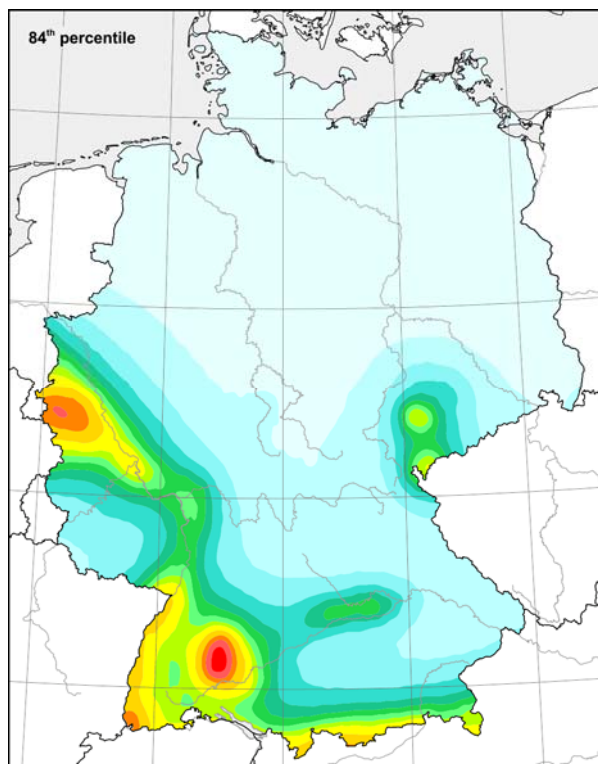
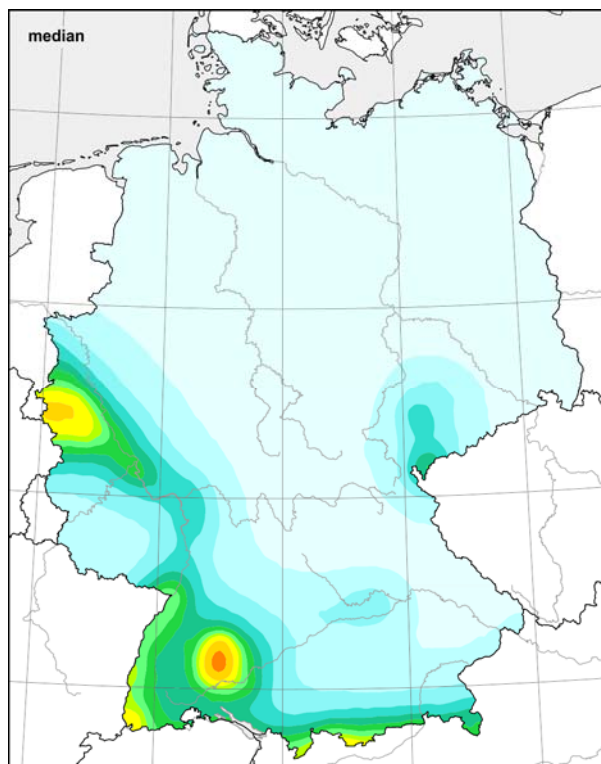


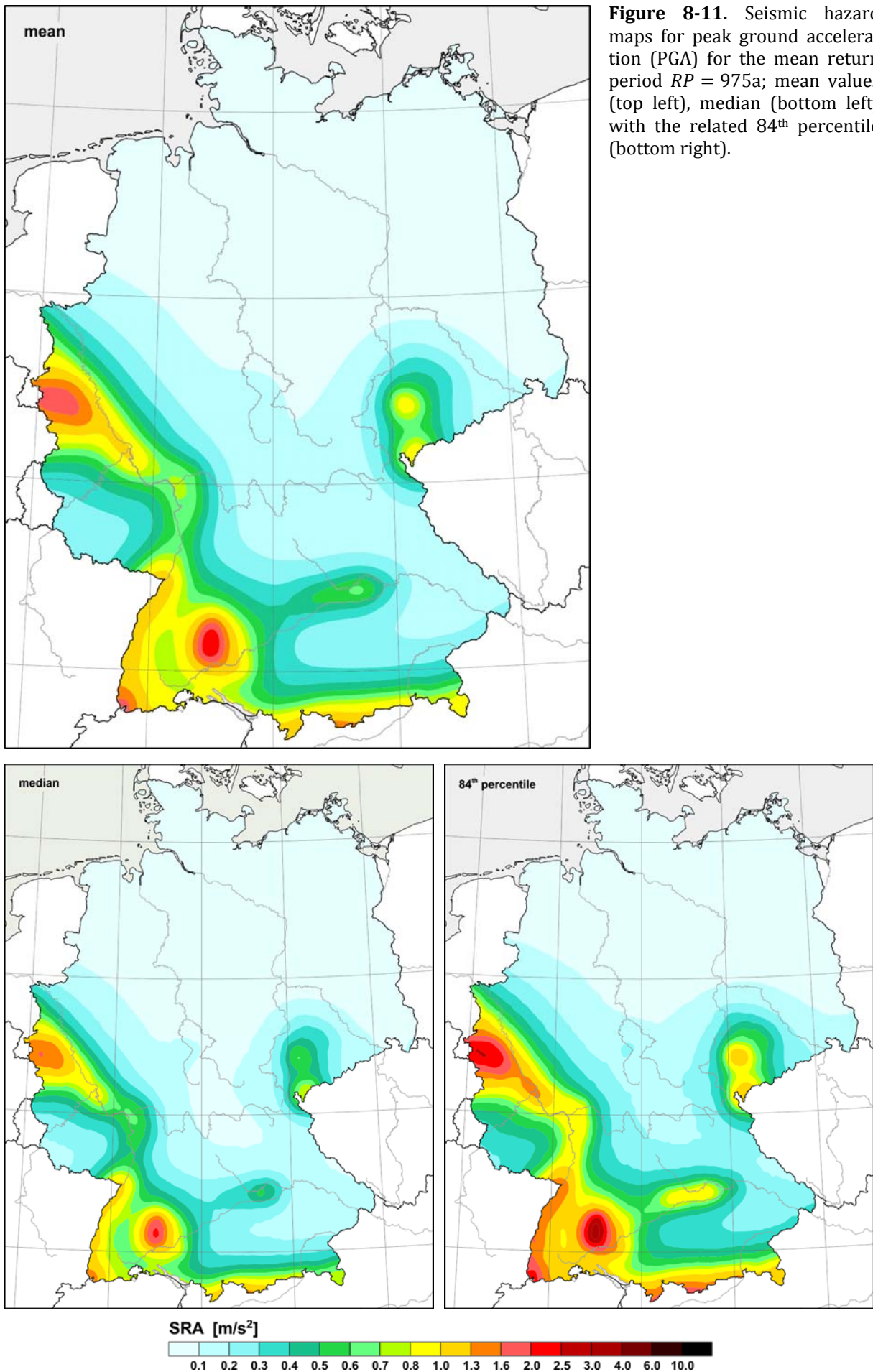


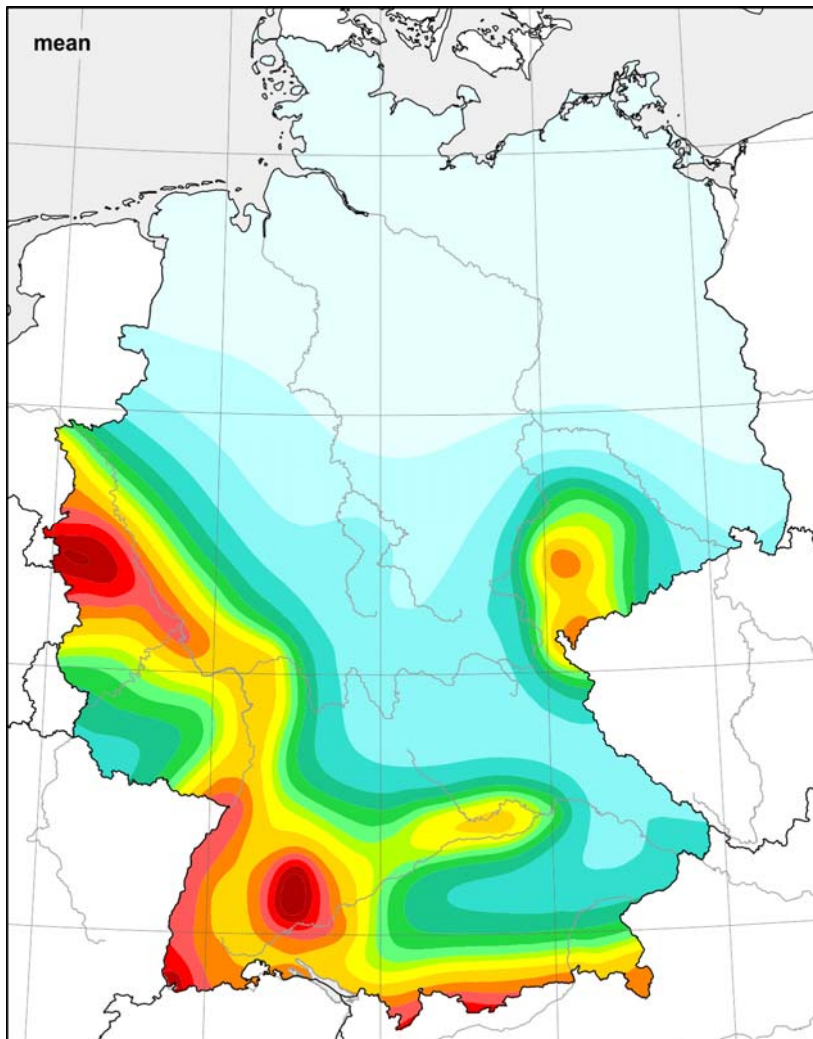
**Figure 8-9.** Seismic hazard maps for the response acceleration amplitudes at 0.20 s spectral period for the mean return period  $RP = 2475a$ ; mean values (top left), median (bottom left) with the related 84<sup>th</sup> percentile (bottom right).



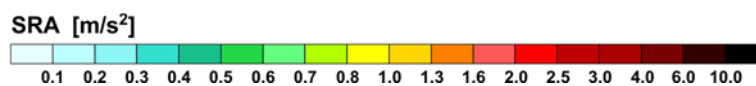
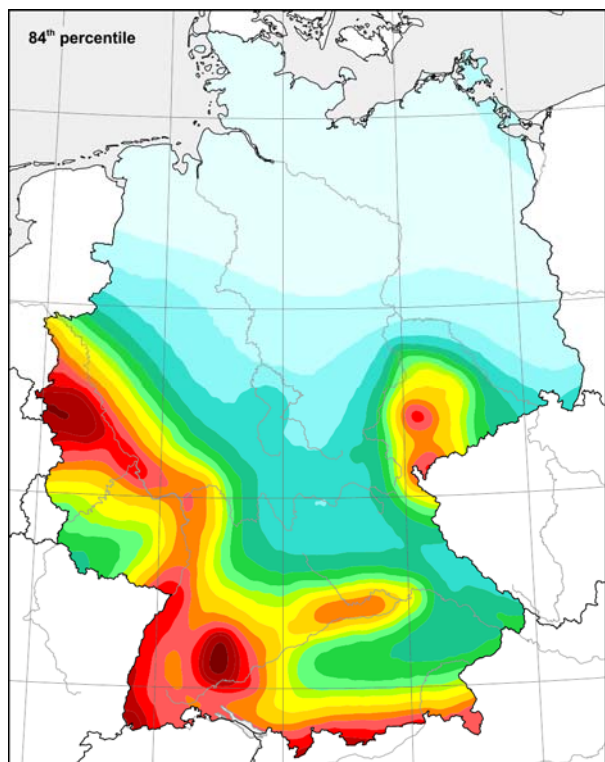
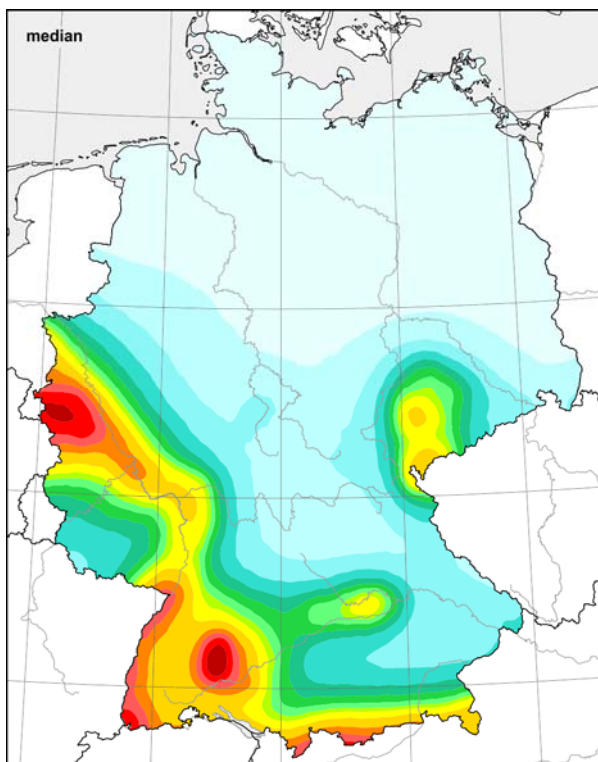
**Figure 8-10.** Seismic hazard maps for peak ground acceleration (PGA) for the mean return period  $RP = 475a$ ; mean values (top left), median (bottom left) with the related 84<sup>th</sup> percentile (bottom right).

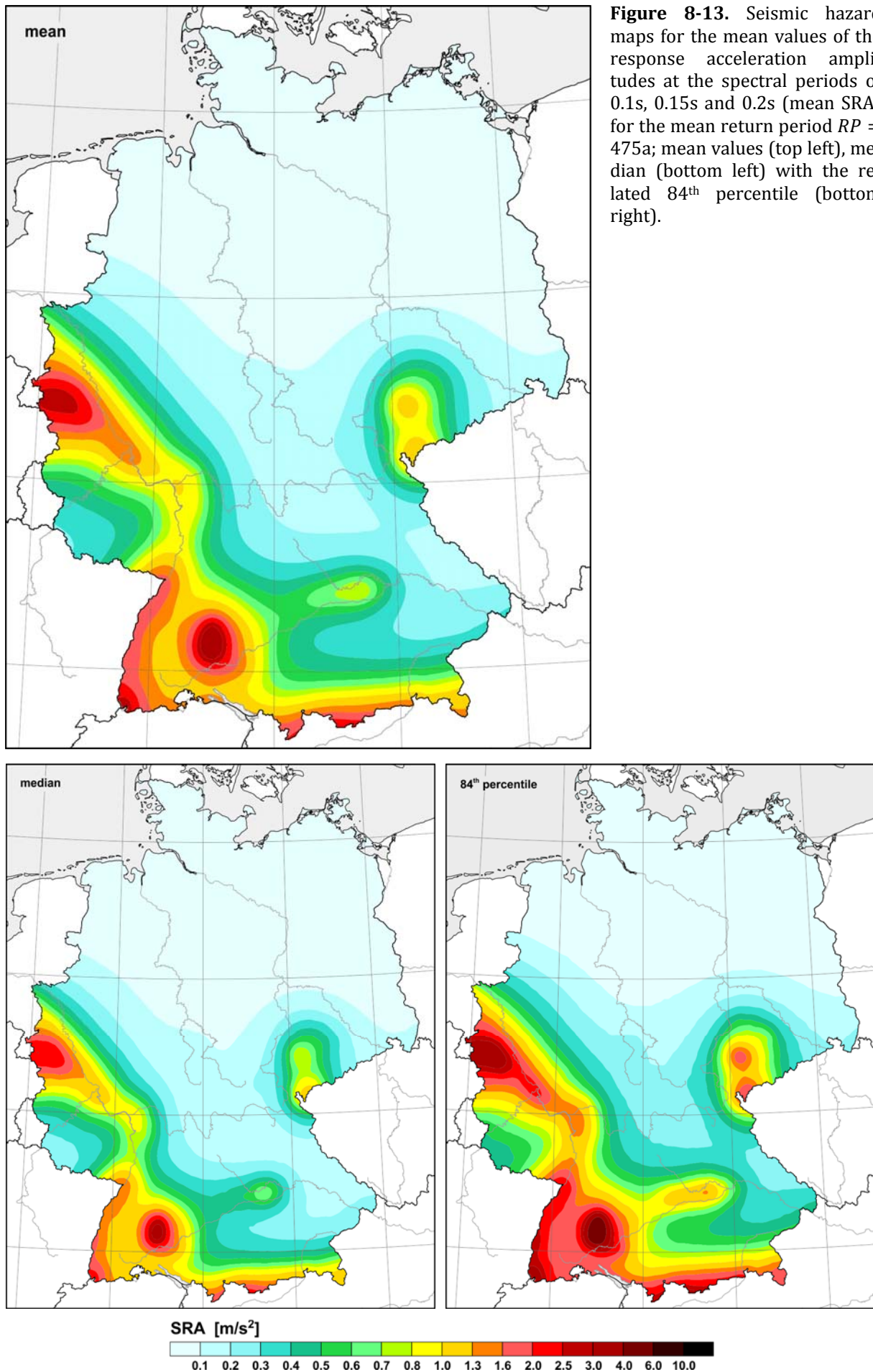




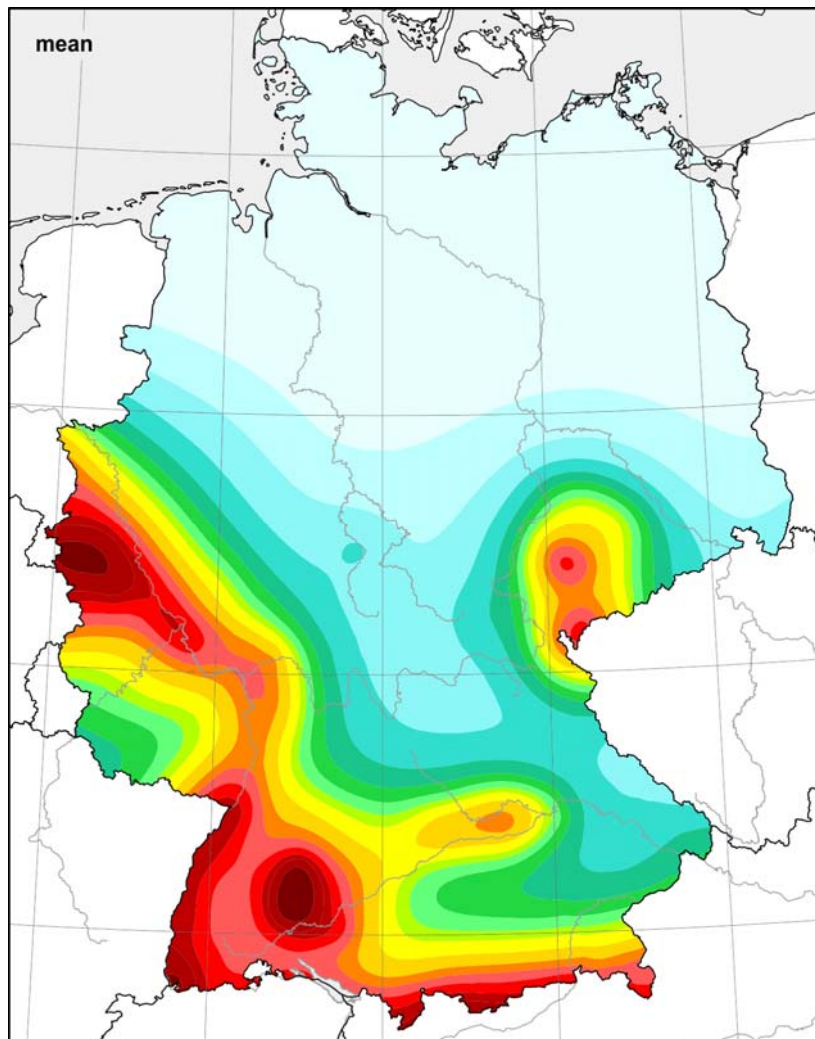


**Figure 8-12.** Seismic hazard maps for peak ground acceleration (PGA) for the mean return period  $RP = 2475a$ ; mean values (top left), median (bottom left) with the related 84<sup>th</sup> percentile (bottom right).

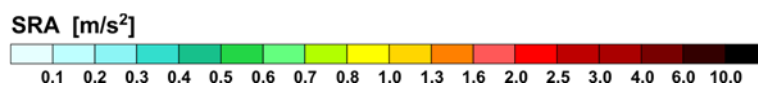
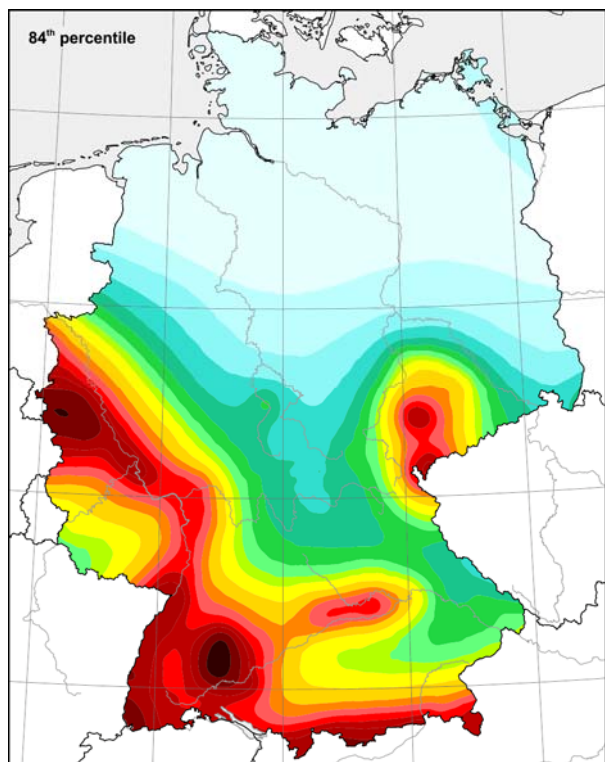
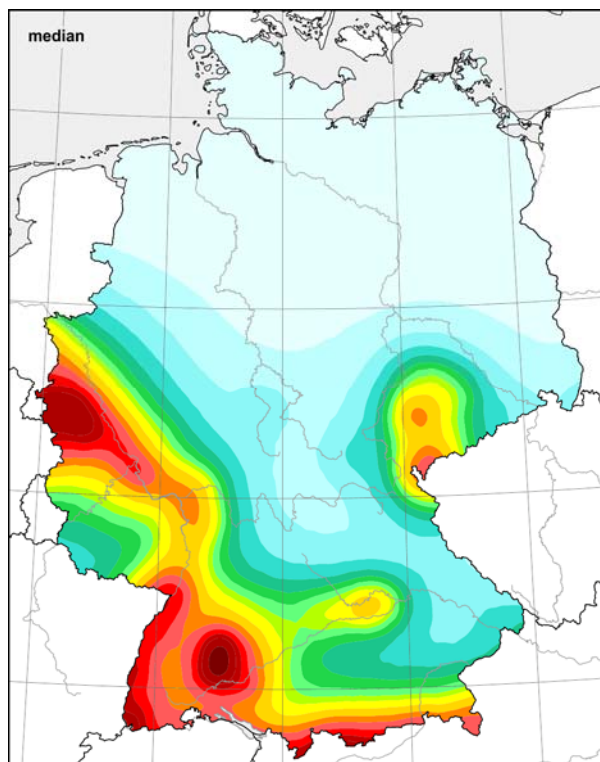


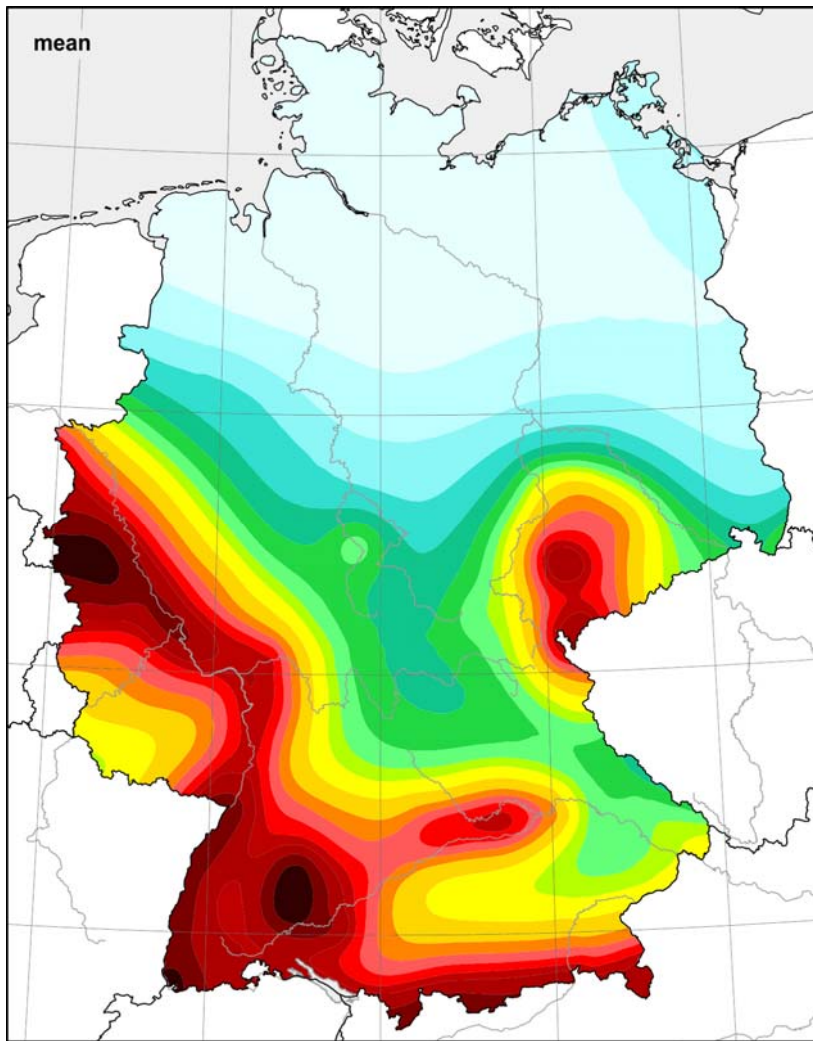


**Figure 8-13.** Seismic hazard maps for the mean values of the response acceleration amplitudes at the spectral periods of 0.1s, 0.15s and 0.2s (mean SRA) for the mean return period  $RP = 475a$ ; mean values (top left), median (bottom left) with the related 84<sup>th</sup> percentile (bottom right).

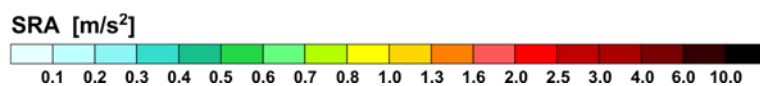
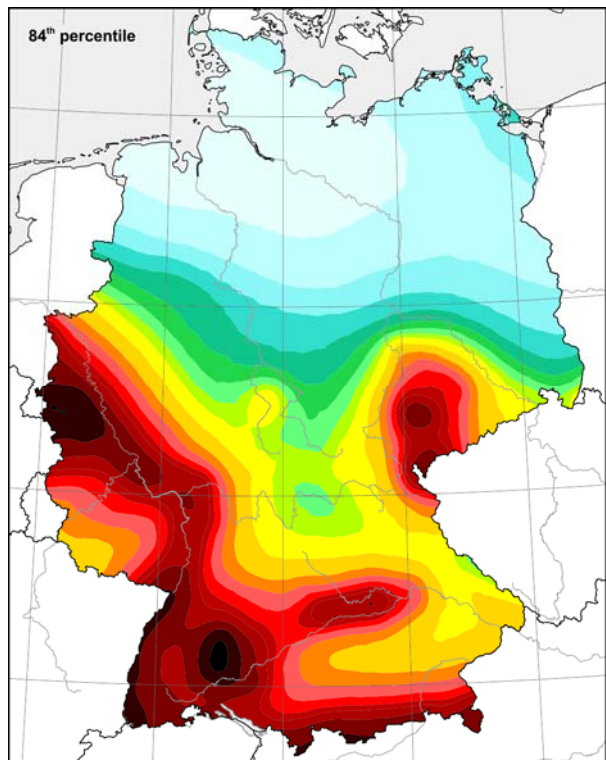
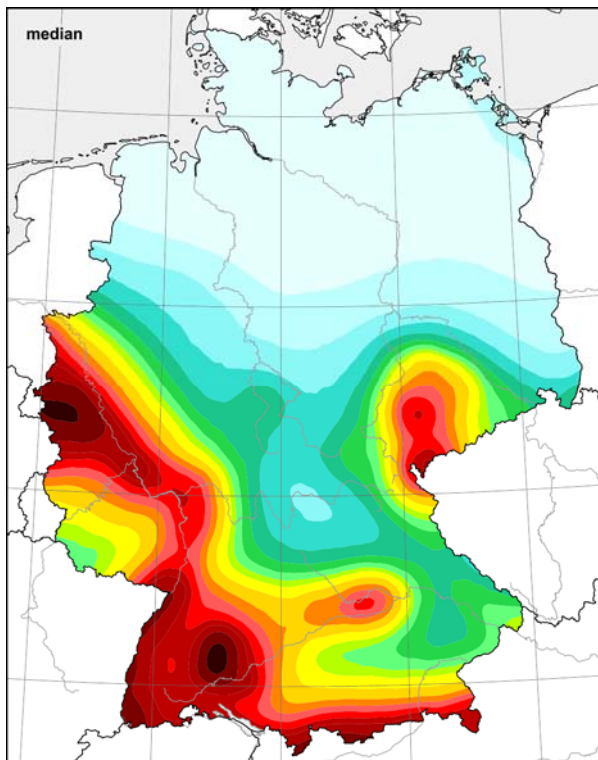


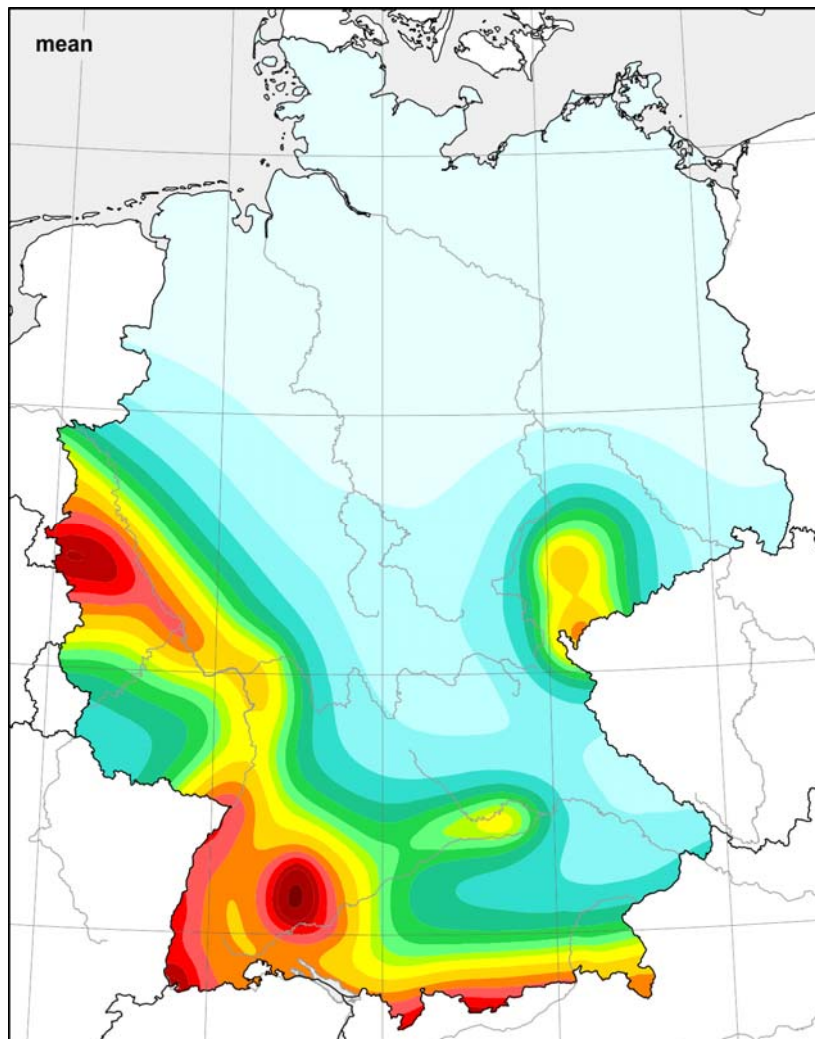
**Figure 8-14.** Seismic hazard maps for the mean values of the response acceleration amplitudes at the spectral periods of 0.1s, 0.15s and 0.2s (mean SRA) for the mean return period  $RP = 975a$ ; mean values (top left), median (bottom left) with the related 84<sup>th</sup> percentile (bottom right).



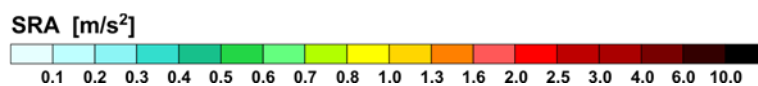
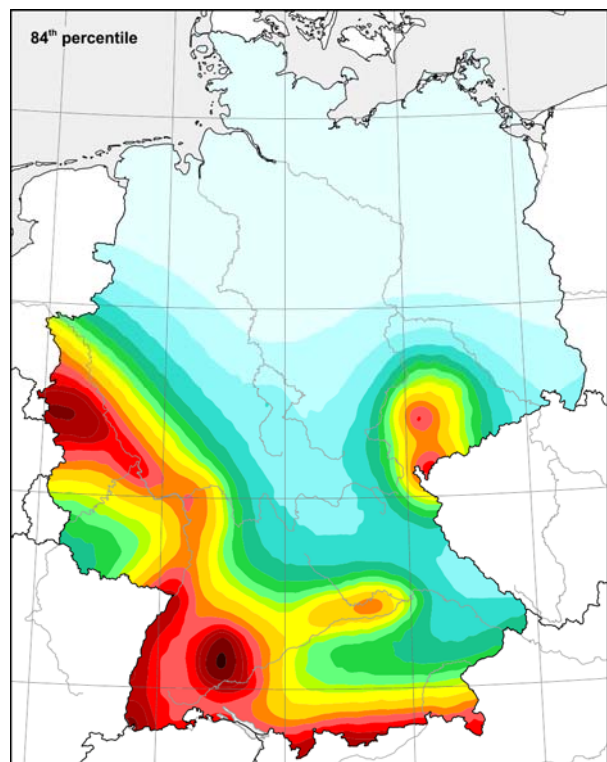
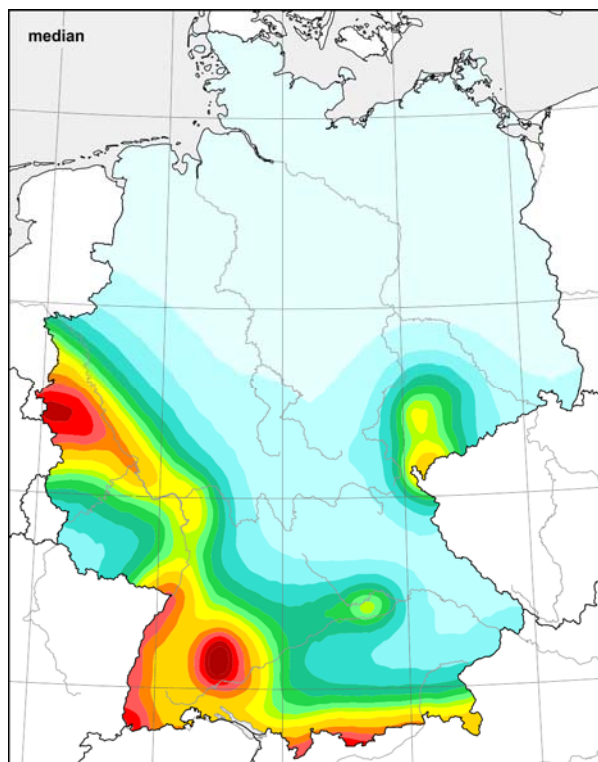


**Figure 8-15.** Seismic hazard maps for the mean values of the response acceleration amplitudes at the spectral periods of 0.1s, 0.15s and 0.2s (mean SRA) for the mean return period  $RP = 2475a$ ; mean values (top left), median (bottom left) with the related 84<sup>th</sup> percentile (bottom right).





**Figure 8-16.** Seismic hazard maps for the maximal values of the response acceleration amplitudes at the spectral periods of 0.1s, 0.15s and 0.2s (max SRA) for the mean return period  $RP = 475a$ ; mean values (top left), median (bottom left) with the related 84<sup>th</sup> percentile (bottom right).





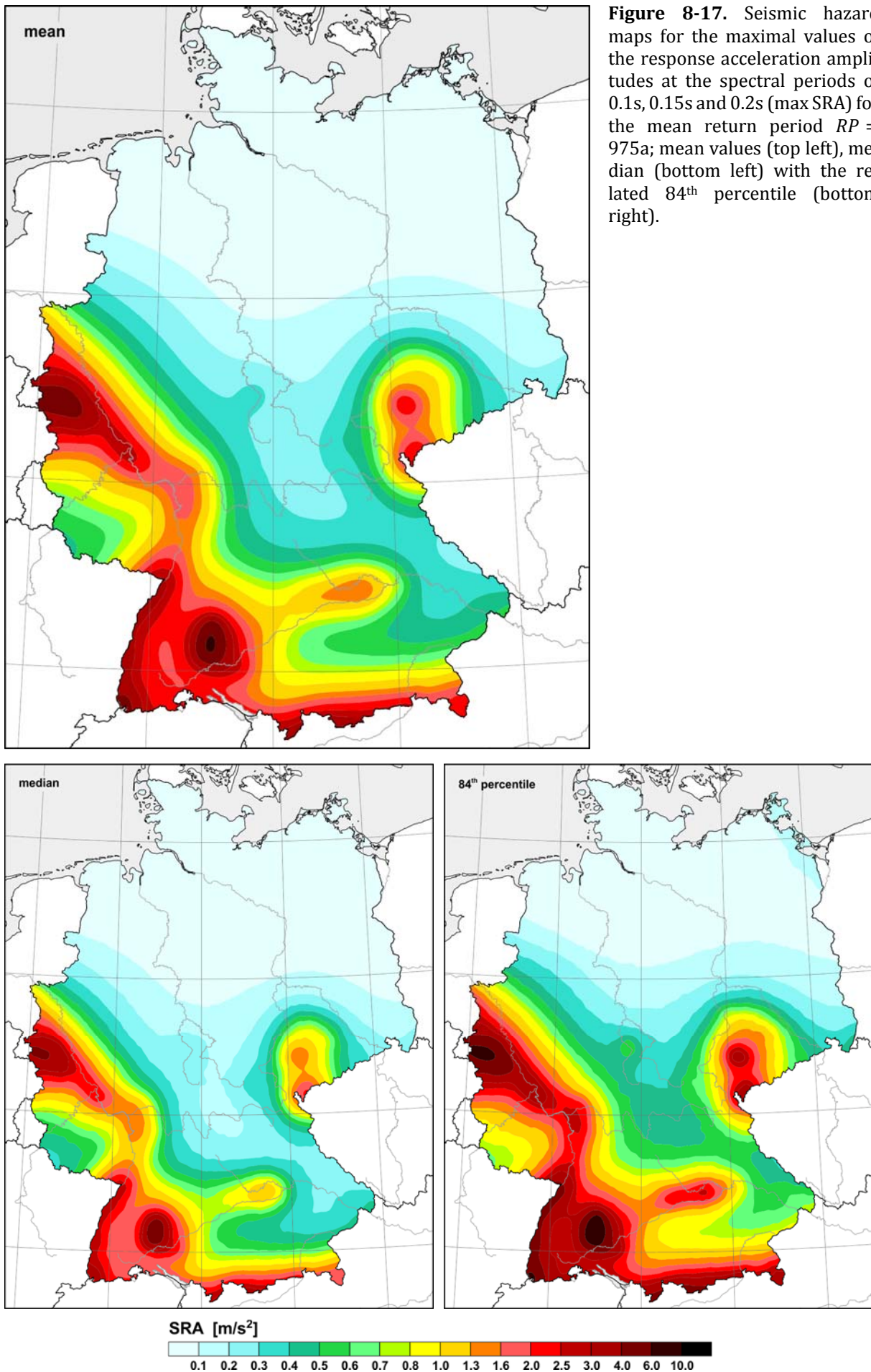


**Figure 8-17.** Seismic hazard maps for the maximal values of the response acceleration amplitudes at the spectral periods of 0.1s, 0.15s and 0.2s (max SRA) for the mean return period  $RP = 975a$ ; mean values (top left), median (bottom left) with the related 84<sup>th</sup> percentile (bottom right).

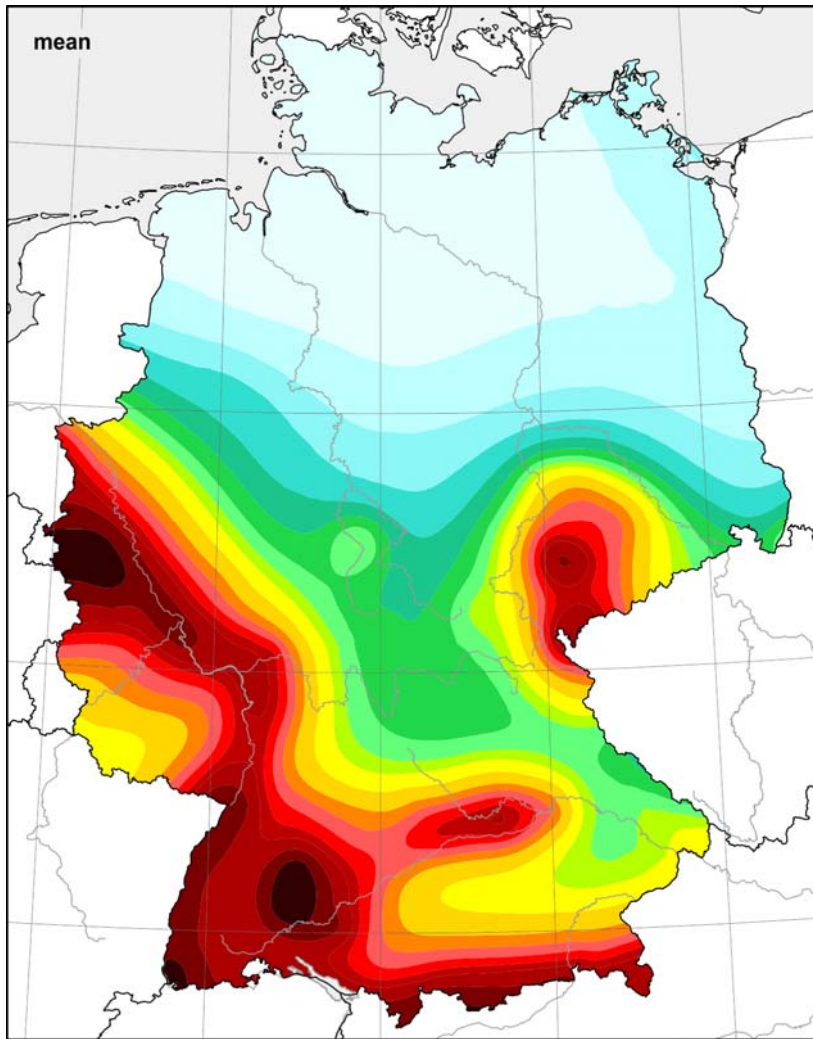
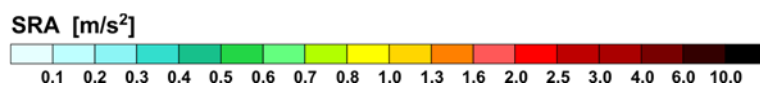
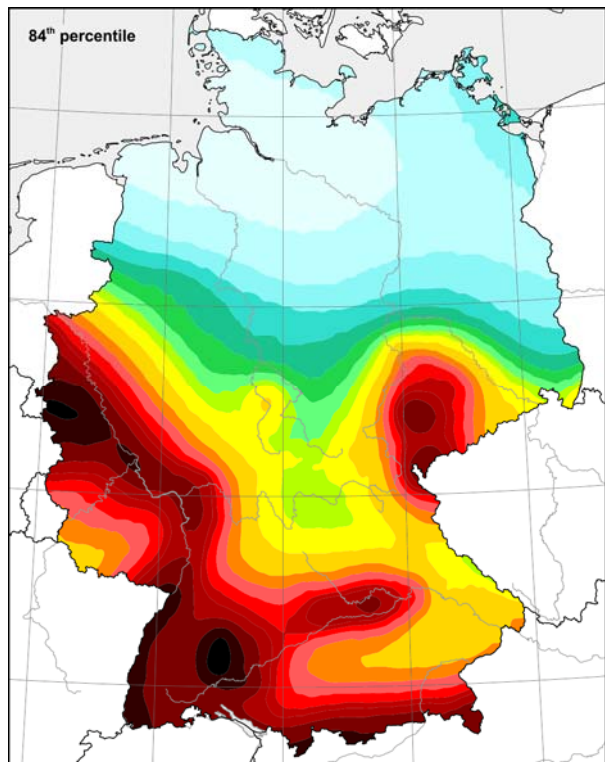
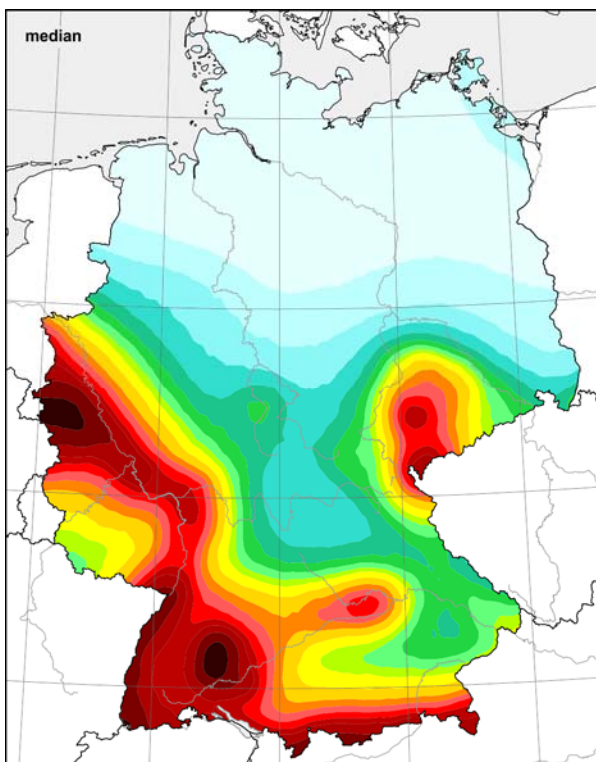


**Figure 8-18.** Seismic hazard maps for the maximal values of the response acceleration amplitudes at the spectral periods of 0.1s, 0.15s and 0.2s (max SRA) for the mean return period  $RP = 2475a$ ; mean values (top left), median (bottom left) with the related 84<sup>th</sup> percentile (bottom right).



## 8.2. Deaggregations

Deaggregations provide an interesting insight into the composition of the seismic hazard at a site for respective hazard levels and ground motion parameters (cf. chapter 9.1 of Grünthal *et al.* 2018); i.e. which rates of magnitude-distance bins govern the seismic hazard for the given parameters. As an example, we here provide the deaggregations for the centres of Aachen, Cologne, Gera, Karlsruhe, Stuttgart and Tuttlingen (Fig. 8-19).

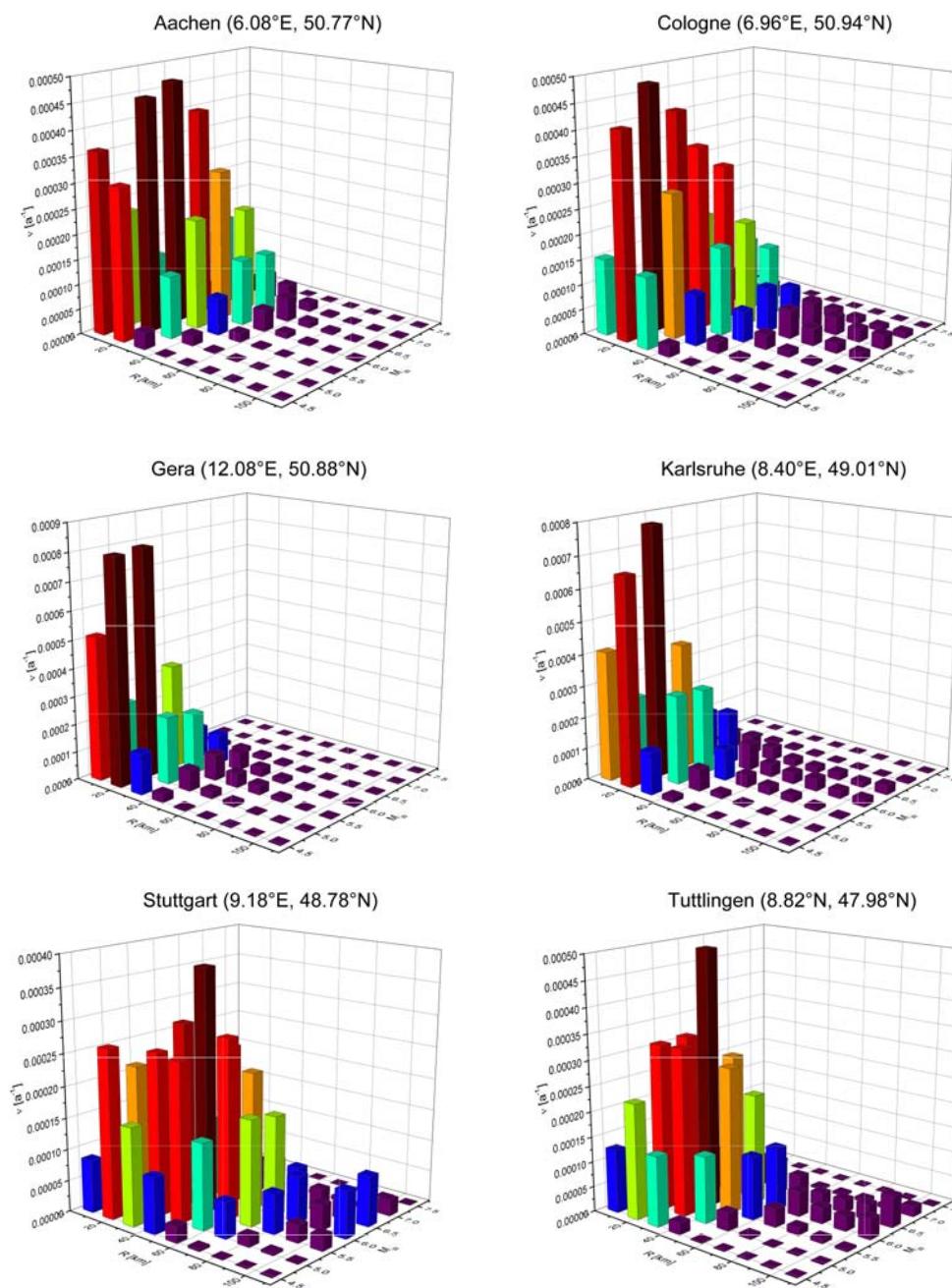


**Figure 8-19.** Deaggregations in form of the rates of magnitude-distance bins for the centres of Aachen, Gera, Cologne, Karlsruhe, Stuttgart and Tuttlingen for PGA and  $RP = 475a$ .

### 8.3. The parameters of the EC 8 elastic design spectral shapes

The central result of the PSHA concerning the project presented here are UHS for any geographic point within Germany (cf. chapter 9.1 in *Grünthal et al. 2018*). These UHS are accessible under the specific project related web portal [http://www.gfz-potsdam.de/EqHaz\\_D2016](http://www.gfz-potsdam.de/EqHaz_D2016), wherefrom the UHS can also be downloaded. The 19 calculated spectral periods in the range of 0.02-3.0 s as backbone for constructing the UHS were

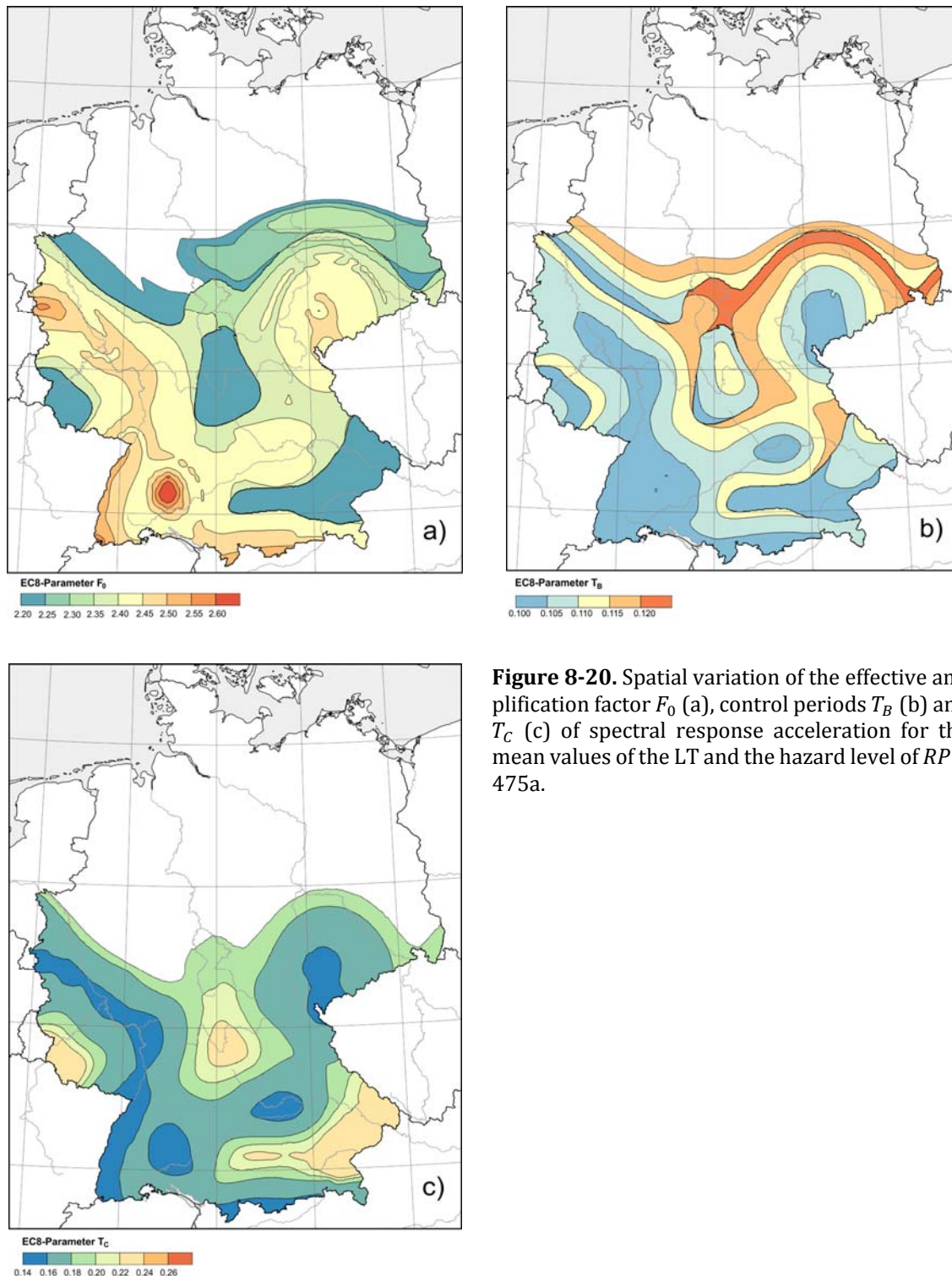


**Figure 8-20.** Spatial variation of the effective amplification factor  $F_0$  (a), control periods  $T_B$  (b) and  $T_C$  (c) of spectral response acceleration for the mean values of the LT and the hazard level of  $RP = 475a$ .

also used for the fit according to the shape of the EC 8 elastic design spectra. These EC 8 spectra are characterized by the following parameters: the effective amplification factor  $F_0$ ; i.e. the ratio between the plateau of the design spectra and PGA, and the control periods  $T_B$ ,  $T_C$  and  $T_D$ . The parameters  $F_0$ ,  $T_B$  and  $T_C$  show a significant spatial pattern within the target area, which is depicted in Figs. 8-20a-c for the mean values of the LT and the hazard level of  $RP = 475a$ .  $T_D$ , the transition period from constant velocity to constant displacement within the spectrum, can only be accessed with large uncertainties mainly due to missing calculated spectral data for larger periods since respective parameters for additional periods are not provided with the GMPE adopted in this analysis.

## 9. Comparison with results of the new Swiss earthquake hazard model

A comparison of the new earthquake hazard model CH2015 for Switzerland (Wiemer *et al.* 2016) with the new German model D2016 has already been made in Grünthal *et al.* (2018) in terms of median PGA maps for  $RP = 475a$  and for  $v_{S30} = 800\text{m/s}$  north and south of the common state border. Both maps coincide very well.

Further comparisons are presented in the following concerning UHS and hazard curves at points within Germany near to the common border. We selected two sites, one immediately north of Basel (46.6°N, 7.6°E) and another one east of Schaffhausen (47.7°N, 8.7°E).

The first comparison is made for seismic hazard curves in form of exceedance probabilities within 50 years for the spectral response acceleration of  $T = 0.2\text{ s}$  (Fig. 9-1) in terms of  $g$ ; i.e. the gravitational acceleration, and for  $v_{S30} = 1105\text{ m/s}$ , which is used as the basis for the results according to the new Swiss project (Wiemer *et al.* 2016) provided via the link as part of the given reference. The curves are shown for median and mean values. Their coincidence is striking. None of them lies above the other, but they cross each other two or three times within the probability range up to  $10^{-4}$ .

The comparison of the UHS according to both projects are shown in Fig. 9-2 in form of the response spectra for the median, the 84<sup>th</sup> and the 16<sup>th</sup> percentile for  $RP = 475a$ . The UHS are also provided in terms of  $g$  and for  $v_{S30} = 1105\text{ m/s}$ . For both locations, which are the same as shown and discussed above in terms of the hazard curves, the peaks of the median

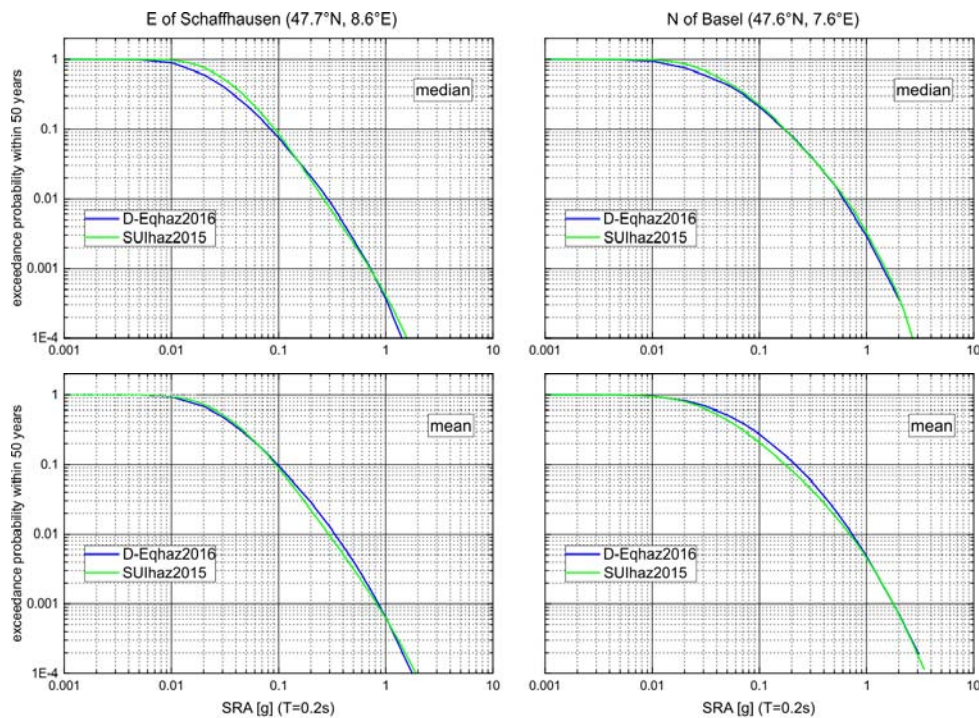


**Figure 9-1.** Seismic hazard curves for two sites immediately north of Basel (left) and east of Schaffhausen (right) as exceedance probabilities within 50 years for the spectral response acceleration of  $T = 0.2$  s in terms of  $g$ ; i.e. the gravitational acceleration, for  $v_{S30} = 1105$  m/s according to the new Swiss project CH2015 (Wiemer *et al.* 2016; <http://www.efehr.org/en/hazard-data-access/hazard-curves/c>) compared with the curves after the D2016 model (Grünthal *et al.* 2018). The curves are shown for median and mean values.

curves are slightly higher according to the D2016 model and significantly higher for the 84<sup>th</sup> percentile. The shape of the 16<sup>th</sup> percentile curve is in one of the two cases practically the same. The maximum spectral amplitudes are reached at almost the same periods, but with slightly lower values for the D2016 model. However, the UHS according to the D2016 model are narrower than those after the Swiss model CH2015, which results in two crossing points of the spectra in case that the one model shows larger peak values. The intersecting points of the median spectral curves are, in both cases, at or near to 0.06 s and at or near to 0.2 s; i.e. just the spectral period used for the graphs of Fig. 9-1. The third spectral period, where the values are almost identical, is for both cases the spectral point which defines the median PGA.

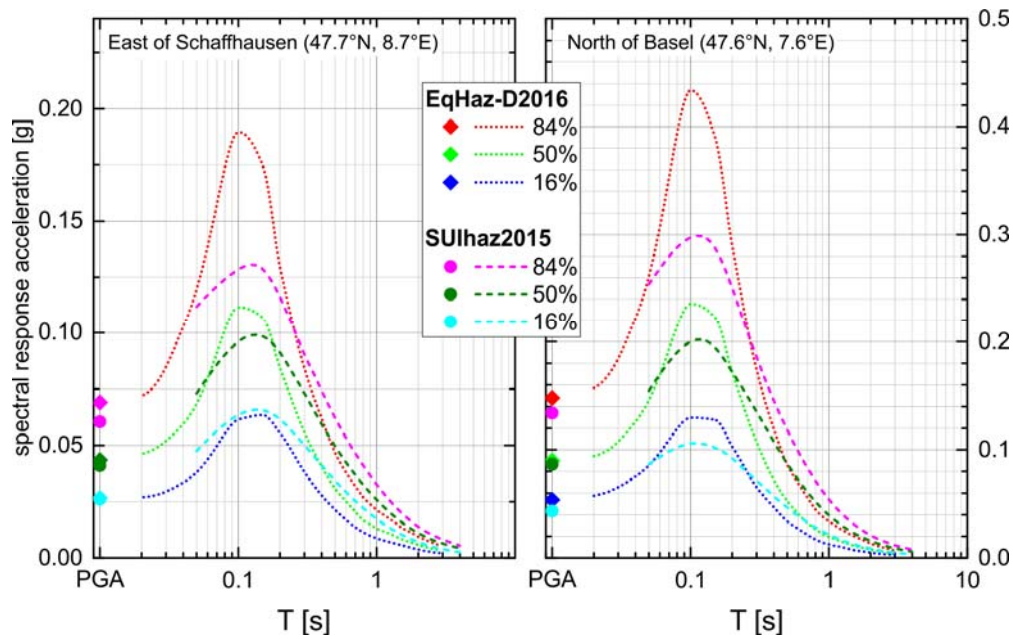


**Figure 9-2.** Comparison of UHS according to the new Swiss project SUIhaz2015 (Wiemer *et al.* 2016) with those after the D2016 model (Grünthal *et al.* 2018). The response spectra are shown for the median, the 84<sup>th</sup> and the 16<sup>th</sup> percentile, for RP = 475 a, in terms of  $g$  and for  $v_{S30} = 1105$  m/s.

## 10. Available Datasets

The main input data of the earthquake model for the probabilistic seismic hazard assessment of Germany, version 2016, are: (1) the geometry of five SSZ models A, B, C, D, E and of the CSS model; (2) the assignment of individual sources to the different superzone models ( $M_{max}$ ,  $b$ -value, depth, tectonic regime and smoothing kernel) and (3) the seismicity rates of all sources given as  $M_{max}$  depending Gutenberg-Richter parameters  $a$  and  $b$  with their covariances  $C_{aa}$ ,  $C_{ab}$  and  $C_{bb}$  (Grünthal *et al.* 2018, Chapter 5.2). These data are published via GFZ Data Services by Grünthal *et al.* (2018a).

The geometry data of the five SSZ models are provided by ESRI shapefiles (Model\_A.shp, Model\_B.shp, Model\_C.shp, Model\_D.shp, Model\_E.shp). Each individual area source of a SSZ model is given by a polygon with geographic coordinates (reference system WGS84) and several describing attributes (Table 10-1). The CSS model of the Lower Rhine graben is described by the shapefile CSS\_Lower\_Rhine\_Top.shp in form of polylines with geographic coordinates (reference system WGS84), each representing the trace of a fault plane upper edge. The polylines are taken from the European Database of Seismogenic Faults (EDSF) compiled in the

framework of the Project SHARE, WP3 Task 3.2 (Basili et al. 2013). The additional CSS attributes of the shape file are explained in Tab. 10-2.

**Table 10-1.** Shapefile attributes of SSZ models. Attributes marked by (\*) are only related to model A.

| Attribute  | Description   | Type    |
|------------|---|---------|
| Name       | source name built from model name and source number within the model (e.g. C05) | string  |
| SourceNo   | source number within a SSZ model (e.g. 5)                                       | integer |
| DepthGr    | depth group number according to Fig. 6-1 and Table 6-1                          | integer |
| TectGr     | tectonic group number according to Fig. 7-1 and Table 7-1                       | integer |
| bGr*       | common $b$ -value group number according to Fig. 5-1                            | integer |
| MmaxGr*    | $M_{max}$ group number according to Fig. 4-2 and Table 4-1                      | integer |
| KernelGr*  | kernel group number according to Fig. 3-7 and Tab. 3-2                          | integer |
| TerraneGr* | tectonic terrane group number according to Fig. 4-1                             | integer |

**Table 10-2.** Shapefile attributes of the CSS models. Related values are given in Tab. 3-1.

| Attribute | Description                       | Type   |
|-----------|-----------------------------------|--------|
| Name      | CSS name according to EDSF        | string |
| TotalL    | CSS total length [km]             | double |
| TotalW    | CSS total depth [km]              | double |
| TotalA    | CSS total area [km <sup>2</sup> ] | double |
| MaxDepth  | maximal depth of CSS              | double |
| FaultType | fault type                        | string |
| MaxMw     | $M_{max}$ of CSS                  | double |
| SigMw     | standard deviation of $M_{max}$   | double |

The parameters  $a$  and  $b$  of the frequency-magnitude relation (Tab. 5-1a-e, Tab. 5-2) are provided by EXCEL files (Model\_A\_Param.xlsx, Model\_B\_Param.xlsx, Model\_C\_Param.xlsx, Model\_D\_Param.xlsx, Model\_E\_Param.xlsx, CSS\_Param.xlsx). These files contain the two versions of the minimum magnitude for fit in two different table sheets (high and low).



## 11. References

- Basilic R, Kastelic V, Demircioglu MB, Garcia Moreno D, Nemser ES, Petricca P, Sboras SP, Besana-Ostman GM, Cabral J, Camelbeeck T, Caputo R, Danciu L, Domac H, Fonseca J, García-Mayordomo J, Giardini D, Glavatovic B, Gulen L, Ince Y, Pavlides S, Sesetyan K, Tarabusi G, Tiberti MM, Utkucu M, Valensise G, Vanneste K, Vilanova S, Wössner J (2013): The European Database of Seismogenic Faults (EDSF) compiled in the framework of the Project SHARE, (Share - The European Database of Seismogenic Faults). DOI: <http://doi.org/10.6092/INGV.IT-SHARE-EDSF>
- DIN EN 1998-1:2010-12 (2010) Eurocode 8: Auslegung von Bauwerken gegen Erdbeben – Teil 1: Grundlagen, Erdbebeneinwirkungen und Regeln für Hochbauten. DIN Deutsches Institut für Normung e.V. Berlin
- DIN EN 1998-1/NA:2011-01 (2011) National Annex - Nationally determined parameters - Eurocode 8: Design of structures for earthquake resistance - Part 1: General rules, Seismic actions and rules for buildings. DIN Deutsches Institut für Normung e.V. Berlin
- Grünthal G (2014) Induced seismicity related to geothermal projects versus natural tectonic earthquakes and other types of induced seismic events in Central Europe. *Geothermics* 52: 22-35; <http://doi.org/10.1016/j.geothermics.2013.09.009>
- Grünthal G, Mayer-Rosa D, Lenhardt W (1998) Abschätzung der Erdbebengefährdung für die D-A-CH-Staaten - Deutschland, Österreich, Schweiz. *Bautechnik* 75(10): 753-767
- Grünthal G, Stromeyer D, Bosse C, Cotton F, Bindi D (2018) The probabilistic seismic hazard assessment of Germany: version 2016, considering the range of epistemic uncertainties and aleatory variability. *Bull Earthquake Engineering* :1-57, <http://doi.org/10.1007/s10518-018-0315-y>
- Grünthal,G, Stromeyer D, Bosse C (2018a): The Source Model of the Probabilistic Seismic Hazard Assessment (PSHA) of Germany - Version 2016. V. 1.0. GFZ Data Services, <http://doi.org/10.5880/GFZ.2.6.2018.001>
- Hakimhashemi A, Grünthal G (2012) A statistical method for estimating catalog completeness applicable to long-term nonstationary seismicity data. *Bull Seismol Soc Am* 102(6): 2530-2546; <http://doi.org/10.1785/0120110309>

- Heidbach O, Custodio S, Kingdon A, Mariucci MT, Montone P, Müller B, Pierdominici S, Rajabi M, Reinecker J, Reiter K, Tingay M, Williams J, Ziegler M (2016) World Stress Map Database Release 2016. GFZ Data Services, <http://doi.org/10.5880/WSM.2016.001>
- Miller AC, Rice TR (1983) Discrete approximation of probability distributions. Management Science 29(3): 352–362. <http://doi.org/10.1287/mnsc.29.3.352>
- Vanneste K, Camelbeeck T, Verbeek K (2013) A model of composite seismic sources for the Lower Rhine Graben, Northwest Europe. Bull Seismol Soc Am 103(2A): 984-1007, <http://doi.org/10.1785/0120120037>
- Wiemer St, Danciu L, Edwards B, Marti M, Fäh D, Hiemer St, Wössner J, Cauzzi C, Kästli Ph, Kremer K (2016) Seismic Hazard Model 2015 for Switzerland (SUIhaz2015). Technical Report, Swiss Seismological Service (SED) at ETH Zurich, <http://doi.org/10.12686/a2>